SEDIMENTOLOGY the journal of the International Association of Sedimentologists

Sedimentology (2023) **70**, 1413–1471 doi: 10.1111/sed.13089

Bioclastic bottom-current deposits of a Devonian contourite terrace: Facies variability and depositional architecture (Tafilalt Platform, Morocco)

HEIKO HÜNEKE*, M. ARWED GIBB*, OLIVER MAYER*, JORIT F. KNIEST*, PAUL MEHLHORN*, LAURA M. GIBB*, Z. SARAH ABOUSSALAM†, R. THOMAS BECKER†, AHMED EL HASSANI‡ and LAHSSEN BAIDDER§

**Institut für Geographie und Geologie, Universität Greifswald, Jahn-Strasse 17a, Greifswald, 17489, Germany (E-mail: hueneke@uni-greifswald.de)*

†Institut für Geologie und Paläontologie, Westfälische Wilhelms-Universität Münster, Corrensstr. 24, Münster, 48149, Germany

‡Hassan II Academy of Sciences and Technology, Km 4 Avenue Mohammed VI, Rabat, Morocco

§Faculty of Sciences Aïn Chock, Geosciences Laboratory, Hassan II University, BP 5366 Maârif, Casablanca, Morocco

Associate Editor – John Reijmer

ABSTRACT

The study examines bioclastic carbonate contourites that arise from the broad spectrum of bottom-current related sedimentary processes ranging from deposition to erosion. The result of the intermittent accumulation of sediment are thin and condensed successions with abundant hiatuses. Such bottom-current deposits are poorly known, since the broadly accepted contourite-facies model, the bi-gradational sequence, characterizes environments of contourite depositional systems as a continuous accretion of fine-grained siliciclastic sediments. To increase current understanding of the carbonate facies within hiatal contourite records, the Eifelian–Frasnian of the Tafilalt Platform in Morocco was investigated. The succession is divided into five facies associations that are interpreted to reflect pelagic sedimentation and deposition from bottom currents on a contourite terrace, a gently inclined section of the upper slope of Gondwana shaped by a water-mass interface. Contourite deposition was mainly controlled by oxic clear-water currents (documented by moderately to completely bioturbated limestones with abundant hydrogenetic ferromanganese nodules, and low organic-carbon contents), at times also by an anoxic water mass (featured by organic-rich coquinas with absent to sparse bioturbation and predominantly syngenetic framboidal pyrites). Biostratigraphic data and the overall depositional architecture display palaeoceanographic hydrodynamic processes associated with a shifting water-mass interface. The inner terrace was characterized by an along-slope contourite channel and a small mounded drift at its downslope margin. Energetic bottom currents furthermore caused abraded surfaces, i.e. plain areas of non-deposition and localized erosion, and sandy condensation layers. The microfacies reflects repeated alternation between suspension deposition, winnowing of fines, bedload traction, dynamic sediment bypassing and reworking, together with concomitant seafloor cementation. Coquinas of mainly planktonic and nektonic organisms are identified as integral parts of bi-gradational contourite sequences showing inverse and normal grading. Hiatal lag concentrations of carbonate intraclasts, ferromanganese nodules and conodonts often drape hardgrounds and erosional surfaces at the midpoint of these frequently incomplete sequences. This Devonian case provides the

opportunity to investigate the spatial and temporal variability of the bed-scale contourite sequence, also with regard to the drift-scale depositional architecture. In addition, the identified high-resolution record is a starting point for unravelling the pattern of oceanic circulation in the Devonian greenhouse world.

Keywords Anti-Atlas, bi-gradational sequence, bioclastic contourite, carbonate contourite, cephalopod limestone, contourite channel, contourite terrace.

INTRODUCTION

Although contourite drifts are widespread in modern deep-marine environments and are valuable archives of palaeoenvironmental changes (e.g. Knutz, 2008; Betzler *et al.*, 2017; de Weger *et al.*, 2020; Toucanne *et al.*, 2021), evidence of bottom-current deposits in ancient sedimentary series is rare and their identification remains problematic (Hüneke & Stow, 2008; Rebesco *et al.*, 2014; Shanmugam, 2017; Eberli & Betzler, 2019). Since detailed outcrop studies usually form the cornerstones of facies models, the fossil contourites problem hinders the refinement of diagnostic bed-scale criteria (Reolid *et al.*, 2020; Hüneke *et al.*, 2021). Consequently, the potential of contourite deposits for palaeoceanographic and palaeoclimatic studies remains largely unexplored, particularly in the Mesozoic and Palaeozoic record, because drift-scale depositional features and basin-wide contourite erosional features have rarely been documented (Duan *et al.*, 1993; Hüneke, 2006, 2007; Surlyk & Lykke-Andersen, 2007; Eberli *et al.*, 2019; Hübscher *et al.*, 2019; Rodrigues *et al.*, 2021).

The specific features of modern carbonate drifts are mainly known from the Marion Plateau (Isern *et al.*, 2005; Eberli *et al.*, 2010), the Maldives (Betzler *et al.*, 2013, 2017; Lüdmann *et al.*, 2013, 2018; Lindhorst *et al.*, 2019; Reolid *et al.*, 2019; Reolid & Betzler, 2019) and the Bahamas (Mulder *et al.*, 2012, 2019; Betzler *et al.*, 2014; Tournadour *et al.*, 2015; Chabaud *et al.*, 2016; Lüdmann *et al.*, 2016, 2018; Wunsch *et al.*, 2017, 2018; Paulat *et al.*, 2019). Many of these studies confirmed the consecutive occurrence and the diagnostic value of normal-to-inverse (bi-gradational) facies sequences (Stow & Faugères, 2008), although the variable bulk densities of bioclastic materials and the early-marine seafloor cementation result in carbonate-specific characteristics (Eberli & Betzler, 2019). The bi-gradational sequence, which is the generally accepted contourite facies model that displays the gradual changes in flow velocity of the bottom current (Faugères *et al.*, 1984; Gonthier *et al.*, 1984; Stow *et al.*, 2002; Stow & Faugères, 2008), is derived from mud-dominated contourite drifts. Examinations of modern contourite settings have shown that partial sequences, including omission surfaces in the central part of the bi-gradational sequence, and even hiatus-bounded sandy contourite intervals, related to prolonged phases of erosion or non-deposition, are at least as common as complete sequences (Stow & Faugères, 2008; Rebesco *et al.*, 2014; Stow & Smillie, 2020). Despite this known variability, so far only a few studies have systematically explored the spatial manifestation of this sequence within contourite depositional systems. Recently, facies models for sandy contourites associated with channels have been published (Brackenridge *et al.*, 2018; de Weger *et al.*, 2020, 2021; de Castro *et al.*, 2020a,b, 2021).

Much less is known about the variability of contourite sequences, in particular of bioclastic composition, from contourite environments characterized by low sediment supply rates, dynamic sediment bypassing, winnowing and episodic erosion. Such conditions result in overall low net accumulation rates that characterize sedimentation on contourite terraces (Viana & Faugéres, 1998; Hernández-Molina *et al.*, 2009, 2016a,b, 2017; Mutti *et al.*, 2014; Miramontes *et al.*, 2019, 2020, 2021; Steinmann *et al.*, 2020; de Castro *et al.*, 2021; Wilckens *et al.*, 2021), in parts of periplatform carbonate drifts (Mulder *et al.*, 2012, 2019; Betzler *et al.*, 2014; Chabaud *et al.*, 2016), and in sediment-transfer areas of contourite depositional systems (Hernández-Molina *et al.*, 2006, 2014; Mulder *et al.*, 2013; de Castro *et al.*, 2020a).

The aim of this study is to explore fossil bioclastic contourites of calcareous composition that

were formed under conditions of very low net accumulation rates. To document such an environment, the Devonian Tafilalt Platform in the eastern Anti-Atlas of Morocco was analysed. The analysis of this platform aims to refine facies models of carbonate contourites and to establish a database for future work on palaeoceanographic changes in the Devonian.

This paper investigates the Eifelian–Frasnian succession of the Tafilalt Platform, based on extensive fieldwork in south-eastern Morocco and by means of a comprehensive microfacies approach. The objectives of this study are to: (i) obtain high-resolution records of bed to microfacies-scale erosional and depositional features from different parts of the platform; (ii) evaluate the lateral facies variability; (iii) determine the drift-scale features based on architecture, general stacking patterns and dimensions of the stratigraphic units, together with the distribution and range of biostratigraphic gaps; and (iv) unravel the sedimentary processes and hydrodynamic conditions that produced the contourite system. Ideal preconditions are the extensive stratigraphic database, large-scale accessible outcrops and an overall weak tectonic deformation. The late Frasnian to early Famennian Kellwasser limestones are not considered in this study, since this facies was formed under the exceptional conditions of a major mass-extinction event and rapid sea-level changes (Stigall, 2012; McGhee *et al.*, 2013; Carmichael *et al.*, 2019; Percival *et al.*, 2020), which are not relevant to the long-term depositional history on the Tafilalt Platform and its overarching controls.

The results of this contourite study will have important consequences for future research. First, instead of pelagic processes, bottom-current-induced processes will be put forward as a main cause of condensed sediment accumulation on deep-marine platforms. Second, the interpretation of thickness variations on the Gondwanan continental margins can be broadened from exclusively considering tectonically-induced subsidence rates and associated gravity processes to also include the morphological perspective of a contourite depositional system and the distribution of depocentres. Third, investigating the link between oceanic anoxic events and intensified bottom-current controlled sedimentation is essential for prospective palaeoceanographic reconstructions and the analysis of Devonian evolutionary events (e.g. Bond *et al.*, 2004; Racki, 2005; Becker *et al.*, 2020; Percival *et al.*, 2020).

STUDY AREA AND GEOLOGICAL SETTING

The Devonian cephalopod limestones are part of the 3 to 4 km thick, early–mid Palaeozoic succession deposited on continental terraces of the passive north-western margin of Gondwana (Soulaimani *et al.*, 2003; Raddi *et al.*, 2007; Baidder *et al.*, 2008, 2016; Michard *et al.*, 2008; Soulaimani & Burkhard, 2008). The present work focuses on the Tafilalt area, where the east–west trending Anti-Atlas belt intersects with the north-west/south-east-trending Ougarta belt, both formed during the Variscan (Alleghanian–Hercynian) collision of Laurussia and Gondwana during the Pennsylvanian to Cisuralian (Fig. 1). Large-scale open anticlines and synclines, formed by thick-skinned inversion tectonics with superimposed folding events (Burkhard *et al.*, 2006; Baidder *et al.*, 2016), provide excellent outcrops to study regional thickness variations and the architecture of the sedimentary units.

The Palaeozoic sequence overlying the Pan-African Basement begins with the Middle Cambrian in most of the eastern Anti-Atlas, initiated by the activity of synsedimentary ENE-trending normal faults. Rather monotonous quartziferous to argillaceous shallow-marine deposits of the Saharan platform specify the Ordovician–Silurian period, including ice-marginal deposits and tunnel valleys incised during the late-Ordovician glaciation (e.g. Destombes *et al.*, 1985; Clerc *et al.*, 2013; Ghienne *et al.*, 2014). The Middle–Late Devonian deposits show remarkable thickness and facies variations, illustrating the coeval disintegration of the northern Sahara platform (Wendt, 1985; Baidder *et al.*, 2008; Ouanaimi & Lazreq, 2008). Basin formation occurred through extension and synsedimentary normal faulting, which resulted in block tilting, slumping and local sedimentary reworking (Wendt & Belka, 1991; Baidder *et al.*, 2008; Wendt, 2021b). Devonian magmatism of calcalkaline intra-plate basalts was restricted to the Lochkovian/Pragian in the eastern Tafilalt, which resulted in the accumulation of up to 100 m of volcaniclastic sediments at Hamar Laghdad (Brachert *et al.*, 1992; Montenat *et al.*, 1996; Belka, 1998; Franchi *et al.*, 2015). Variscan metamorphism of the Devonian rocks is low to very low throughout the Tafilalt. Diagenetic and anchizonal illite-crystallinity values are predominant (Ruiz *et al.*, 2008). Conodont-alteration-index (CAI) values range from 3 to 5, suggesting a burial palaeotemperature between 120°C and 310°C (Belka, 1991).

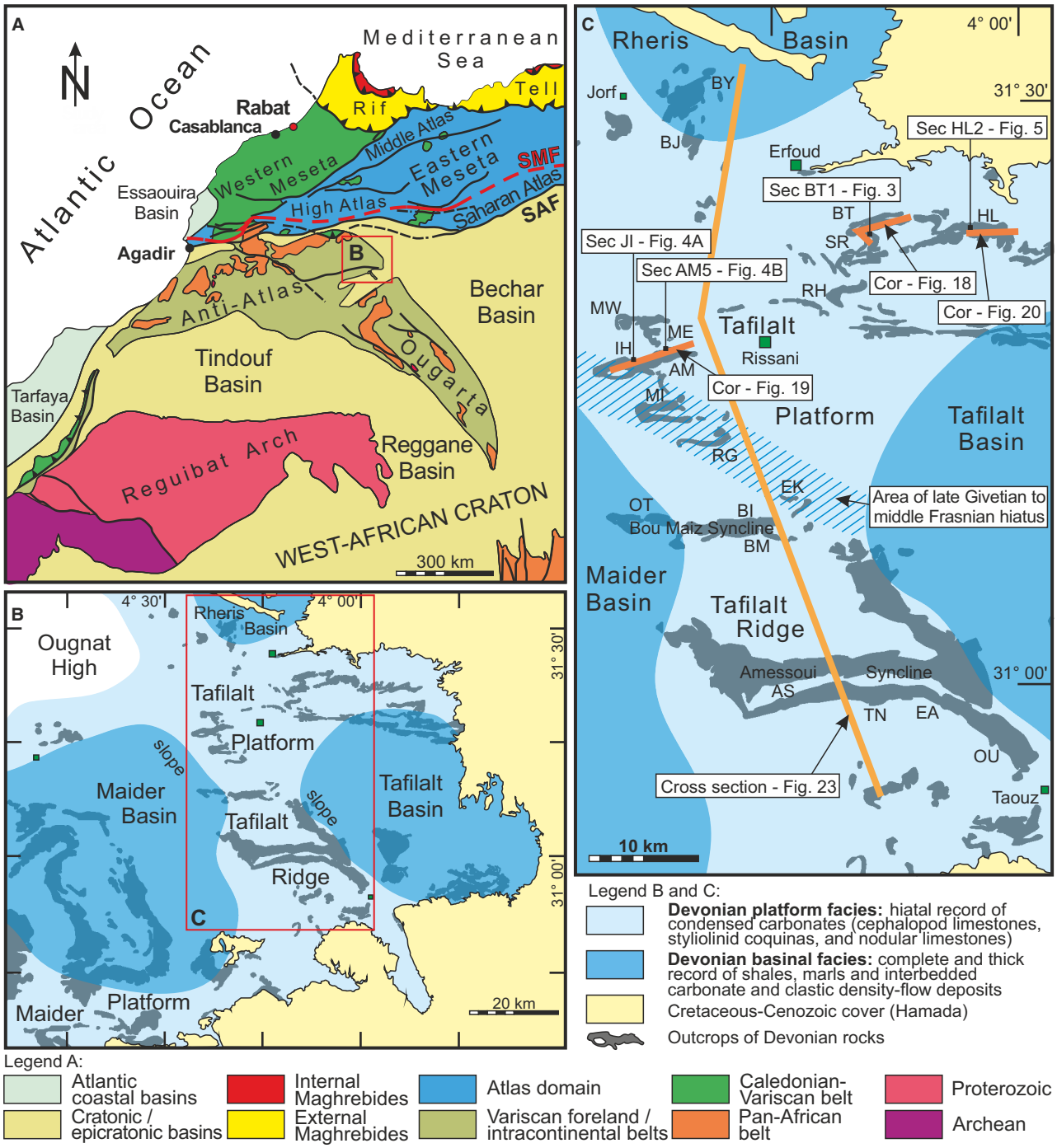

Fig. 1. Geological setting of Tafilalt Platform and locations. (**A**) Tectonic map of north-westernmost Africa showing the northern part of the West African Craton and the adjoining fold belts (modified from Michard *et al.*, 2008), with location of the Tafilalt area (framed). SAF, South Atlas Fault; SMF, South Meseta Fault. (**B**) Overall lithofacies pattern and palaeogeography of the Tafilalt area during late Givetian and early Frasnian (modified from Wendt *et al.*, 1984; Wendt & Aigner, 1985; Belka & Wendt, 1992). The Ougnat High was probably a land area. (**C**) Location sections exemplified in this study. AM, Jebel Amelane; AS, Amessoui Syncline; BI, Bou Ifahrherion; BJ, Bine Jebilet; BM, Bou Maiz; BT, Bou Tchrafine; BY, Barrage el Yhoudi; EA–El, Atrous; EK, El Kachla; HL, Hamar Laghdad; IH, Jebel Ihrs; ME, Mdoura East; MI, Mech Irdane; MW, Mdoura West; OT, Ottara; OU, Ouaoufilal; RG, Rich Gaouz; RH, Rich Haroun; SR, Seheb el Rhassal; TN, Tizi Nersas; Sec, section; Cor, correlation scheme.

Tafilalt Platform

The Tafilalt Platform is a distinct palaeogeographic element during the Middle and Late Devonian (Wendt, 1985, 1989; Wendt & Belka, 1991; Lubeseder *et al.*, 2010), extending across the eastern Ougnat–Ouzina Axis and the Ougnat–Erfoud High (Baidder *et al.*, 2008, 2016). Two rapidly subsiding blocks formed the Maider and Tafilalt basins to the west and east (Fig 1B). The Tafilalt Basin is the western termination of the Bechar–Reggane Basin in western Algeria, of which the major part is hidden under Upper Cretaceous and Tertiary deposits (Wendt, 2021a). In the north, Wendt & Belka (1991) identified the Rheris Basin, which is the margin of a large subsiding area that connects to the Meseta Domain (Hoepffner *et al.*, 2006; Baidder *et al.*, 2008). The Meseta–Anti-Atlas boundary is an ENE-trending transpressional dextral fault called the South-Meseta-Fault (Hoepffner *et al.*, 2006; Michard *et al.*, 2010), which is located about 100 km north of the Tafilalt Platform (Fig. 1A). It was active during the Devonian, separating the stable craton (Anti-Atlas) in the south from a rifted continental domain of thinned crustal blocks (Western and Eastern Meseta) or an oceanic domain (Palaeotethys) further north (see discussion in Stampfli & Borel, 2002; El Hassani *et al.*, 2003; Burkhard *et al.*, 2006; Hoepffner *et al.*, 2006; Baidder *et al.*, 2008; Michard *et al.*, 2010; Stampfli *et al.*, 2011, 2013; Accotto *et al.*, 2021).

A condensed limestone succession (5–50 m) characterizes the Middle to Late Devonian Tafilalt Platform (Wendt *et al.*, 1984), consisting of: (i) thoroughly bioturbated nodular and well-bedded cephalopod limestones, mainly showing a texture of bioclast wackestone with abundant planktonic (styliolinids, nowakiids) and nektonic biota (cephalopods, placoderms), together with low-diversity benthos; (ii) bedded crinoid limestones that include patches of encrusting crinoid holdfasts often preserved in life position; (iii) beds of organic-rich planktonic styliolinid and brachiopod coquinas, i.e. well-sorted packstones and grainstones preserving low-angle cross-bedding and lamination; (iv) quartz-rich brachiopod coquinas; and (v) hardgrounds. Episodic influence of bottom currents has been inferred from the overall low net accumulation rate, current-oriented orthoconic nautiloids and styliolinids, imbricated goniatite shells, and abundant shell concentration, mainly styliolinid coquinas (Wendt, 1988, 1995; Wendt & Belka, 1991; Walliser & Reitner, 1999; Aboussalam & Becker, 2011). In addition, widespread submarine erosional features have been identified on the Tafilalt Platform (Aboussalam & Becker, 2011; Wendt, 2021b). A shallowing towards a euphotic shelf and a land area in the south is indicated by the increasing abundance of benthic organisms, gravity-flow deposits with redistributed photic-zone reef builders (coral–stromatoporoid biostromes) and quartziferous brachiopod coquinas, which occur in the southern part of the Tafilalt Ridge (Fig. 1C; Amessoui Syncline) (e.g. Massa *et al.*, 1965; Wendt *et al.*, 1984; Aboussalam, 2003; Aboussalam & Becker, 2011; Becker *et al.*, 2013; Hartenfels *et al.*, 2018).

A much thicker record (100–400 m) of hemipelagic and density-flow deposits characterizes the slope aprons into the Maider and Tafilalt basins on both sides of the platform (Lubeseder *et al.*, 2010), consisting of: (i) well-bedded laminated marls and calcareous mudstones, rich in lithic peloids and locally quartz, forming rhythmic limestone–marl couplets; (ii) normally-graded limestone beds showing lamination and cross-lamination together with complete and partial Bouma-sequences, interpreted as turbidites; (iii) mud-rich conglomerates, representing debrites; (iv) slump deposits; and (v) thin beds of brachiopod and styliolinid coquinas, i.e. textures of well-sorted packstone and grainstone locally showing low-angle cross-bedding and cross-lamination.

Mud mounds are a characteristic morphosedimentary feature of the eastern Tafilalt Platform (Fig. 2). Although most of the mud mounds at Hamar Laghdad developed during the Emsian, some also accreted during the Eifelian–Givetian, especially the famous Hollard Mound at the eastern end of the ridge (e.g. Töneböhn, 1991; Brachert *et al.*, 1992; Belka, 1998; Aitken *et al.*, 2002; Hartenfels *et al.*, 2018; Klug *et al.*, 2018). Tabulate corals (auloporids and thamnoporids) and crinoids are the most common organisms that colonized the mounds, while calcareous algae and stromatoporoids are absent. The palaeoenvironment has been interpreted as a deep-water, below fair-weather wave base but probably within the range of major storms and under control of bottom currents (Brachert *et al.*, 1992; Klug *et al.*, 2018).

Stratigraphic framework

The Eifelian–Frasnian sections investigated here are part of the Bou Tchrafine (d4) to Achguig (d6) formations (Hollard, 1963, 1981; Hartenfels *et al.*, 2018). A number of marker beds have been recognized in the succession of cephalopod limestones,

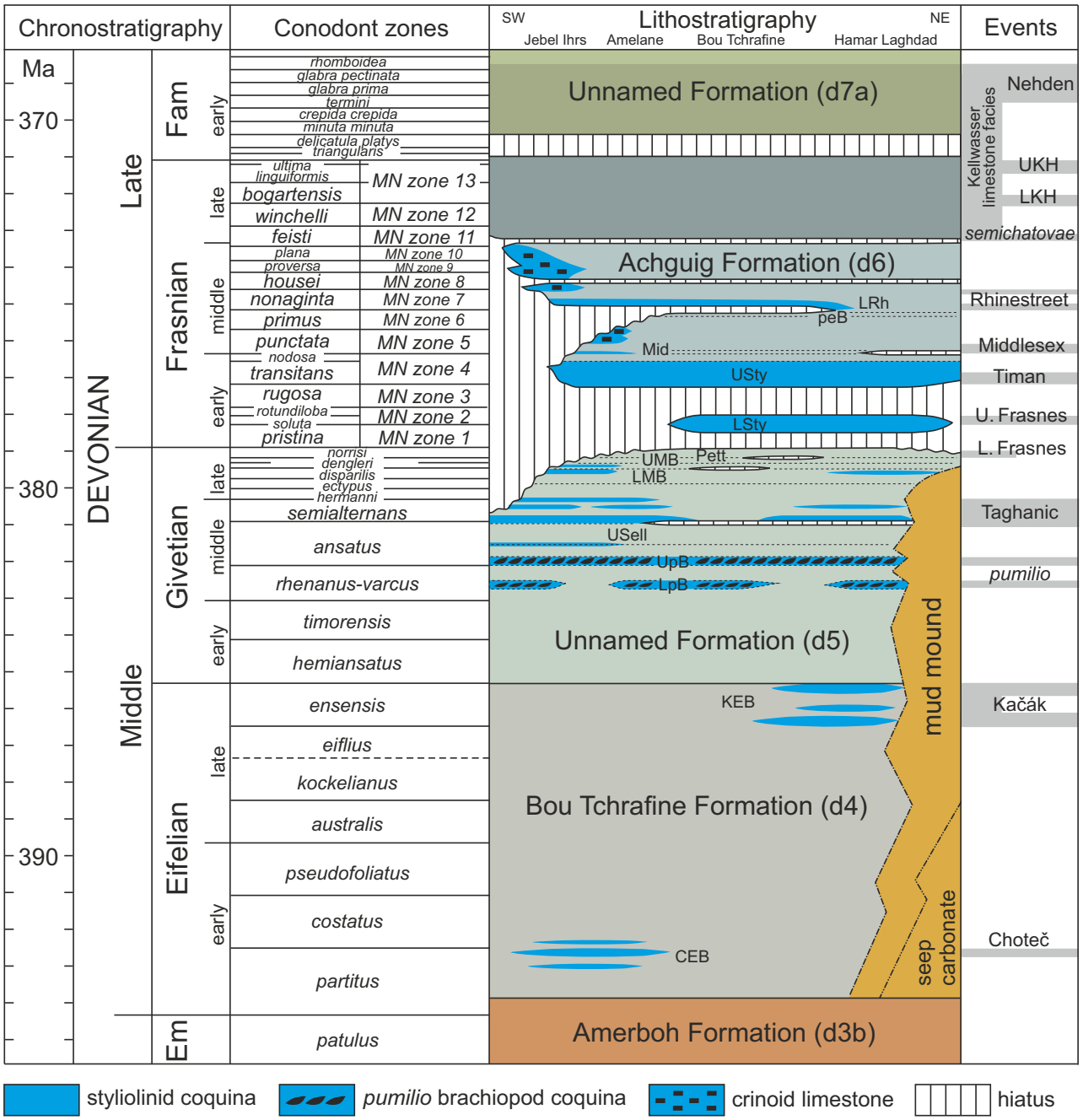

Fig. 2. Stratigraphic scheme of Middle and early Late Devonian cephalopod limestones and associated deposits of the Tafilalt Platform. Highlighted are the stratigraphic position of hiatuses and the occurrence of coquinas, which are a substantial part of marker beds (based on publications in Becker *et al.*, 2013; Hartenfels *et al.*, 2018; and own data). Devonian timescale, chronostratigraphy, conodont zonation, lithostratigraphy and global events from Becker *et al.* (2020). CEB, Choteč Event Bed; KEB, Kačák Event Bed; LKH, Lower Kellwasser Horizon; LMB, Lower Marker Bed; LpB, Lower *pumilio* Bed; LRh, Lower Rhinestreet equivalents; LSty, Lower Styliolinite Frasnes Event; Mid, Middlesex Styliolinite; MN, Montage Noire conodont zonation; PeB, pebble Bed; Pett, *Petteroceras* Bed; UKH, Upper Kellwasser Horizon; UMB, Upper Marker Bed; UpB, Upper *pumilio* Bed; Usell, Upper *Sellagoniatites* Bed; USty, Upper Styliolinite Timan Event.

which are laterally discontinuous (pinching out locally) but can be traced across the whole Tafilalt Platform and locally into the basins (Fig. 2). These marker beds are characterized by a combination of specific sedimentary features (for example, organic-rich beds, particle-supported depositional texture, beds rich in ferromanganese nodules) and a typical fauna (for example, abundant styliolinids, *pumilio*-type brachiopods, specific goniatites). Examples are the Lower and Upper *pumilio* Beds (LpB and UpB) or the Lower and Upper Styliolinite Beds (LSty and USty, Fig. 2). Detailed biostratigraphic work identified these marker beds as isochronous lithostratigraphic units (Belka & Wendt, 1992; Belka *et al.*, 1997, 1999; Aboussalam & Becker, 2007, 2011; Gouwy *et al.*, 2007; and publications edited by Becker *et al.*, 2013; Hartenfels *et al.*, 2018). The latter authors detailed several biostratigraphic gaps (Fig. 2), which are frequently associated with the known marker beds. In successions sampled bed-by-bed, the gaps can be reliably identified by conodonts, because these skeletal elements consist of apatite and would be preserved even under the influence of carbonate dissolution. In case conodonts of certain zones and subzones are missing, the duration of the biostratigraphic gaps can be estimated, since the Devonian conodont zonation is chronostratigraphically scaled (Becker *et al.*, 2020). The most widespread biostratigraphic gaps, those of the *norrisi* (*ca* 200 ka) and MN 2–3a zone (*ca* 800 ka), occur in the early Frasnian succession and can be traced across the whole Tafilalt Platform (Fig. 2). They occur at the base of organic-rich marker beds (Lower and Upper Styliolinite Bed), which consist of styliolinid packstone and grainstone (styliolinid coquinas). In many cases, both the hiatuses and the marker beds were formed in times of rapid global extinctions or radiations (Fig. 2), which have been described as Devonian bioevents (e.g. House, 1985, 2002; Racki, 2005, 2020; Becker & Kirchgasser, 2007; Brett *et al.*, 2012; Gereke & Schindler, 2012; Becker *et al.*, 2016, 2020).

Palaeoceanographic setting

The Tafilalt Platform formed at the outer rim of a broad epicontinental sea that extended over large parts of North Africa (Lüning *et al.*, 2003, 2004; Craig *et al.*, 2008; Soua, 2014). It was located at the transition to the slope aligned along the South Meseta Fault separating the Meseta domain from mainland Gondwana (Baidder *et al.*, 2008; Michard *et al.*, 2010).

There are only few conceptual models of ocean circulation for the Devonian that are based on an analogy with the modern world, where deep-water formation occurs at high latitudes (Heckel & Witzke, 1979; Copper, 1986; Oczlon, 1990; Wendt, 1995; Dopieralska *et al.*, 2006; Hüneke, 2006; Dopieralska, 2009; Crasquin & Horne, 2018; Abram & Holz, 2020). These models are conflicting in many regards, not least because of the contradicting published plate-tectonic and palaeogeographic reconstructions (e.g. Ziegler, 1989; Van der Voo, 1993; Dalziel *et al.*, 1994; McKerrow *et al.*, 2000; Tait *et al.*, 2000; Golonka, 2002, 2020; Stampfli & Borel, 2002; Lewandowski, 2003; Torsvik & Cocks, 2004, 2013; von Raumer & Stampfli, 2008; Stampfli *et al.*, 2013; Domeier & Torsvik, 2014; Blakey, 2016). In particular, the plate tectonic position of the north-western margin of Gondwana is somewhat controversial, especially its palaeolatitude and its geographical relation to eastern North America and the terrain assemblage of southern Europe. Nevertheless, there is agreement that a low-latitudinal deep-marine realm (Prototethys, Paleotethys, Rheic, Rhenohercynian Ocean), which included a set of terrane assemblages (Armorica, Galatia, Hanseatic), separated the north-western Gondwana margin from Laurussia in the north. Considering the distribution of coral–stromatoporoid reefs in the southern periphery of this wide subtropical realm, the Moroccan margin of Gondwana drifted northward during the Devonian, probably shifting the Tafilalt area from 40° to 30° south of the equator within an expanded tropical reef zone (Copper, 2002; Golonka, 2002, 2020; Kiessling, 2002; Eichholt & Becker, 2016).

Oceanographic models infer an eastward-directed (warm) surface current along the northern margin of Gondwana as part of a large anticlockwise circulation cell between Gondwana and Laurussia (Heckel & Witzke, 1979; Oczlon, 1990; Hüneke, 2006; Abram & Holz, 2020). Eastward-directed currents of (cold) deep water masses probably affected intermediate and deeper parts of the Gondwanan continental slope (Crasquin & Horne, 2018). The gradual narrowing of the oceanic gateways between the continental plates and the intermediate terranes triggered the intensification of both shallow-marine and deep-marine current systems during the Devonian (Hüneke, 2006). Regional circulation patterns in the Tafilalt area have been reconstructed from the orientation of orthoconic cephalopods (Wendt, 1995) and

neodymium isotopic data (Dopieralska, 2009), indicating an eastward flow of the surface water mass during the Eifelian–Frasnian.

INVESTIGATED OUTCROPS, MATERIAL AND METHODS

The current study is based on extensive fieldwork conducted in the early 2010s in a project that focused on the high-resolution stratigraphy of the Devonian platform and basin successions in the Eastern Anti-Atlas and the Moroccan Meseta. Subsequent fieldwork during annual field campaigns from 2016 to 2019 concentrated on the Eifelian to Frasnian succession of cephalopod limestones and associated lithologies on the Tafilalt Platform (Fig. 1C). Microfacies and bed-scale sedimentary features were documented in detailed sedimentary graphic logs, resulting from bed-by-bed examination and tight thin-section sampling. Four representative and well-dated key sections from Bou Tchrafine (Fig. 3), Jebel Ihrs (Fig. 4A), Jebel Amelane (Fig. 4B) and Hamar Laghdad (= Hmar Lakhdad) (Fig. 5) are exemplified in detail in this paper to unravel the facies successions and their vertical and lateral changes. From the same areas in the central, south-western and north-eastern parts of the Tafilalt Platform, stratigraphic correlation schemes show the large-scale stratigraphic architecture (Fig. 1C). These correlation schemes are based on 45 sections logged along the kilometre-long scarp slopes to explore overall thickness variations, lateral continuity of marker beds and shell concentrations, the range and regional distribution of biostratigraphic gaps, and principal stacking patterns of the stratigraphic units.

The stratigraphic framework is mainly based on the comprehensive database that was accumulated for the Tafilalt Platform using conodonts and ammonoids (see Bultynck, 1986; Walliser *et al.*, 1995; Becker & House, 1994, 2000; Belka *et al.*, 1999; Aboussalam, 2003; Aboussalam & Becker, 2007, 2011; Gouwy *et al.*, 2007; Narkiewicz & Bultynck, 2010; and publications in Becker *et al.*, 2013; Hartenfels *et al.*, 2018). Numerous supplemental conodont samples were evaluated from crucial intervals for biostratigraphic control. In addition, lithostratigraphic correlation was achieved by lateral tracing of marker beds and bed boundaries.

The database includes 890 thin sections, most of them prepared at a size of 7 × 10 cm in order to document sedimentary structures and microfacies variation at the bed scale. Samples for thin sections were obtained from all different lithologies and from all parts of the measured sections. Individual key beds were documented with up to ten thin sections to investigate subtle facies variations across the beds and along their lateral continuation, in particular transitions across bed boundaries into the underlying and overlying lithologies. All thin-section photomicrographs and scans shown in the figures are oriented vertically unless stated otherwise. For thin section analysis, the textural classification of Dunham (1962) and Embry & Klovan (1972) was used and considers the recommendations by Flügel (2010) and Lokier & Al Junaibi (2016). The analysis of dense shell concentrations, termed coquinas, was based on the criteria of Kidwell (1991a). The relative percentage frequency of different components was determined by means of the visual-comparison charts of Baccelle & Bosellini (1965) and Matthew *et al.* (1991). The extent of biogenic reworking was quantified using the bioturbation index (BI) of Taylor & Goldring (1993).

The mineralogical composition of ferromanganese nodules and hardgrounds was determined using X-ray diffraction (Bruker D8 Advance; Bruker Corporation, Billerica, MA, USA). For quantification of total carbon (TC), finely-ground samples were analysed with a CNS elemental analyser (EuroEA 3000; Eurovector, Pavia, Italy). In a second step, the amount of total inorganic carbon (TIC) was determined by measuring the released CO_2 after dissolving the carbonate content with hot 50% H_3PO_4 (EuroEA 3000). The subtraction of TIC from TC-content revealed the amount of total organic carbon (TOC). Calibration was performed using Eltra standards (pure $CaCO_3$). The analytical precision is ±1.66% for TC and ±2.0% for TIC. For pyrite morphological analysis, polished slabs (17 samples) were studied under Zeiss-Evo MA10 scanning electron microscope (SEM; Zeiss, Oberkochen, Germany) equipped with secondary electron (SE) probes, back-scatter detector (BSD) and an X-ray spectrometer (EDX). Then, the size of the pyrite framboids and the framboid microcrystals in the SEM pictures (1067 images) were measured using the software ImageJ Fiji (version 2.9.0).

RESULTS: DEPOSITIONAL AND EROSIONAL FEATURES ACROSS THE TAFILALT PLATFORM

Lithologies and microfacies

Five lithologies, each showing a characteristic facies association (FA1 to FA5, Table 1), were

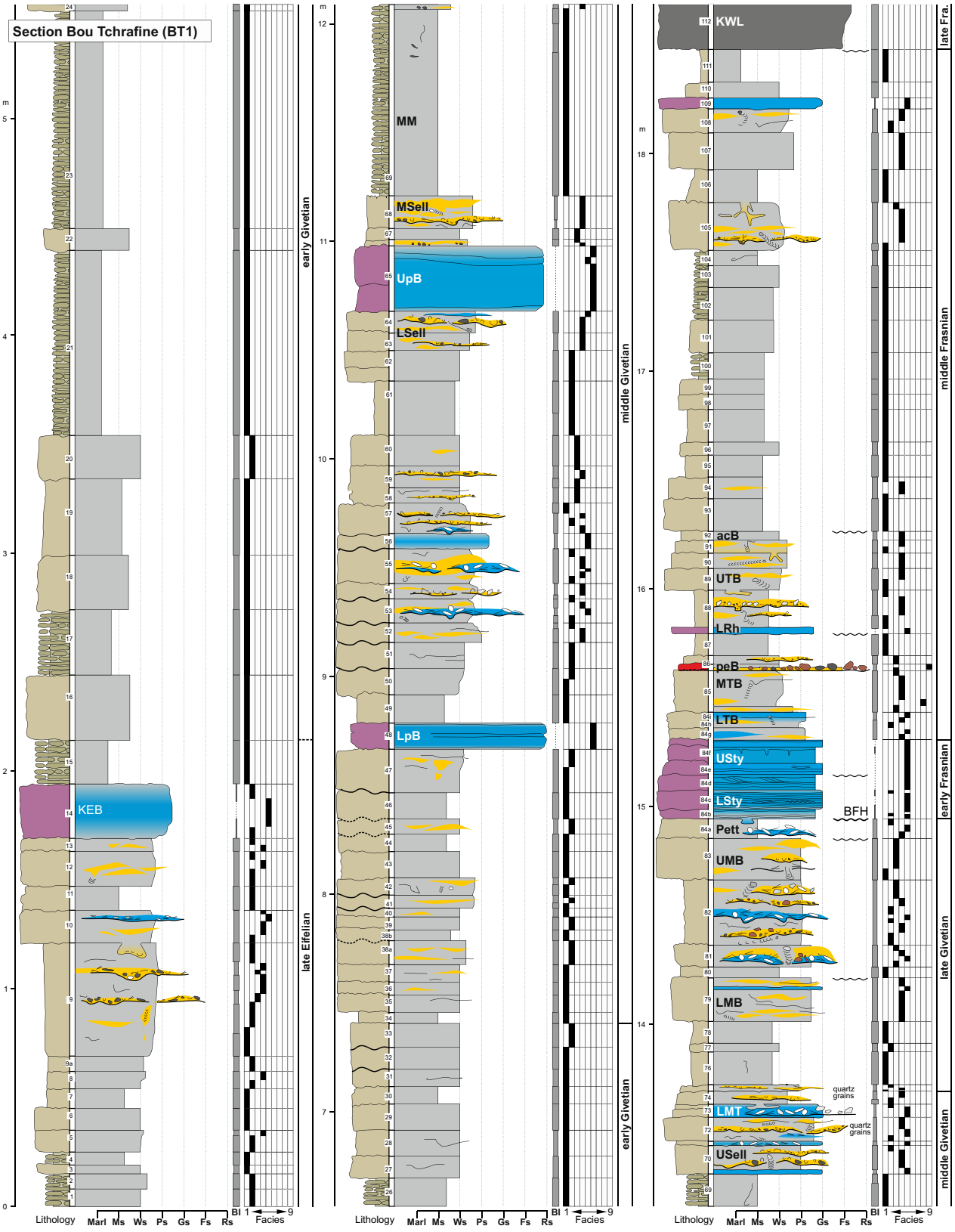

Fig. 3. Sedimentological log key section BT1 (location: 31°22'34.71"N, 4°9'59.35"W) at Bou Tchrafine illustrating lithologies, depositional texture, facies types, sedimentary structures, hiatuses and biostratigraphy of the succession on the central Tafilalt Platform. BFH, Basal Frasnian Hiatus

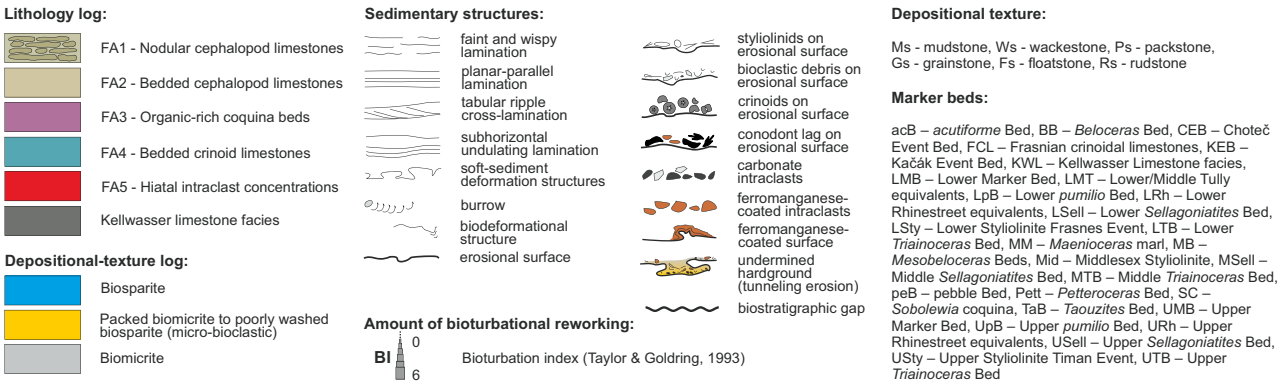

distinguished in the studied sections (Figs 3 to 5): nodular cephalopod limestones (FA1); bedded cephalopod limestones (FA2) (Figs 3 and 6A); organic-rich styliolinid and brachiopod coquinas (FA3) (Figs 6B, 7A, 7B and 8A); medium to thick-bedded crinoid limestones (FA4) (Figs 2, 6C and 6F); and individual beds rich in intraclasts (FA5) (Fig. 7A, D and F). Together, these main lithologies comprise nine microfacies (F1 to F9, Table 2, Figs 3 to 5). The facies of the Eifelian–Givetian mud mounds occurring on the eastern platform are outside the scope of this study.

Nodular cephalopod limestones (FA1)

The nodular limestones and marly nodular limestones vary in thickness from decimetres to several metres (Figs 3 and 6A). They mainly consist of thin-shelled bioclast wackestone to planktonic and nektonic biota floatstone (F1); rarely some bioclast wackestone with faint lamination (F2) (Table 2). Cephalopods (goniatites, orthocones and oncoceratids) and dacryoconarids (styliolinids and nowakiids) are the most characteristic biota (Fig. 9A to D). Thin shells of brachiopods, trilobites, gastropods and entomozoid ostracods are less abundant. The fragile shells are mostly well-preserved, with shell fragments usually associated with burrow structures (Fig. 9E). Indistinct biodeformational structures prevail, leaving a burrow-mottled appearance [bioturbation index (BI) 6 to 5, Figs 3 to 5 and 9]. Trace fossil assemblage is composed of occasional *Chondrites* and *Planolites*; large *Zoophycos* are mainly found in the dark, marly limestones.

Bedded cephalopod limestones (FA2)

Bedded cephalopod limestones form bedsets with thicknesses of decimetres to several metres, especially in the Givetian and the Frasnian (Figs 3 to 5 and 6A). The spectrum of bioclasts corresponds to that of nodular limestones, with the difference that fragmented shells are more common or even prevail (Fig. 10B to F). The lamination preserved in many beds of this lithology is irregular and locally indistinct (Fig. 6E, 7C, 8C and 8D). It relates to variations in depositional texture and/or bioclastic composition (Figs 10A, 10F and 11A to F). Thin (millimetre to centimetre) micro-bioclast packstone (F4) and mottled styliolinid packstone and grainstone (F5.1) are interstratified with thicker intervals of bioclast wackestone with faint lamination (F2) and more rarely thin-shelled bioclast wackestone (F1) (Figs 3 to 5 and 11E, Table 2). The facies of ferromanganese-nodule wackestone (F3) locally forms decimetre-thick layers and complete structureless beds (Figs 6E, 7D and 11G to I). Iron-rich (ochre) nodules consist of goethite and hematite, while todorokite and buserite are the principal oxides identified in manganese-rich (black) nodules. The micro-bioclast packstones (F4) show pinch-and-swell structures and are laterally discontinuous (Figs 10E, 10F and 11E). Burrow-mottled styliolinid packstone and grainstone (F5.1) are irregularly lenticular or form distinct millimetre-thin layers (Figs 7C, 8C, 8D and 10A) that are traceable over tens or hundreds of metres. The Upper *Sellagoniatites* Bed exemplifies millimetre-thin coquinas that can be traced across the entire Tafilalt Platform (USell in Figs 3 and 4).

The facies boundaries are often gradual and display both inverse and (more common) normal grading, i.e. transition from mud to grain-support and vice versa (Fig. 10A). The consecutive inverse to normal-graded (bi-gradational) sequences

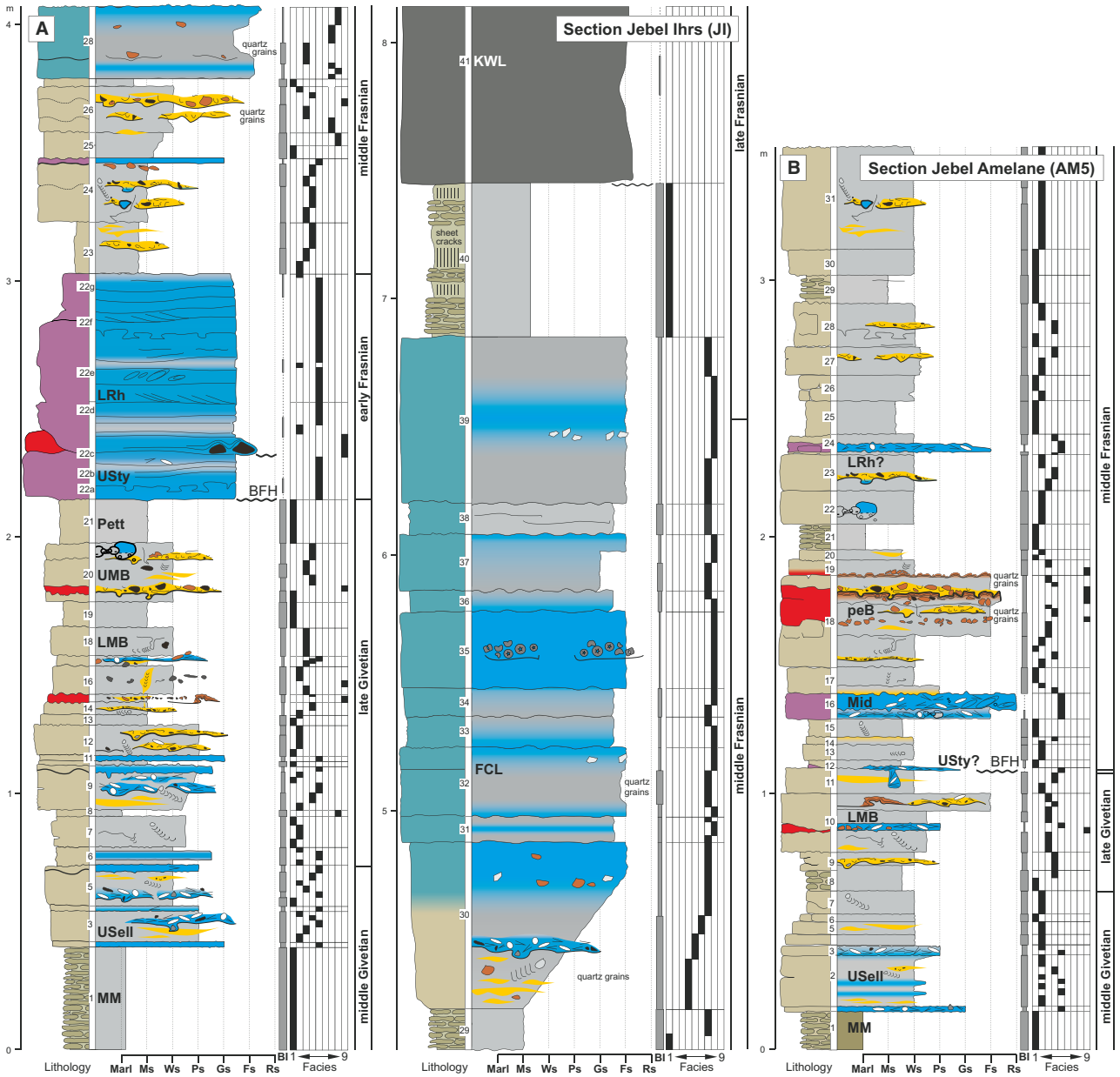

Fig. 4. Sedimentological logs key sections (**A**) JI (location: 31°15'52.54"N, 4°23'30.60"W) at Jebel Ihrs and (**B**) AM5 (location: 31°16'43.2"N 4°21'12.0"W) at Jebel Amelane illustrating lithologies, depositional texture, facies types, sedimentary structures, hiatuses and biostratigraphy of the succession on the southwestern Tafilalt platform. For legend see Fig. 3. BFH, Basal Frasnian Hiatus

display a transition from graded bioclast wackestone (F1.3) to micro-bioclast packstone (F4) and progressively to bioclast wackestone with faint lamination (F2) (Fig. 10F). Less common are bi-gradational sequences with inverse grading from F1.3 to styliolinid packstone (F5.1) and normal grading to F1.2 or F2 (Table 2, Fig. 10A). The thickness of the bi-gradational sequences ranges from a few centimetres to over a metre, with the coarse-grained central interval forming a thin part of the sequence (millimetres to centimetres) (Figs 3 to 5).

A characteristic feature of FA2 are the uneven discontinuity surfaces, some of which show truncations and hardgrounds, locally with ferromanganese encrustations. Laterally, discontinuity

Fig. 5. Sedimentological log key section HL2 (location: 31°22'35.46"N, 4°3'31.91"W) at Hamar Laghdad (= Hmar Lakhdad) illustrating lithologies, depositional texture, microfacies, sedimentary structures, hiatuses and biostratigraphy of the succession on the north-eastern Tafilalt Platform. For legend see Fig. 3. BFH, Basal Frasnian Hiatus

Table 1. Lithologies and sedimentary facies associations (FA) established for the studied Eifelian–Frasnian carbonate deposits on the Tafilalt Platform.

Lithology	Facies association	Prevailing facies	Types of sedimentary deposit	Thickness (m)
Nodular cephalopod limestones	FA1	F1, F2	Pelagites or calcareous muddy contourites	0.2–15
Bedded cephalopod limestones	FA2	F1, F2, F3, F4, F5.1	Calcareous muddy to sandy contourites	0.2–12.0
Organic-rich coquinas	FA3	F5.1, F5.2, F5.3, F6	Calcareous sandy contourites of dysoxic–anoxic water masses	0.01–2.8
Bedded crinoid limestones	FA4	F7, F8	Calcareous sandy contourites of reworked prolific benthic organisms	0.1–5.0
Hiatal intraclast concentrations	FA5	F9.1, F9.2, F3, F4	Gravel-lag contourites	0.01–0.3

surfaces can be traced over tens of metres, but in many cases they transition into gradual facies boundaries as described above. In other cases, succeeding discontinuity surfaces laterally merge into a single one (Fig. 8C). These discontinuity surfaces frequently form the sharp base of microbioclast packstone (F4) and styliolinid packstone and grainstone layers (F5) (Figs 10F and 11A to F). Above the discontinuity surfaces, the bioclastic laminae are often enriched in similar-sized conodonts and quartz grains (Fig. 10E).

Trace fossil assemblage is composed of *Chondrites*, *Planolites* and ?*Teichichnus*. Below hardgrounds, *Planolites* burrows locally show a sharp upper limit and a more diffuse lower limit. Large networks of *Thalassinoides* are common on the tops of the beds of this facies association (Fig. 8E). The preservation of the sedimentary lamination typically varies from sharp-cut to completely disturbed due to moderate to intense bioturbation (BI 3–6, Figs 3 to 5, 8C and 11A).

Organic-rich coquina beds (FA3)

Organic-rich coquinas form distinct dark beds or bedsets with thicknesses of up to 2.8 m (Figs 3 to 5 and 6B). Individual beds locally show bedform-related morphologies, like crests and troughs of subaqueous dunes (Fig. 8A and B). More rarely, organic-rich coquinas constitute isolated or laterally-chained lenses. Bed boundaries are typically clear-cut. Previous biostratigraphic work (Fig. 2) and additional conodont data revealed that, in many cases, biostratigraphic gaps occur at the base of separate FA3 beds or bedsets (Figs 3 to 5). Less common are biostratigraphic gaps within bedsets associated with layers of intraclasts (see FA5). The organic-rich coquinas consist of styliolinid packstone and grainstone (F5) or *pumilio*-type brachiopod rudstone (F6) (Table 2). Bioturbation is absent to sparse (BI 0–1, Figs 3 to 5 and 13A). *Planolites*-like burrows were found in a few beds.

The most prominent features of styliolinid-rich coquinas (F5) are traction structures (Table 2), which occur as: (i) subhorizontal, slightly undulating lamination (Fig. 6B); (ii) planar-parallel lamination; and (iii) subordinated ripple cross-lamination (Figs 7B, 12B, 12F and 13D). Locally, small-scale low-angle cross-stratification was identified. The lamination is frequently characterized by irregularly alternating packstone and grainstone laminae with recurring gradational trends (Figs 12A, 12B and 13A). The conical styliolinid shells are well-preserved and commonly show telescoping (Fig. 13B and F). Fragmented shells are less common (Fig. 13D to F). Whole and fragmented shells of brachiopods, trilobites, crinoids and large cephalopods (goniatites and orthoconic cephalopods) are locally present (up to 30%) (Figs 12A, 12F and 13H). Most beds of parallel-laminated styliolinid packstone (F5.2) display conical dacryoconarid shells oriented parallel to the lamination; shell size and specific orientation vary from laminae to laminae (Fig. 13B, C and G). Some of the thicker laminae show subtle inverse and normal grading by varying shell size or mud content (Fig. 13A). In beds with cross-laminated styliolinid grainstone (F5.3), the shells are oriented parallel to cross-lamination; aligned within the planes of current-ripple slip faces (Figs 12F and 13H).

Pumilio-type brachiopod rudstone beds (F6) display inverse and normal grading at the base and the top (Fig. 12C to E), respectively.

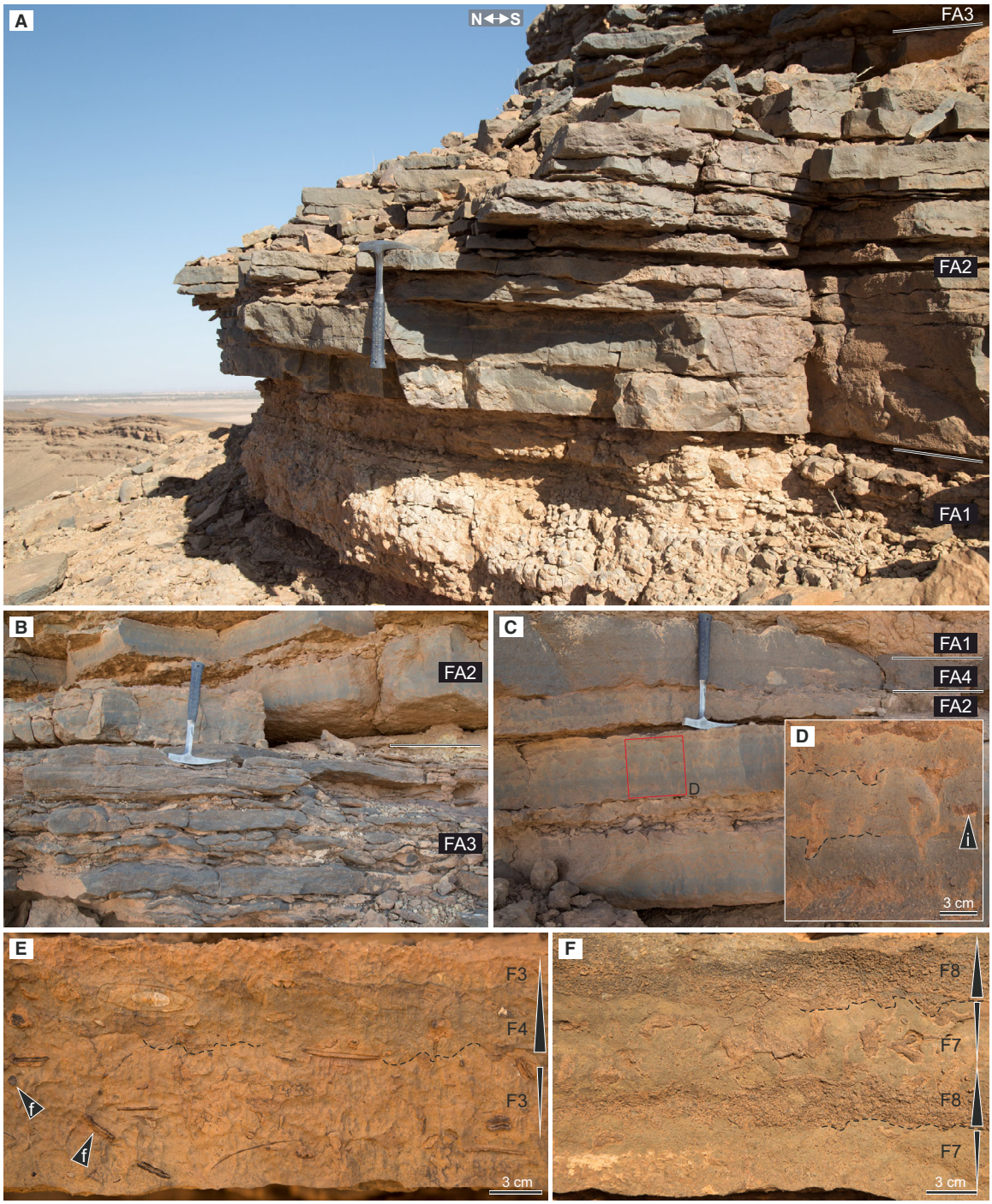

Fig. 6. Outcrop lithologies Givetian–Frasnian limestones at Jebel Ihrs. (**A**) Nodular cephalopod limestones (FA1), bedded cephalopod limestones (FA2) and organic-rich coquinas (FA3). Section JI, beds 1 to 22 (Fig. 4A). (**B**) Organic-rich coquinas (FA3) consisting of styliolinid packstone and grainstone (F5) overlain by bedded cephalopod limestones (FA2). Section JI, beds 22 to 26 (Fig. 4A). (**C**) Bedded cephalopod limestones (FA2) and bedded crinoid limestones (FA4). Section JI, beds 23 to 29 (Fig. 4A). (**D**) Detail of bed 26 showing bioturbationally-mottled erosional surfaces (dashed) draped by layers of micro-bioclast packstone rich in intraclasts (i) (F4). (**E**) Bedded cephalopod limestone (FA2) rich in ferromanganese-coated bioclasts and intraclasts (f) showing erosional discontinuity surfaces draped by layers of micro-bioclast packstone. Section IH5 (see Fig. 19), late Givetian, *Petteroceras* Bed (Pett). (**F**) Bedded crinoid limestone (FA4) showing inverse and normal grading between interstratified layers of crinoid floatstone and rudstone (F7/F8), together with laterally-discontinuous erosional surfaces (dashed). Section IH5 (see Fig. 19), middle Frasnian. Hammer is 32 cm long.

Articulate brachiopod shells occur tightly packed and at places parallel to cross-lamination. Connected by a gradual transition, the lowermost and uppermost parts of the beds tend to show disarticulated and smaller shells with more abundant styliolinids of the same size.

Total organic carbon (TOC) content of the analysed samples varies between 0.9% and 3.0% (Table 3). Samples with high TOC values (for example, UpB, LSty, USty, LRh) typically show abundant pyrite framboids with mean diameters <5 μm and microcrystals <0.4 μm (Fig. 14). The organic matter forms aggregations in the interstitials between styliolinid shells (Fig. 13D to F) and is finely distributed within mud-rich layers (Fig. 13A).

Bedded crinoid limestones (FA4)

Bedded crinoid limestones, in the middle Frasnian interval at Jebel Ihrs (Figs 2, 6C and 6F), have thicknesses ranging from several decimetres to a few metres (Fig. 4). This lithology consists of gradually interstratified layers and beds of crinoid floatstone (F7) and laminated crinoid rudstone (F8) (Fig. 6F, Table 2). Facies sequences exhibit normal grading and less common inverse grading, which is defined by variation in grain size, particle composition and the content of interstitial mud (Fig. 15A and B). Large amounts of crinoid ossicles together with a few other benthic elements (solitary rugose corals, auloporids, trilobites and brachiopods) and diverse nektonic and planktonic fauna (cephalopods and styliolinids) characterize this facies. Crinoid ossicles are mainly disarticulated; some layers include chains of connected ossicles and (reworked) crinoid holdfasts. Bioclasts and intraclasts are occasionally coated by calcareous and ferromanganese microstromatolitic crusts (Fig. 15). Bioturbation is sparse to common (BI 1–4, Figs 4, 6D and 6F).

Hiatal intraclast concentrations (FA5)

In the late Givetian and Frasnian, intraclast layers up to a few decimetres thick or intraclast-bearing surfaces occur (Fig. 7A, D and F). They are associated with biostratigraphic gaps (see Fig. 2) or hardgrounds and minor erosional surfaces (Figs 4 and 5). Above such hiatus surfaces, often specific particle concentrations are present, consisting almost exclusively of phosphatic conodonts or ferromanganese-coated particles, i.e. grains with a high specific weight. Large goniatite shells are locally enriched in larger numbers (Fig. 4A, UMB). Carbonate–intraclast floatstones (F9.1) and ferromanganese–intraclast floatstones (F9.2) document the variability of this FA (Table 1). The former is mainly associated with biostratigraphic gaps in FA3 (Fig. 7A), as evidenced by conodont data (Fig. 2), as the latter only occurs on erosional surfaces and hardground in FA2 (Fig. 7D to F).

Thicker layers display complex internal microstratigraphic relationships with small-scale truncating unconformities (irregular) and scour marks (U-shaped) together with composite sedimentary structures (Fig. 16A to D). Facies palimpsests feature ferromanganese-nodule floatstone (F3) and micro-bioclast packstone (F4). Quartz grains (extraclasts) are locally abundant (Fig. 16D to F). Burrows below such layers may accommodate tubular infills of otherwise unpreserved (because they are bypassed or eroded) sediments. In some cases, sediments of this facies seal cavities below hardgrounds that were undermined by tunnelling erosion.

Stratigraphic architecture

The large-scale variation in sediment thicknesses and facies of the Eifelian–Frasnian cephalopod limestones and interbedded lithologies was obtained by correlation and lateral tracking of marker beds (Fig. 17). Stratigraphic correlation schemes from the central Tafilalt Platform at Bou Tchrafine (Fig. 18), the south-western part at Jebel Amelane and Jebel Ihrs (Fig. 19) and the north-eastern part at Hamar Laghdad (Fig. 20) exemplify the stratigraphic architecture and are described in the following sections.

Central Tafilalt Platform (Bou Tchrafine)

The Eifelian to Frasnian succession (Fig. 2) of mainly nodular and bedded cephalopod limestones (Figs 3, 17A and 18) represents a sediment-starved stratigraphic succession covering about 21 Myr, including condensed beds in the late Givetian to middle Frasnian. Bedsets of both nodular and well-bedded limestones (Table 1) form tabular stratigraphic units with minor thickness variations (Fig. 18). The Eifelian interval is about 14 m thick. The pre-*pumilio* Givetian has a thickness of *ca* 7 m, the post-*pumilio* Givetian *ca* 4 m, and the (pre-Kellwasser) Frasnian succession *ca* 3.5 m. These thicknesses indicate overall very low net-accumulation rates varying between 0.6 and 2.8 mm kyr^{-1}.

A widespread biostratigraphic gap occurs at the base of the early Frasnian (Basal Frasnian Hiatus, BFH, Fig. 17A) and spans the lower

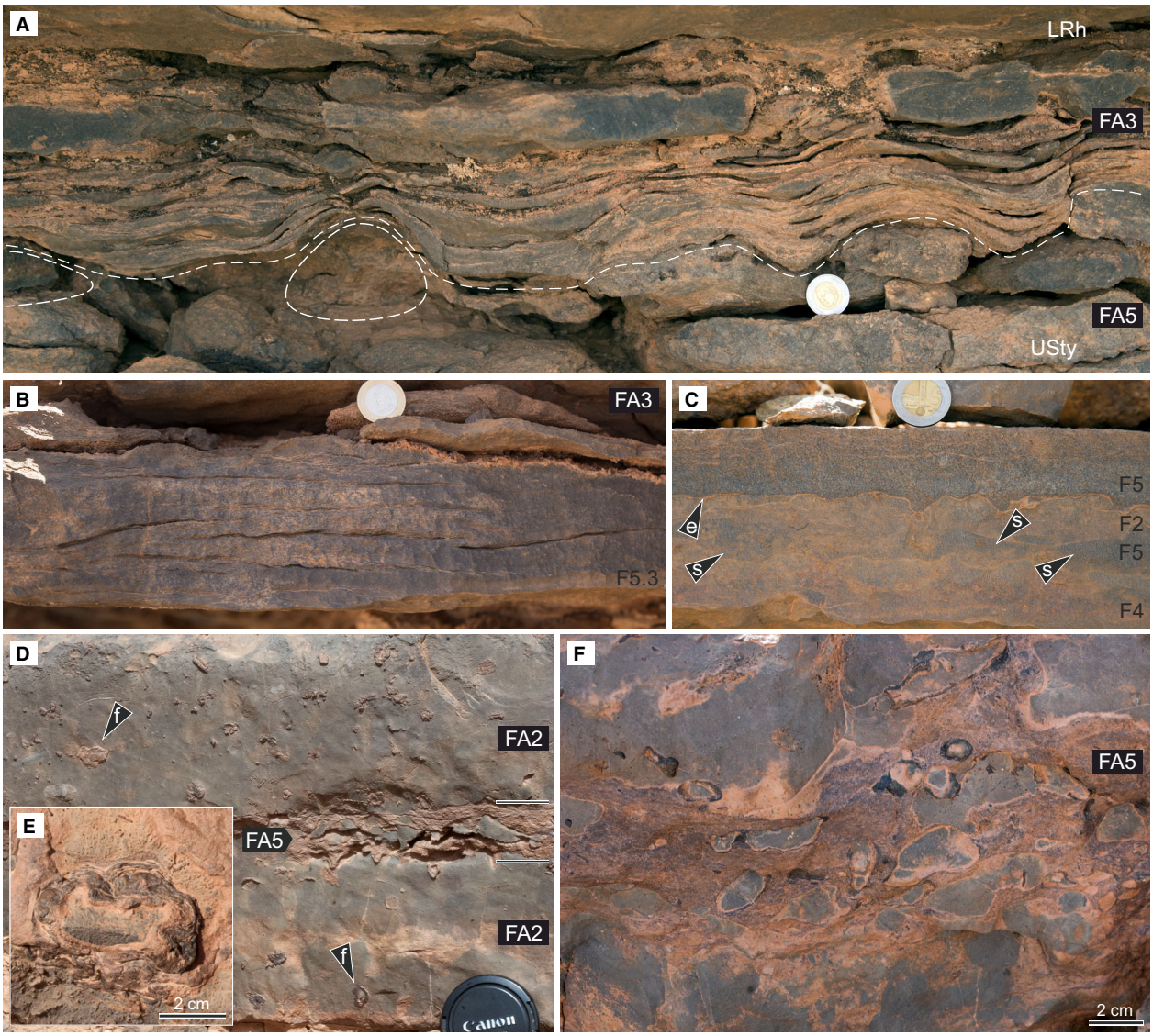

Fig. 7. Outcrop lithologies Givetian–Frasnian limestones at Jebel Ihrs and Jebel Amelane. (**A**) Bed of intraclasts (FA5) between organic-rich coquinas (FA3), consisting of styliolinid packstone and grainstone (F5) and showing draped lamination. The dashed line indicates the biostratigraphic gap between Upper Styliolinite (USty) and the Lower Rhinestreet Styliolinite (LRh) (compare Figs 2, 17 and 19). Section IH6, early–mid Frasnian. (**B**) Organic-rich coquina (FA3) of styliolinid grainstone (F5.3) showing cross-lamination. Section IH5, early Frasnian, USty. (**C**) Bedded cephalopod limestone (FA2) with styliolinid coquinas (F5) that form irregular lenses (s) and a continuous layer at the top. Note erosional discontinuity surface (e). Section JI, bed 9, late Givetian (see Fig. 4A). (**D**) Layer of intraclasts (FA5) within bedded cephalopod limestones (FA2), rich in ferromanganese-coated bioclasts and intraclasts (f). Section AM5, bed 10, late Givetian, Lower Marker Bed (Fig. 4B). (**E**) Detail of (D) showing ferromanganese-coated intraclast. (**F**) Intraclast bed (FA5). Section AM5, bed 18, middle Frasnian (peB) (Fig. 4B). Coin is 25 mm, lens cover 75 mm in diameter.

parts of conodont zone MN1 (Fig. 2). Five additional hiatuses occur in the late Givetian to middle Frasnian succession (Figs 3 and 18). Numerous minor breaks in sedimentation are indicated by erosional surfaces and hardgrounds, which are locally covered by intraclast layers (F9) and seafloor-abraded cephalopod shells.

Organic-rich coquinas (FA3) were repeatedly identified within the Givetian–Frasnian record

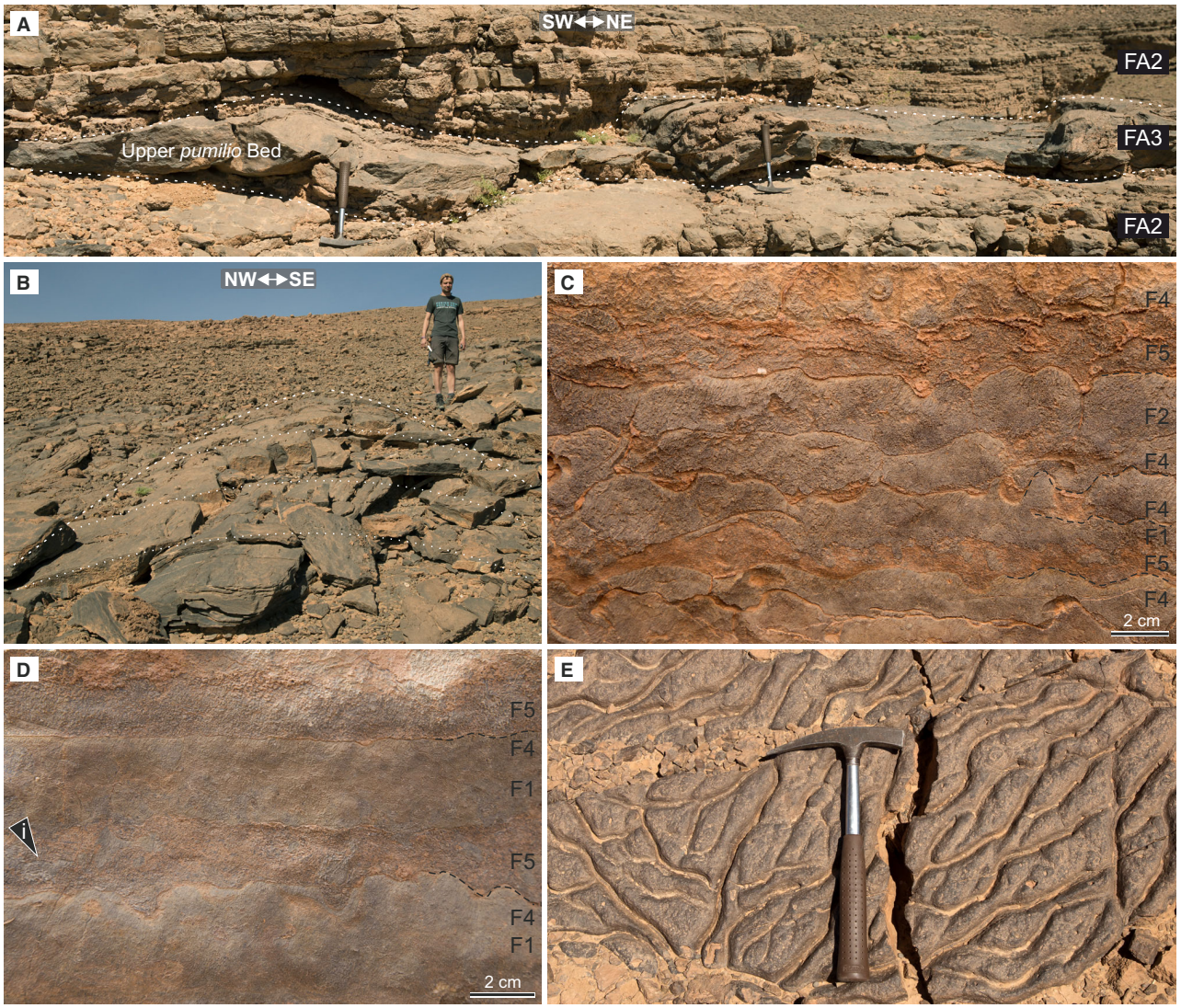

Fig. 8. Outcrop lithologies Givetian–Frasnian limestones at Hamar Laghdad. (**A**) Bedded cephalopod limestones (FA2) and organic-rich coquina (FA3) of brachiopod rudstone (F6) showing asymmetrical sinusoidal bedform morphology. 350 m west of the Hollard Mound, Middle Givetian, Upper *pumilio* Bed. (**B**) Organic-rich coquina (FA3) of brachiopod rudstone (F6). Note oblate hemispheroidal morphology (sand dune or tail) elongated towards the observer. Section HL10, Upper *pumilio* Bed. (**C**) Bedded cephalopod limestone (FA2) showing succession of irregular erosional discontinuity surfaces and hardgrounds draped by thin layers of micro-bioclast packstone (F4) and styliolinid packstone (F5). Section HL2, bed 19 (Fig. 5), late Givetian. (**D**) Bedded cephalopod limestone (FA2) with layers of styliolinid packstone (F5), micro-bioclast packstone (F4) and bioclast wackestone (F1), which are bounded by sharp erosional contacts and hardgrounds. Note abundant intraclasts (i). Section HL2, bed 19 (Fig. 5), late Givetian. (**E**) Bedding plane of bedded cephalopod limestones (FA2) showing network of *Thalassinoides*-like traces (compare relief of discontinuity surfaces in vertical sections of C and D). Section HL4.2, middle Frasnian. Hammer is 31 cm long.

(Figs 3 and 18). A characteristic bedset with parallel and cross-laminated styliolinid coquinas (F5, Table 2) is present in the early Frasnian. These beds cover the basal–Frasnian hiatus and enclose another biostratigraphic gap (Fig. 3, bed boundary 84e/f) comprising the main parts of MN zones 2 and 3 (between LSty and USty in Fig. 2). Across a distance of 600 m towards the south (BT8–BT10 in Fig. 18), the lowermost beds of these coquinas vary in thickness (from 8 to 40 cm). Additional thin styliolinid coquinas occur in the middle Givetian (Upper

Table 2. Facies types (F1 to F9) and main sediment characteristics of the studied Eifelian–Frasnian successions on the Tafilalt Platform. Third column: Names of facies types are italics, short names in bold.

Facies		Stratification	Name, short name and microfacies	Sedimentary structures	Interpretation of depositional processes	
F1		Well-bedded, flaser-bedded, and nodular-bedded bed sets	***Thin-shelled bioclast wackestone*** *to floatstone of planktonic and nektonic biota*: dacryoconarids (styliolinids, nowakiids) are ubiquitous, cephalopods common; less common biogens: thin-shelled brachiopods, trilobites, gastropods, ostracods and crinoids; bimodal grain-size distribution (bioclasts and micrite) *End members illustrate high variability:*	Bioturbationally mottled or homogenized sediment; indistinct burrows delimited by subtle packing-density and colour differences	***Pelagic carbonates***: settling of pelagic carbonate mud and larger skeletal elements (plankton and nekton); some benthic organisms; intensive bioturbation	**PELAGITE/CONTOURITE**
F1.1	**WACKESTONE**	Amalgamated beds common	***Styliolinid wackestone*****:** monotonous, low-diverse nektonic and planktonic fauna; mainly styliolinids and thin-shelled molluscs	Local discrete burrows difficult to be differentiated from the host sediment	Focussing of carbonate mud	
F1.2		Well-bedded, wavy and parallel bounding surfaces	***Grain-rich bioclast floatstone*** *to wackestone*: highly diverse nektonic and planktonic fauna plus benthic elements, clusters of large cephalopods, varying packing density	Moderate bioturbation with some distinct burrows; overall slightly mottled appearance; fragmented dacryoconarids are mostly related to biogenic traces	Increased primary production in surface water, favouring a diverse nektonic and planktonic fauna; or redistribution of pelagic carbonate mud by weak bottom currents **(C1 and C5 divisions of bigradational contourite sequences)**	
F1.3		Textural massive, laterally continuous beds and bed sets	***Graded*** *styliolinid* ***bioclast wackestone*** *to packstone*: loosely- to densely-packed styliolinids, nowakiids and other thin-shelled bioclasts in clusters, pockets, lenses and laminae	Indistinct normal and inverse grading due to variable packing-density (coarse-tail grading); mottling is moderate to prominent	Variation in primary productivity; or variable release of particles from suspension within a weak but fluctuating bottom current **(C1 and C5 divisions of bigradational contourite sequences)**	

Table 2. (continued)

Facies		Stratification	Name, short name and microfacies	Sedimentary structures	Interpretation of depositional processes	
F2	**WACKESTONE**	Well-bedded, flaser-bedded, and nodular-bedded bed sets	***Bioclast wackestone with faint lamination*: predominating nektonic and planktonic fauna (e.g. styliolinids, cephalopods); laminae-specific particle amount, grade of fragmentation and change in packing density; high percentage of fragmented biogens and out-sized mud clasts**	Faint irregular lamination, subtle normal and inverse coarse-tail grading, associated with omission surfaces, minor erosional surfaces and hardgrounds; moderate diffuse bioturbation plus distinct traces	***Calcareous muddy contourites*: deposition of carbonate mud and shells from suspension within a tranquil but fluctuating bottom current; temporal sedimentary omission and winnowing of carbonate mud; C1 and C5 divisions of bigradational contourite sequences**	**CONTOURITE**
F3		Individual beds and lamina sets, lateral variability in bed thickness	***Ferromanganese-nodule wackestone** and floatstone*: abundant ferromanganese-coated and -impregnated intraclasts, bioclasts, and oncoids (rare ooids), together with planktonic and nektonic fauna (e.g. cephalopods and styliolinids); high percentage of shell debris and out-sized mud clasts	Associated with erosional surfaces, hardgrounds and hiatuses; insignificant bioturbation; infill of burrows, borings in hardgrounds and of cavities below hardgrounds	***Calcareous muddy contourites*: ferromanganese encrustation during halts of sedimentation; relocation and mixing of material from different sources within a tranquil bottom current; C1, C2, C4 and C5 divisions of condensed bigradational contourite sequences**	
F4	**PACKSTONE – GRAINSTONE**	Individual beds and lamina sets within beds of other facies types	***Micro-bioclast packstone*: heavily fragmented thin-shelled skeletal grains; bioclastic debris of fine sand to silt size; locally rich in intraclasts, quartz grains and conodonts; unimodal grain-size distribution with a broad spread**	Irregular, but distinct lamination, often corresponding to bed-internal erosional surfaces; inverse and normal grain-size grading; local fills of pockets and micro-scours; insignificant bioturbation, except distinct traces	***Calcareous silty contourites*: bottom-current-induced reworking, redistribution and fragmentation of fragile skeletal elements related to bedload mobilization caused by a moderate bottom current; intensive winnowing of carbonate mud; C2 and C4 divisions of bigradational contourite sequences**	
F5		(A) Local fill of sediment traps (e.g. burrows, scours, below larger bioclasts). (B) Individual lenses and discontinuous layers interstratified with other facies (F2, F3, F4) (C) tabular beds and bedsets displaying horizontal	***Styliolinid packstone and grainstone**, locally rudstone*: striking monomict or oligomict composition – abundant whole dacryoconarid shells (mainly styliolinids, nowakiids) forming grain-supported fabrics; locally rich in bivalves, crinoids or cephalopods	Well-preserved traction structures, or structureless or interlaminated with carbonate mud and crystal silt; frequently associated with hiatuses, hardgrounds or erosional surfaces; degree of bioturbation is highly variable, but usually low	***Calcareous sandy contourites*: bottom-current-induced winnowing of mud, bedload transport of sand-sized styliolinids (and other bioclasts), particle sorting and alignment; intermittent deposition of silt-sized fragments from suspension; C3 divisions of bigradational contourite sequences**	

Table 2. (continued)

Facies	Stratification	Name, short name and microfacies	Sedimentary structures	Interpretation of depositional processes
	lamination and cross-lamination (D) laterally-chained lenses	*End members illustrate high variability:*		and **stand-alone C3 units** bounded by hiatuses
F5.1		*Burrow-**mottled styliolinid packstone** and grainstone*: styliolinid micro-coquinas; polymodal orientation patterns of conical styliolinid shells; clusters of complete cephalopod shells and shell debris	Structureless; irregular-chaotic fabrics or complete bioturbational reworking of primary structures; local bioturbational mottling and indistinctly delimited burrows	Bottom-current-induced winnowing of mud and deposition from migrating bedload with subsequent homogenisation caused by intensive bioturbation; or chaotic fabric due to superimposed multiple depositional events
		CONTOURITE		
		PACKSTONE – GRAINSTONE		
F5.2		***Parallel-laminated styliolinid packstone** and grainstone*: alternating packstone and grainstone laminae with frequent gradational trends (plus drapes of mud and crystal silt); often lamination-parallel orientation of conical styliolinid shells (mainly bimodal patterns)	Subhorizontal-undulating lamination displaying normally-graded laminae and small scours; planar-parallel lamination; coarsening- and fining-upward micro-sequences; local discrete vertical burrows	Deposition from migrating bedload sheets; flow deceleration cause dumping of suspended sediment, effectively suppressing traction and inducing bed accretion; depositional shear sorting; fast accumulation inhibits bioturbation
F5.3		***Cross-laminated styliolinid grainstone** to packstone, locally rudstone*: alignment of styliolinid and cephalopod shells within planes of ripple slip faces (bimodal orientation patterns of styliolinids: perpendicular and parallel to the ripple crest)	Current-ripple cross-lamination; bioturbation is rare to absent	Deposition from migrating current ripples; current-induced orientation of dacryoconarid shells related to flow conditions and bedform topography; fast accumulation inhibits bioturbation

Table 2. (continued)

Facies	Stratification	Name, short name and microfacies	Sedimentary structures	Interpretation of depositional processes
CONTOURITE				
F6	Parallel-sided individual beds	*Thin-shelled* ***pumilio-type brachiopod rudstone***, *with interlayers of packstone and grainstone:* mainly micromorphic brachiopods, interlayers with abundant styliolinids; typical sequences: packstone of disarticulated brachiopods and styliolinids (base), rudstone of bivalved brachiopods (centre), packstone of disarticulated brachiopods (top)	Faint parallel lamination with gradational boundaries; invers-to-normal grading; rare cross lamination; bioturbation almost absent	***Calcareous sandy contourites***: bottom-current induced transport and sorting of micromorphous brachiopods (plus styliolinids and mud) of undetermined origin; deposition from bedload and suspension; **(C2), C3 and (C4) divisions of bigradational contourite sequences**
RUDSTONE – FLOATSTONE – PACKSTONE				
F7	(A) Parallel-sided individual beds and bed sets (B) Laminae and layers within beds of other facies (F7, F8)	***Crinoid floatstone*** *and packstone:* abundant disarticulated (less common connected) crinoid ossicles, together with additional skeletal elements of benthic organisms (solitary corals, trilobites, brachiopods) and bioclasts from nektonic and planktonic biota (cephalopods, styliolinids)	Gradually interbedded with F8, showing invers and normal grading; locally bounded by erosional surfaces; moderate to strong bioturbation; discrete traces rarely identified	***In-situ benthic carbonate production and calcareous muddy contourites***: prolific benthic communities (crinoid meadows) benefiting from increased food supply by weak bottom currents; subsequent reworking and redistribution of disarticulated skeletal elements; enhanced deposition of carbonate mud from suspension; **C1, (C2), (C4) and C5 contourite divisions**
F8		*Irregularly-****laminated crinoid rudstone***, *packstone and grainstone:* large disarticulated crinoid ossicles predominate, plus bioclasts of solitary corals, brachiopods, cephalopods, dacryoconarids, trilobites and less common bryozoans; (ferromanganese-impregnated) intraclasts are locally abundant	Gradually interbedded with F7, showing inverse and normal grading; locally distinct (bed-internal) erosional surfaces; bioturbation is rare	***Calcareous sandy contourites***: reworking and redistribution of benthic skeletal elements by energetic bottom currents; deposition from bed load and suspension; winnowing of carbonate mud and particle sorting according to the fluctuating flow strength; **C3 divisions of bigradational contourite sequences**

Table 2. (continued)

Facies	Stratification	Name, short name and microfacies	Sedimentary structures	Interpretation of depositional processes
F9	Erosional, intraclast-bearing surfaces or layers up to a few decimetres-thick, associated with biostratigraphic gaps and minor hiatuses	***Intraclast floatstone***, *rudstone, wackestone and packstone, locally rich in extraclasts* (*mainly quartz grains*): mainly intraclasts of carbonate mud and micro-bioclast packstone; intraclasts of styliolinid grainstone are less frequent *End members illustrate high variability:*	Irregular and truncating boundaries; complex internal microstratigraphic relationships characterized by small-scale unconformities and scour marks; common facies and fabric palimpsests (transition to F2, F3, F4)	***Gravel-lag contourites:*** deposits of vigorous, temporal erosional bottom currents; formed by reworking of indurated sediments, prolonged sediment bypassing and long-lived winnowing; dynamic interplay between depositional, erosional and authigenic processes (cementation, precipitation)
				CONTOURITE
F9.1		***Carbonate–intraclast floatstone***, *rudstone and packstone:* intraclasts are locally-derived from the substrate; covers erosional surfaces and hardgrounds; drapes and scour fills mainly on facies F3, F4 and F5; clasts of styliolinid grainstone in beds of facies F5	Traces accommodate tubular infills of bypassed sediments; rare borings	*Carbonate gravel-lag contourites*: bottom currents activate synsedimentary seafloor cementation under favourable conditions of the Devonian calcite sea; subsequent erosion and temporal reworking of semi-lithified sediments
				RUDSTONE – FLOATSTONE – PACKSTONE
F9.2		***Ferromanganese–intraclast floatstone***, *rudstone and packstone:* coatings of ferromanganese oxyhydroxides on individual particles (intraclasts, bioclasts, quartz grains), as fine encrusted horizons (hardgrounds, laminae), or as nodules (oncoids, ooids); locally ferromanganese impregnation of background sediment	Variably burrowed and local borings	*Ferro-manganese gravel-lag contourites*: very slow precipitation of ferromanganese oxyhydroxides from seawater in association with temporal erosion and sediment bypassing; extremely low sediment accumulation rates induced by the presence of energetic bottom currents

Sellagoniatites Bed, USell) and in the middle Frasnian (Lower Rhinestreet Event, LRh). Organic-rich coquinas (FA3) of brachiopod rudstone (F6, Table 2) occur as two separate beds in the middle Givetian (Lower and Upper *pumilio* beds). The Upper *pumilio* Bed shows an increase in thickness from north (<3 cm) to south (>30 cm) along the western Bou Tchrafine scarp (BT2–BT10 in Fig. 18). The marker beds reflect a uniform tabular architecture, also with regard to the interbedded cephalopod limestones (FA1 and FA2).

South-western Tafilalt Platform (Jebel Amelane, Jebel Ihrs)

The tabular Eifelian to middle Givetian stratigraphic units can be traced from the central Tafilalt Platform to the south-western margin and show minor thickness and facies variations (Fig. 18). The same holds for the late Givetian to middle Frasnian limestones; however, they are missing in the western and southern scarps of Jebel Ihrs (Fig. 19A, section IH1, IH2, IH2.1), and further south at Mech Irdane, Rich Gaouz and El Kachla (Fig. 1C). As a consequence, the late Frasnian Kellwasser Limestone rests disconformably on middle Givetian cephalopod limestones in this area. Hence, the various short-ranging stratigraphic gaps identified on the central Tafilalt Platform converge towards the south-west into a long-ranging hiatus of about 7 Myr that cuts down into the late and middle Givetian (Fig. 2). This area of truncated late Givetian limestones was identified as a channel trending south-east/north-west (Fig. 1C). Middle Frasnian crinoid limestones (FA4) are locally present at Jebel Ihrs (Fig. 19A, section IH1) and at Mech Irdane (Fig. 1C).

Between the north-eastern channel margin and the platform interior, the late Givetian and Frasnian succession shows a distinct lateral variation in facies and sediment thickness, as documented along the upper scarps of Jebel Amelane and Jebel Ihrs (Figs 17B, 17C and 19). Over a distance of 6 km, the thickness of the late Givetian varies between 0 m and 2 m, whereas the (pre-Kellwasser) Frasnian varies between 1.2 m and 5.5 m in thickness. The thickest intervals occur in a 2 km wide zone bordering the channel margin at Jebel Ihrs (Fig. 19). Within that zone, Frasnian organic-rich styliolinid coquinas (FA3) and crinoid limestones (FA4) form thick bedsets (Table 1, Fig. 4) that are laterally discontinuous and pinch out towards the south-west (i.e. the channel) and the north-east (i.e. the platform interior) (Fig. 19A). The Frasnian organic-rich styliolinid coquinas (FA3) at Jebel Amelane occur as discrete beds, thinning over a short distance (AM5 in Fig. 19B).

The mounded bedsets of FA3, 1.5 m in thickness close to the channel, directly cover the basal Frasnian hiatus. They represent the Upper Styliolinite and the Lower Rhinestreet Styliolinite (Fig. 17B), which are separated by an intraclast-bearing hiatus (Fig. 7A). The interbedded cephalopod limestones and the Lower Styliolinite are not preserved (compare Fig. 2).

Close to the channel margin at Jebel Ihrs, crinoid limestones of FA4 constitute thick bedsets in the late middle Frasnian (Figs 17 and 19). They are stacked on top of the mounded styliolinid coquinas of FA3, and have a maximum thickness of almost 3.0 m close to the channel margin. Consequently, FA3 and FA4 deposits of packstone to rudstone make up more than 60% of the Frasnian succession in this zone, which contrasts with a maximum of 5% in other parts of the Tafilalt Platform (Fig. 18).

North-eastern Tafilalt Platform (Hamar Laghdad)

At Hamar Laghdad, distinct variations in sediment thicknesses and facies in the Givetian–Frasnian succession were documented near the Eifelian–Givetian mud mounds (Fig. 20). Similar to their occurrence in central parts of the Tafilalt Platform, the Eifelian nodular and bedded limestone bedsets (Table 1) form tabular stratigraphic units with moderate thickness variation. The thickness of the pre-*pumilio* Givetian, however, decreases from 18 m in the west to 5 m in the east in close proximity to the Hollard Mound (HL2 to HL4.2 in Fig. 20). The post-*pumilio* Givetian varies between 2 m and 5 m, and the (pre-Kellwasser) Frasnian succession between 2 m and 6 m. Many of the short-ranging hiatuses identified in the central platform occur in the Hamar Laghdad area as well (Figs 5 and 20).

The organic-rich coquinas (FA3) show a remarkable increase in thickness in close proximity to the Hollard Mound (HL10 in Fig. 20). The lower Frasnian styliolinid coquinas (F5) show a local maximum in thickness of up to 4.5 m at a distance of about 200 m south-west from the mound base, before it wedges out in front of the mound slope. The middle Givetian brachiopod coquinas (F6) preserve bedform-related depositional morphologies (dune or sediment tail) near the mud mound (Fig. 8B) with

remarkable bed thicknesses of up to 0.4 m (Lower *pumilio* bed) and 1.2 m (Upper *pumilio* bed).

INTERPRETATION

Bed-scale contourite features

The facies associations recognized on the Tafilalt Platform are interpreted using hydrodynamic criteria such as variations in: (i) the ratio of carbonate mud to skeletal grains; (ii) grain size; and (iii) shell fragmentation; together with (iv) traction structures; and (v) patterns of shell orientation (e.g. Southard & Bouguchwal, 1990; Kidwell, 1991a; Martín-Chivelet *et al.*, 2008; Flügel, 2010; Rebesco *et al.*, 2014; Eberli & Betzler, 2019). Additional criteria used were grain composition, extent of bioturbation, trace-fossil assemblages, and features of seafloor related cementation and mineral precipitation (e.g. Wilkin *et al.*, 1996; Uchman & Wetzel, 2011; Föllmi, 2016).

Pelagic deposits (FA1)

FA1 sediments are interpreted as pelagic deposits because they lack hydrodynamic sedimentary structures and show a predominance of shells of calcareous plankton and nekton embedded in carbonate mud (Tables 1 and 2). The fragile shell preservation and vertically embedded cephalopod shells underline an overall tranquil depositional environment. The absence of light-dependent (phototrophic and photosymbiotic) benthos signals accumulation below the euphotic zone. The well-preserved cephalopod shells indicate deposition in a water depth less than 300 m, which has been calculated based on the implosion depth for such shells (Hewitt, 1996). This interpretation aligns with previous studies on cephalopod limestones of the Tafilalt Platform (Wendt *et al.*, 1984; Wendt & Aigner, 1985; Lubeseder *et al.*, 2010) and other areas (Tucker, 1974, 1990). The low–diverse trace fossil assemblage, tentatively assigned to the *Zoophycos* ichnofacies (see Hubbard *et al.*, 2012; Svarda, 2012), is compatible with a pelagic origin.

Where FA1 is part of bi-gradational sequences together with bedded cephalopod limestones, however, the facies association may also signify fine-grained contourites resulting from pirated pelagic rain and remobilized pelagic mud in response to weak bottom currents (see below). The subtle vertical variation in skeletal grains and carbonate mud, such as in F1.3 (Table 2), may agree with a variation in primary productivity in the surface waters and a variable release of particles from suspension within a tranquil but fluctuating bottom current. The syn-depositional intensive bioturbation makes it impossible to clearly distinguish pelagites from muddy carbonate contourites removed from a bottom nepheloid layer, also because both facies represent conceptual extremes in a continuum of deep-sea sedimentary processes (see Rebesco *et al.*, 2014).

The origin of the lime mud constituting Palaeozoic deep-sea carbonates is unclear (Servais *et al.*, 2016). Munnecke & Servais (2008) identified different types of calcareous microfossils and nannofossils in Silurian carbonates of Gotland and concluded that calcareous plankton most probably existed already during the Palaeozoic. Tucker (1990) has suggested that the lime mud of Palaeozoic deep-sea carbonates could well be derived from the breakdown of macroskeletons, which requires a fragmentation process. In general, plankton exhibit a dramatic diversification in the Devonian (Whalen & Briggs, 2018).

Clear-water bottom-current deposits (FA2)

In FA2, the sequences of F1, F2, F3 and F4 (for example, Fig. 3 beds 3–10, 89–106), occasionally with F5.1 (for example, Fig. 3 beds 69–83, Fig. 5 beds 4–23), showing bi-gradational patterns with inverse and normal grading (Table 2), are interpreted as contourite sequences based on the criteria described by Gonthier *et al.* (1984), Stow *et al.* (1986) and summarized by Stow & Faugères (2008). Indicative are the gradual variations in depositional texture, mean grain size and degree of shell fragmentation, which were caused by the long-term fluctuation in the dynamic properties of the bottom current combined with low sediment supply. Sediment-specific features, resulting from the available evolutionary stock of Devonian skeletal elements, are those described for fossil contourites (Hüneke & Stow, 2008; Hüneke, 2013), including indistinctly defined particle-size grading, abundant intraclasts, hardground-covered omission surfaces (for example, Fig. 4A beds 1–13, Fig. 5 beds 4–23) and other effects of early-marine seafloor cementation (Eberli & Betzler, 2019).

The coquinas with whole shells (F5.1) represent sand-sized bioclastic contourites and constitute the C3 contourite sequence intervals (Fig. 21A), as coquinas made up of heavily fragmented shells (F4) are silt-sized bioclastic contourites and represent the C2 and C4 intervals

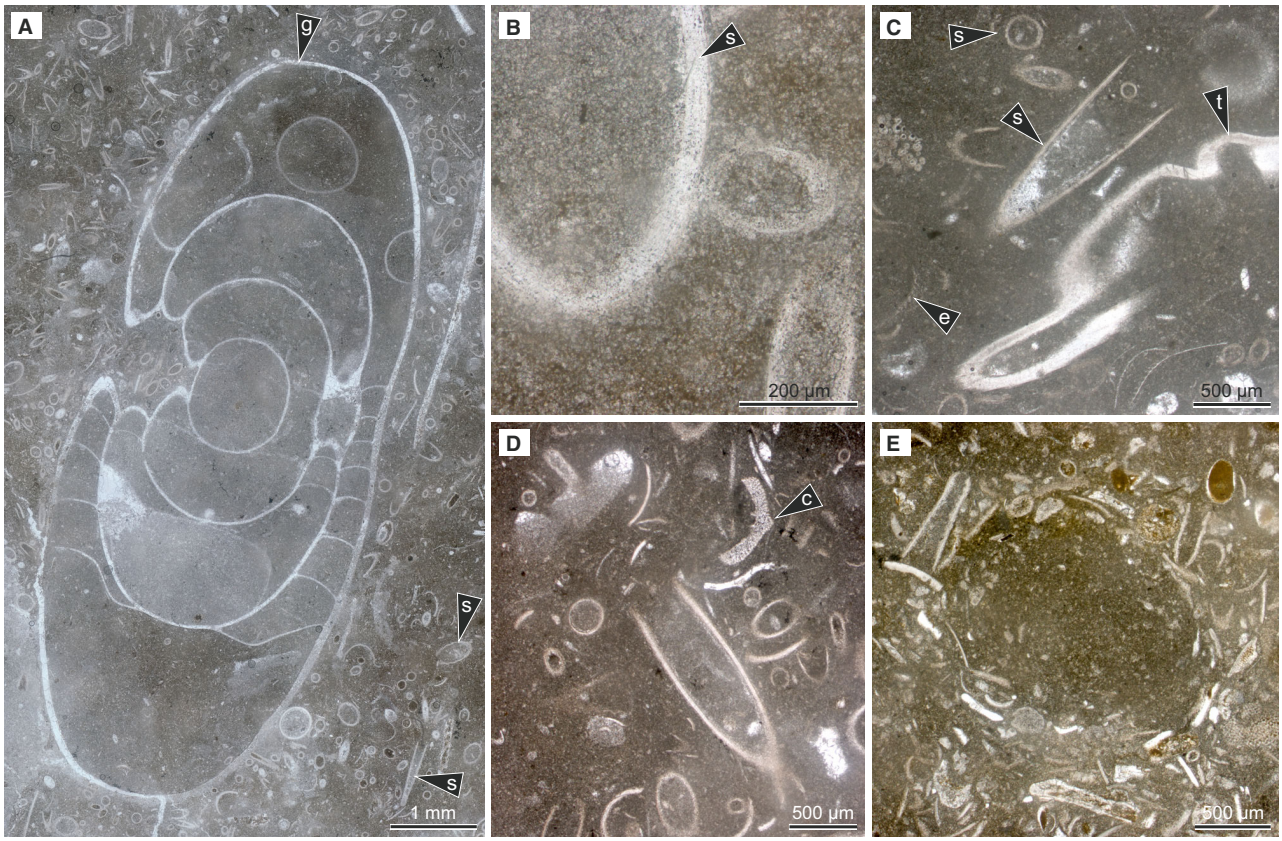

Fig. 9. Microfacies Facies Association 1 (FA1), Eifelian–Frasnian, Tafilalt Platform. (**A**) Thin-shelled bioclast floatstone (F1), biomicrite, showing abundant styliolinids (s) and goniatite (g) (*Maenioceras*). Thin section BT-57b, middle Givetian, *rhenanus-varcus* Zone. (**B**) Detail of (A) showing styliolinid shells (s) and fine-grained matrix with most grains smaller than 10 µm. (**C**) Styliolinid wackestone (F1.1) with abundant well-preserved styliolinids (s), entomozoans (e) and trilobite shell (t) showing characteristic bimodal grain-size distribution. Note well-preserved shells. Thin section HL2-4, middle Givetian. (**D**) Styliolinid wackestone (F1.1) with crinoid arm element (c). Thin section ME-46. (**E**) Thin-shelled bioclast wackestone (F1) with abundant shell fragments being associated with *Planolites* burrow. Thin section JI-20/2/, late Givetian.

(Fig. 21B and C). The latter display textural inversions resulting from disintegration of the fragile shells in response to varying hydrodynamic energy (Folk, 1962). The occurrence of silt-sized quartz grains (Fig. 10E) agrees with an increase in hydrodynamic energy. The coquinas are identified as: (i) hiatal or condensed shell concentrations; and, more rarely, (ii) lag concentrations (Kidwell, 1991a,b). The condensed concentrations (Figs 10A and 11A) formed because finer-grained sediment was never deposited out of suspension (total bypassing) at peak-flow conditions, or resulted from alternating small-scale deposition and erosion (dynamic bypassing). The lag concentrations (Fig. 10F) result from prolonged winnowing of carbonate mud and shell fragmentation. Abundant ferromanganese-coated particles (F3) show many of the microbial structures described by Preat *et al.* (2008) and indicate mostly oxic (to suboxic) conditions and low overall sediment-accumulation rates (e.g. Benninger & Hein, 2000; Föllmi *et al.*, 2011; Hein *et al.*, 2015; Föllmi, 2016), which implies deposition from clear-water bottom currents. Such depositional conditions are confirmed by the large extent of bioturbation (BI 3–6).

Incomplete contourite sequences typically include an erosional surface that separates a coarsening-up unit from an overlying fining-up unit (Fig. 21C, Table 2), displaying a gradual transition from C1 to C2 (for example, F1.3 to F2), abruptly followed by a gradual transition from C4 to C5 (for example, F4 to F1.2). Thin C3 intervals may occur (for example, styliolinid packstone), locally represented by starved ripples. These midcut-out bi-gradational sequences may originate from long-term variation in bottom-

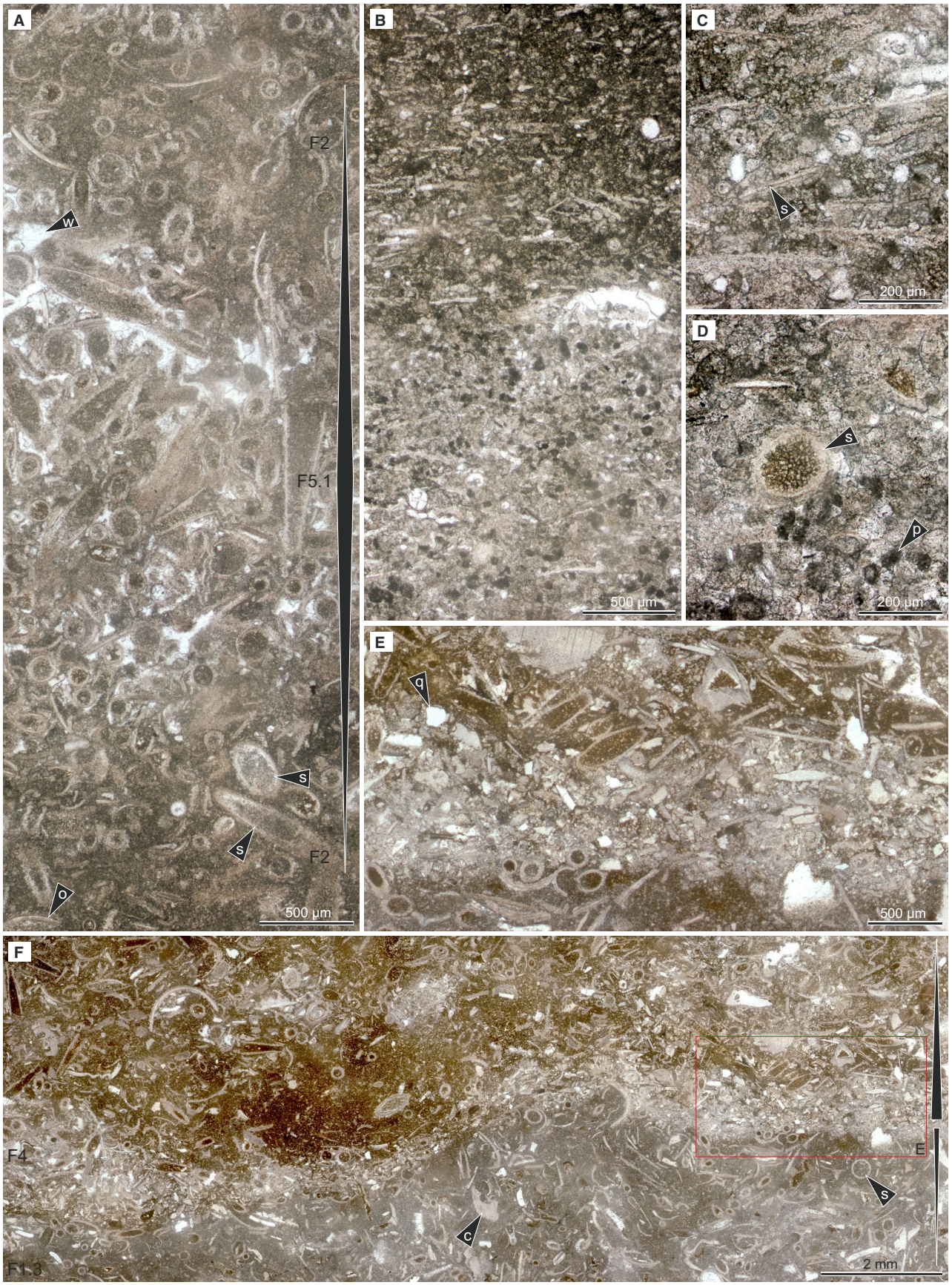

Fig. 10. Microfacies Facies Association 2 (FA2), Eifelian–Frasnian, Tafilalt Platform. (**A**) Bioclast wackestone (F2) gradational interlaminated with styliolinid packstone (F5.1). Note inverse-to-normal grading, washed-out interstitials (w), prevailing styliolinids (s) and rare ostracod shells (o). Thin section BT-70-71-2, top middle Givetian, top of *ansatus* Zone (Upper *Sellagoniatites* Bed). (**B**) Micro-bioclast packstone (F4) showing compositional variation of lamination with abundant fragmented styliolinid shells and peloids. Thin section BT-68-1, middle Givetian, *ansatus* Zone. (**C**) Detail of (B) showing horizontally-aligned styliolinid fragments. (**D**) Detail of (B) showing good sorting of very-coarse-silt-sized and very-fine-sand-sized (micro-bioclastic) fragments. Note circular section of a styliolinid shell (s) and peloids (p). (**E**) Detail of (F) showing prevailing bioclastic debris and abundant quartz of equivalent grain size (q) above erosional surface. (**F**) Graded styliolinid bioclast wackestone (F1.3), truncated and draped by micro-bioclast packstone (F4) displaying erosional contacts. Note prevailing styliolinids (s) and rare crinoid elements (c). Thin section BT-75M, basal late Givetian, *hermanni* Zone.

current velocity, or a temporal variation in local sediment supply (Gonthier *et al.*, 1984; Stow *et al.*, 1986; Stow & Faugères, 2008). The omission of (parts of) the C3 and C2 divisions is related to a prolonged phase of non-deposition and erosion during peak-flow, as has been documented for modern contourite successions (Stow & Faugères, 2008). The intervening erosional surface was frequently transformed into a hardground (Fig. 11A and H). Burrows below the hardground show sharp ceilings, indicating early marine cementation and hardening of the seafloor when the current intensified and the sedimentation rate was extremely reduced (Hüneke, 2013). The C2 and C4 intervals (F2, F3 and F4) include carbonate mud intraclasts (Table 2), which were eroded from the hardened substrate during peak-flow conditions. Reworked intraclasts are a common component in modern carbonate drifts (Chabaud *et al.*, 2016; Lüdmann *et al.*, 2018; Eberli & Betzler, 2019). The C4 division may contain particles with a higher specific weight compared to the calcite bioclasts (ferromanganese nodules, conodonts) and hence may form lags at the base of the normally-graded interval (Fig. 21B and C). All of these features indicate winnowing or a long break in sedimentation halfway through the formation of a bigradational sequence. Furthermore, siliciclastic particles (mainly quartz grains) commonly occur in the C4 intervals (F4), indicating enhanced current-induced supply from more distant (external) sources, as in packstone layers of carbonate contourite sequences on the modern Bahamian slopes (Mulder *et al.*, 2019).

The low-diverse trace fossil assemblage agrees with a contourite environment (see Wetzel *et al.*, 2008; Rodríguez-Tovar *et al.*, 2019; Hovikoski *et al.*, 2020). *Thalassinoides*-like traces on hiatal surfaces (Figs 8C to E and 11A to E), which are frequently filled by coquinas of styliolinid packstone to grainstone (F5), developed on semi-consolidated firmground to hardground substrates due to erosion, non-deposition and chemogenic induration (see Wetzel *et al.*, 2008).

Deposits of energetic dysoxic–anoxic bottom currents (FA3)

The coquinas constituting FA3 (F5 and F6) are interpreted as sand-sized bioclastic contourites forming stand-alone C3 intervals within contourite sequences (see Stow & Faugères, 2008), which in many cases are bounded by hiatuses (Fig. 21D, Table 2). The predominance of particle-supported depositional textures and the omnipresent traction structures evidence deposition from a migrating bedload in response to continuous hydrodynamic traction (Martín-Chivelet *et al.*, 2008; Stow *et al.*, 2009). Widespread shell stacking (telescoping) and layer-specific orientation patterns of the conical styliolinid shells display a unidirectional flow with small direction spread and variable speed (Fig. 13B and F). The vertical variation in styliolinid shell size reflects sorting processes (Fig. 12F). The particle composition – abundant shells of calcareous plankton – indicates bottom-current induced reworking of pelagic carbonate muds occurring within the source area. The absent to sparse bioturbation (BI 0–1) and the elevated TOC values (Table 3), together with the morphology and size distribution of pyrite framboids present in most beds (Fig. 14) suggest sediment deposition from an anoxic water mass (see Berner, 1984; Ekdale & Mason, 1988; Sagemann *et al.*, 1991; Svarda *et al.*, 1991; Wignall, 1994, 2005; Wilkin & Barnes, 1997; Uchman & Wetzel, 2011). The prevalence of small pyrite framboids ($D < 5$ μm) composed of small microcrystals ($d \leq 0.4$ μm) indicates syngenetic formation at the oxic–anoxic interface within the water column with subsequent settling to the seafloor (Wilkin *et al.*, 1996; Liu *et al.*, 2019). Interlayers with a few discrete traces and larger framboidal pyrites ($D > 5$ μm) likely represent periods of dysoxic conditions.

The varying subhorizontal-undulating lamination (Table 2), which includes small-scale scours

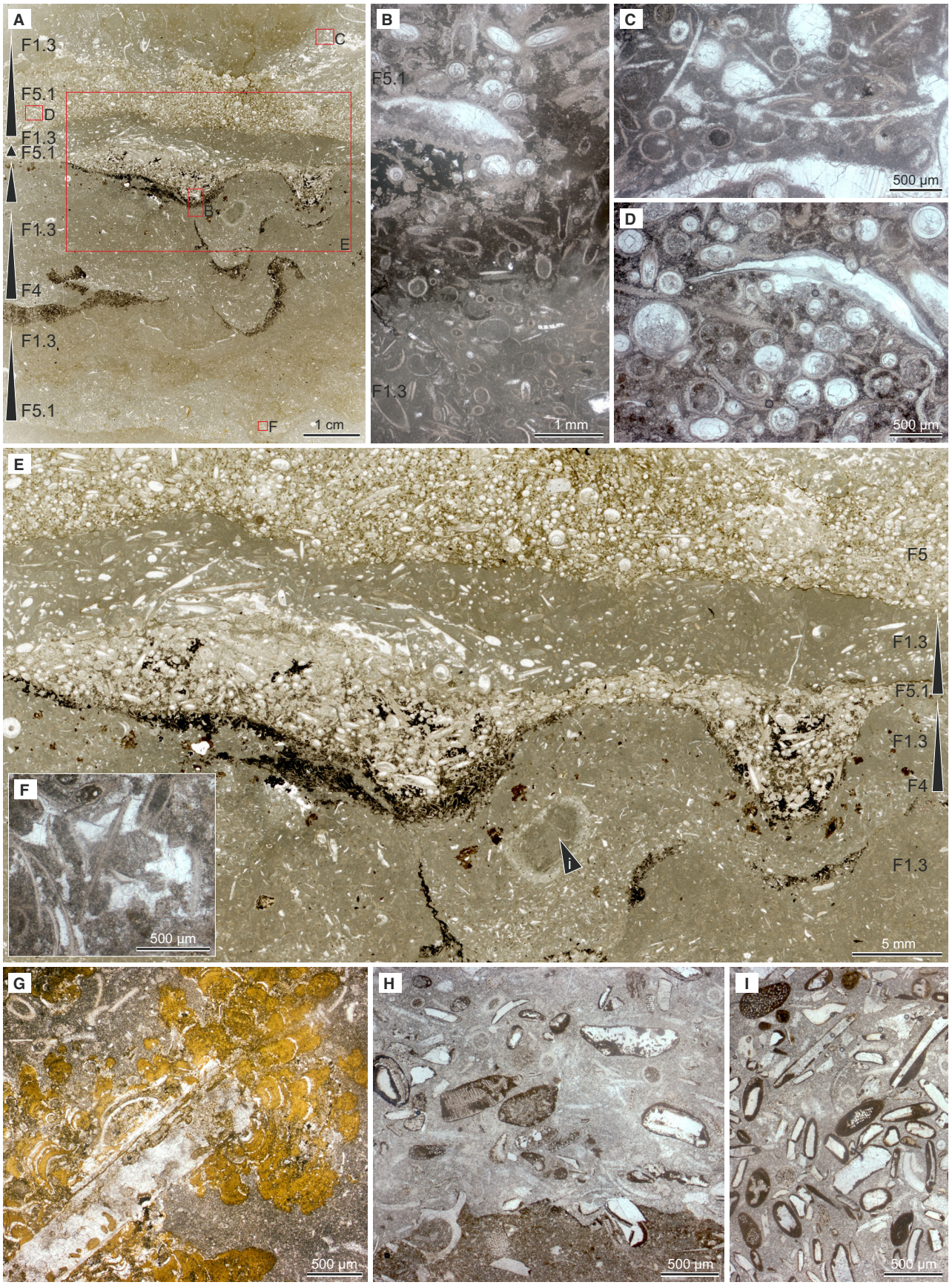

Fig. 11. Microfacies Facies Association 2 (FA2), Eifelian–Frasnian, Tafilalt Platform. (**A**) Thin layers of styliolinid packstone (F5.1), micro-bioclast packstone (F4) and bioclast wackestone (F1.3), which are bounded by sharp erosional contacts, hardgrounds and gradational contacts. Thin section HL2-M-19/1/, late Givetian. (**B**) Detail of (A) showing dark manganese-impregnated hardground on styliolinid wackestone (F1.3) draped by styliolinid packstone (F5.1). (**C**) Detail of (A) displaying gradual transition from particle to mud-support. (**D**) Detail of (A) showing whole and fragmented styliolinid shells including bivalved brachiopod shell (F5.1). (**E**) Detail of (A) highlighting normally-graded layers (F4 to F1.3, F5.1 to F1.3). Note carbonate-mud intraclast (i). (**F**) Detail of (A) showing sparite-filled interstitials in burrow-mottled styliolinid packstone (F5.1). (**G**) Ferromanganese-nodule floatstone (F3) showing large ferromanganese-impregnated *Frutexites* overgrowth around mollusc fragment. Thin section AM5-10c, late Givetian. (**H**) Eroded hardground surface overlain by ferromanganese-nodule wackestone (F3) with abundant ferromanganese-impregnated bioclasts. Thin section BT-86a, middle Frasnian. (I) Ferromanganese-coated bioclasts. Thin section shown in (H).

and normally graded laminae (Fig. 13A), was produced by tenuous traction together with rhythmic suspension fallout, which is consistent with deposition under the influence of weak to moderate, fluctuating bottom currents (Martín-Chivelet *et al.*, 2008). Ripple cross-lamination indicates bedload transport at subcritical flow conditions (Figs 12B and 13H), as planar-parallel lamination from upper-stage-plane beds most likely resulted from bedload sheets (and very low-amplitude bed waves) at Froude near-critical flow conditions (e.g. Allen, 1984; Paola *et al.*, 1989; Ashley, 1990; Southard & Bouguchwal, 1990; Best & Bridge, 1992; Ono *et al.*, 2021).

The brachiopod coquinas (F6), with inverse-to-normal grading (Fig. 21E, Table 2), agree with varying current strength, more specifically, increasing to decreasing flow speed during bed accretion (see Stow & Faugères, 2008). The large amount of styliolinids at the base and in the centre of the Upper *pumilio* Bed (Fig. 12C to E), indicates depositional conditions similar to those derived for the styliolinid coquinas (F5). The prevailing brachiopods, however, point to a specific source area outside of the Tafilalt Platform.

Current-reworked crinoid meadows (FA4)

The bi-gradational stacking of facies F7 and F8 present in the crinoidal limestones of FA4 (Table 2, Fig. 15) can be related to the standard contourite-facies sequence (Gonthier *et al.*, 1984; Stow & Faugères, 2008). The abundance of complete contourite sequences suggests sustainable sediment supply compared to the plankton-dominated bioclastic contourites of FA2 (Fig. 21F). Nevertheless, breaks in sediment accretion occurred (Fig. 6F), since omission surfaces and hardgrounds are locally associated with the C3 intervals (F8). Deposition at oxic to suboxic conditions is confirmed by the occurrence of ferromanganese-coated crinoidal ossicles (e.g. Hein *et al.*, 2015; Föllmi, 2016) and the moderate extent of bioturbation (BI 2–4, Fig. 4). Latter also indicates higher accumulation rates compared to FA2.

The crinoid floatstone facies (F7) resulted from *in situ* benthic carbonate production, which is a specific feature of some modern carbonate–contourite systems (Eberli & Betzler, 2019; Reolid *et al.*, 2019). Carbonate-segregating benthic organisms, such as suspension-feeding crinoids and solitary rugose corals, are most prolific when laterally supplied with food particles by weak bottom currents at water-mass boundaries (Dorschel *et al.*, 2007; Duineveld *et al.*, 2007; Davies *et al.*, 2009; Mienis *et al.*, 2012a,b; Taviani *et al.*, 2016). The Frasnian crinoid meadows were places of preferred mud deposition from the nepheloid layer and were prone to fluctuating flow strengths, resulting in indistinctly laminated and sorted deposits with abundant chains of connected crinoid ossicles (including holdfast). The bi-gradational beds and, on a larger scale, the bedsets of FA7 and FA8 display a long-term change between stimulated benthic carbonate production and intensified sediment reworking as a result of the fluctuating bottom-current flow strength.

Hiatal lag deposits (FA5)

Concentrations of carbonate intraclasts, ferromanganese nodules, large goniatite shells and conodonts in FA5 (Table 1), draping hardgrounds and erosional surfaces, are interpreted as lag deposits. The residuum of mechanically robust shells and highly fragmented less robust shells constituting the matrix clearly results from mechanical erosion. Published conodont data reveal that

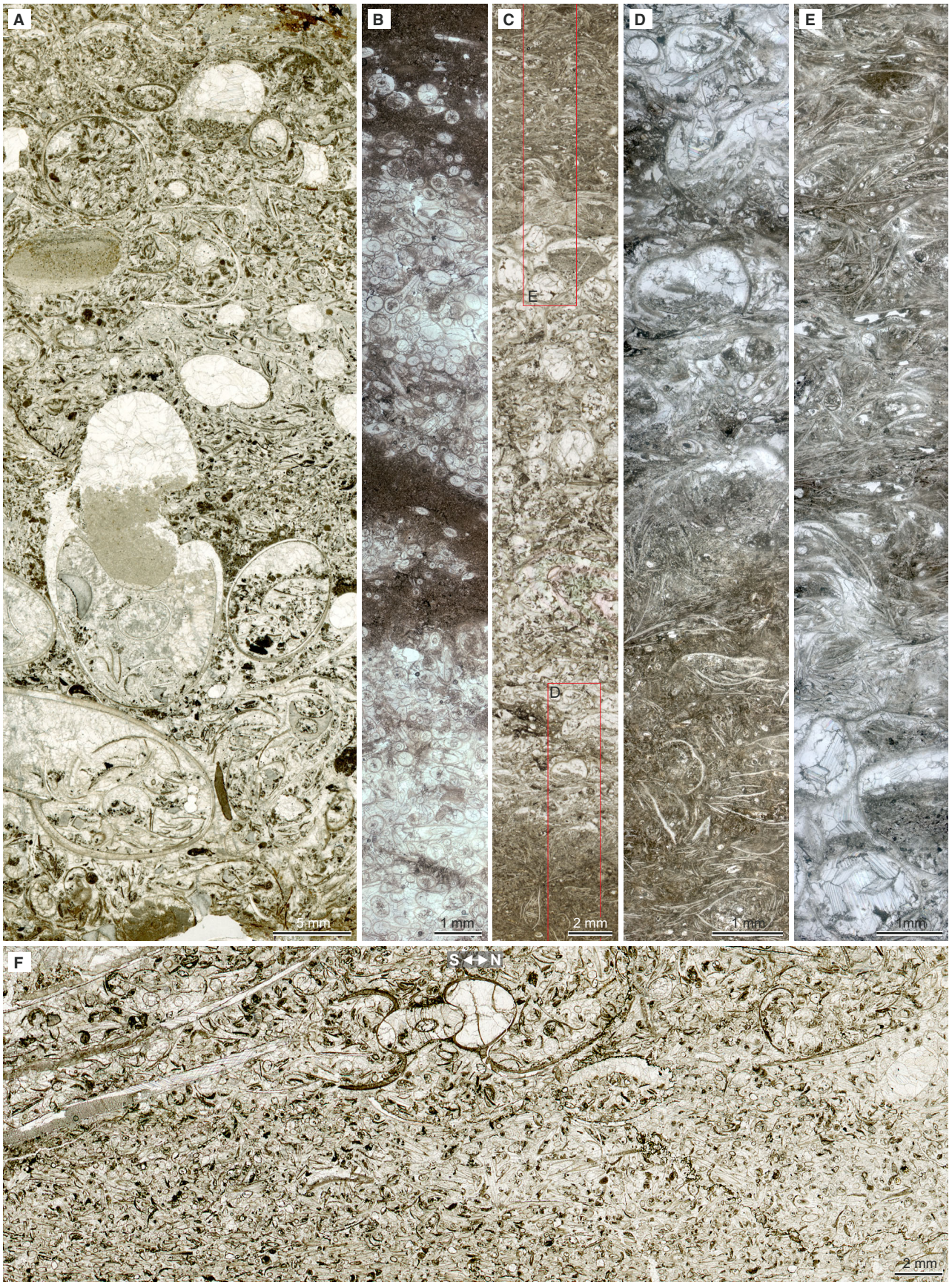

Fig. 12. Microfacies Facies Association 3 (FA3), Eifelian–Frasnian, Tafilalt Platform. (**A**) Styliolinid packstone to grainstone rich in orthoconic cephalopods and goniatites (F5). Note washed-out shell interstitials and subtle inverse-to-normal grading. Thin section AM5-16, Middle Frasnian. (**B**) Cross-laminated styliolinid packstone to grainstone including drapes of fine-grained sediment (F5.3). Thin section BT-84(II–IV), early Frasnian. (**C**) Thin-shelled *pumilio*-type brachiopod rudstone between layers of packstone (F6). Bi-gradational sequences of depositional texture and grain size, formed by disarticulated and bivalved brachiopod shells together with abundant styliolinids. Thin section BT-65UP2(E-W), middle Givetian. (**D**) Detail of (C) that shows increasing shell size and shell thickness together with gradual transition from mud to particle-support, displaying inverse grading. (**E**) Detail of (C) that shows large bivalved brachiopod shells gradually overlain by disarticulated, fragmented and smaller shells, exhibiting normal grading. Note minor amount of styliolinids. (**F**) Styliolinid grainstone gradually overlain by cephalopod rudstone (F5.3) displaying inverse grading. The styliolinid cones in lowermost part are oriented subhorizontally. In upper part, the abundant goniatites (*Manticoceras*) are aligned obliquely due to cross-lamination. Thin section IH1.5-13v2, early Frasnian, USty.

biostratigraphic gaps characterize many of the associated discontinuity surfaces (Fig. 2; Fig. 4A bed 22) or indicate extremely reduced accumulation rates during the formation of these layers (see Wendt, 1988; Aboussalam & Becker, 2007, 2011). The lag deposits are indicative of energetic currents that selectively removed fine-grained particles, excavated and reworked granule to cobble-sized intraclasts from the indurated seabed, and resulted in long periods, exceeding one biozone, with reduced sediment accumulation.

Long-lasting exposure of the seafloor is evidenced by the thick ferromanganese coats around many intraclasts (Fig. 16A and F), shells and on the hardground surface (e.g. Giresse, 2008; Reolid & Nieto, 2010; Föllmi, 2016). Most of the small-sized ferromanganese nodules were formed by hydrogenetic accretion from ambient seawater, as indicated by the regular and closely-packed concentric microstructures, with columnar patterns or rounded segregations. The formation of the hydrogenetic nodules relies on a regular relocation process allowing the nodules to rotate and to remain at the sediment–water interface despite their very low accretion rates (Halbach *et al.*, 1981; Hein & Peterson, 2013). Low overall sediment-accumulation rates are an important precondition (<10 mm kyr^{-1}; Hein & Koschinsky, 2014). Especially contour currents are capable of winnowing and eroding fine-grained sediment, delivering oxygen, and assuring the throughput of iron and manganese ions and colloids used in the accretion of the nodules (Glasby & Read, 1976; Hartmann *et al.*, 1989; Usui *et al.*, 1993; Hein & Peterson, 2013).

The lag deposits mainly drape hiatuses bounding the C3 and C4 intervals of partial contourite sequences in FA2 and FA3 (Fig. 21G, Table 2). Therefore, they can be termed calcareous gravel-lag contourites, chemogenic contourites or ferromanganese contourites (Stow & Faugères, 2008; Rebesco *et al.*, 2014). Such contourites are known from ancient and modern carbonate drifts (Hüneke & Stow, 2008; Rebesco *et al.*, 2014; Eberli & Betzler, 2019).

Drift-scale features

The Eifelian–Frasnian succession with interbedded pelagic limestones and bioclastic contourites formed in response to varying bottom-currents on a contourite terrace (Fig. 22B). This interpretation is based on: (i) the large-scale stratigraphic architecture of the succession; (ii) the overall limited sediment thicknesses; (iii) the occurrence of abundant biostratigraphic gaps; and (iv) the spatial distribution of facies F2, F3, F4 and F9 (Table 2) that could be interpreted as contourites (Stow & Faugères, 2008; Rebesco *et al.*, 2014; Eberli & Betzler, 2019). The documented co-occurrence of widespread depositional and erosional contourite features characterizes contourite terraces, which often correspond to the landward upper part of a plastered drift (Hübscher *et al.*, 2010; Hernández-Molina *et al.*, 2016c; Eberli & Betzler, 2019; Thiéblemont *et al.*, 2019; Miramontes *et al.*, 2021).

Seaward-dipping contourite terraces are typically found on the upper and middle continental slopes at the interfaces of different water masses (e.g. Viana, 2001; Viana *et al.*, 2002a,b; Hernández-Molina *et al.*, 2009, 2014; Brackenridge *et al.*, 2011; Preu *et al.*, 2013; Ercilla *et al.*, 2016; Steinmann *et al.*, 2020; Wilckens *et al.*, 2021). Water-mass interfaces are characterized by energetic geostrophic currents and associated internal waves and eddies (Reid *et al.*, 1977; Yin *et al.*, 2019; Miramontes *et al.*, 2020), which

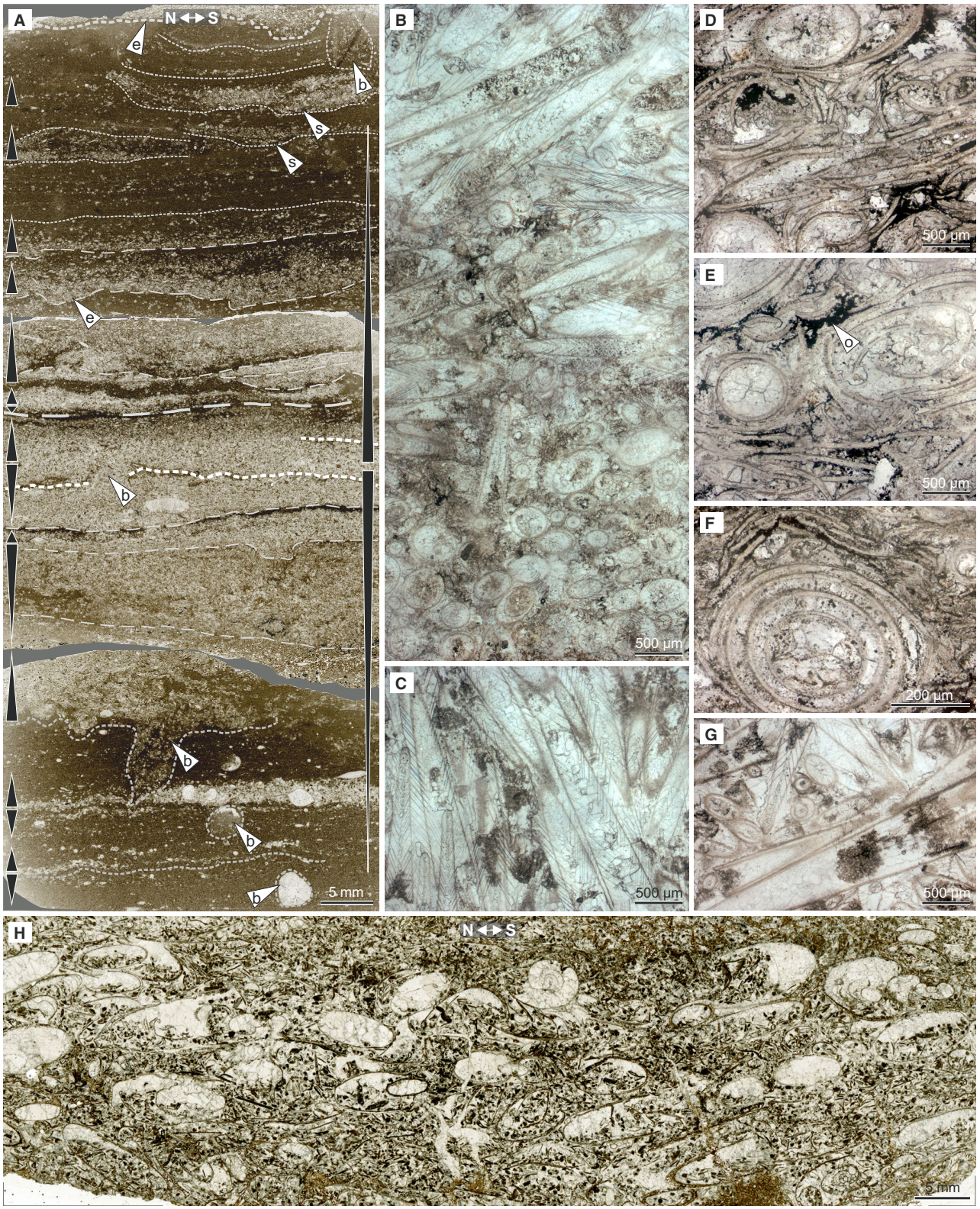

widely shape the slope morphology (e.g. Hernández-Molina *et al.*, 2011; Mulder *et al.*, 2012; Thiéblemont *et al.*, 2019).

In modern carbonate settings, contourite terraces are a common feature of shelves swept by bottom currents such as the Miami and

Fig. 13. Microfacies Facies Association 3 (FA3), Eifelian–Frasnian, Tafilalt Platform. (**A**) Parallel-laminated and cross-laminated layers of styliolinid packstone and grainstone (F5.2 and F5.3), interlaminated with finer-grained sediment (F2 and F4). Black triangles highlight coarsening-upward and fining-upward sequences (right margin), which include inversely-graded and normally-graded intervals (left margin). Note scarce burrowing (b), minor erosional surfaces (e) and scour fills (s). Thin sections BT-84b+c(N-S). (**B**) Laminae of styliolinid grainstone (F5.2) defined by change in shell orientation. Note that the conical styliolinids are aligned perpendicular to the thin-section plane in the lower part (O-sections) and largely parallel to it in the upper part (V-sections). Thin section JI-22c. (**C**) Detail of lower part of (B) in bedding-parallel thin section showing horizontally-aligned conical shells (V-sections). (**D**) Whole and fragmented styliolinid shells in styliolinid grainstone (F5). Thin section JI-22e2.2w. (**E**) Concentrations of black organic matter (o) in interstitials between whole and fragmented styliolinid shells in styliolinid grainstone (F5). Thin section JI-22e2.2w. (**F**) Cone-in-cone stacking of shells in styliolinid grainstone (F5). Thin section JI-22fwV2. (**G**) Irregular orientation of shells in styliolinid grainstone (F5). Thin section BT-84cH5, oriented parallel to bedding. (**H**) Bed of cross-laminated styliolinid rudstone rich in goniatites (F5.3). Note that cephalopods are of almost equal size due to sorting and many shells are embedded with their long axis parallel to the former ripple slipface, i.e. oblique from upper right to lower left. Thin section JI-22e2.4wV2(N-S) (Fig. 4).

Table 3. Total carbon (TC), total inorganic carbon (TIC) and total organic carbon (TOC) content of samples from organic-rich coquinas (FA3).

Facies Association (FA)	Sample	Facies	TC (%)	TIC (%)	TOC (%) = TC–TIC	Stratigraphy
FA3	BT-48	F6	12.04	11.13	0.92	LpB
FA3	IH5-17c	F6	12.24	11.14	1.10	UpB
FA3	BT-84-c	F5	11.48	9.77	1.72	LSty
FA3	BT-II-III	F5	12.06	11.15	0.91	LSty
FA3	HL-24a	F5	11.05	9.87	1.18	LSty
FA3	JI-22-a	F5	11.77	10.50	1.27	USty, Base
FA3	JI-22-b	F5	11.75	10.22	1.53	USty
FA3	JI-22-d	F5	11.63	8.61	3.01	USty
FA3	BT-84-g	F5	11.32	9.98	1.34	USty
FA3	MWE-34	F5	11.32	10.30	1.02	USty
FA3	ME-29	F5	10.62	9.40	1.22	USty
FA3	JI-22f	F5	10.78	9.71	1.07	USty, Top
FA3	IH5-42	F5	11.96	10.45	1.51	LRh
FA3	BT-88-1	F5	11.58	10.19	1.39	LRh
FA3	ME-34	F5	10.63	9.59	1.05	LRh

Pourtalès terraces along the seaward edge of the Florida Platform and the Marion Plateau off the Great Barrier Reef (Mullins & Neumann, 1979; Heck *et al.*, 2004; Hübscher *et al.*, 2010; Eberli & Betzler, 2019). These morphosedimentary features are produced by bottom currents that are driven by the surficial water mass at 300 to 400 m water depth, or at even shallower water depths. The gently sloping terraces alternately take up thin contourite deposits or become eroded to deliver sediment down-current on associated contourite drifts, which are mainly controlled by sea-level changes and changes in the thickness of the surficial water mass (Kenter *et al.*, 2001; Isern *et al.*, 2002, 2005; Eberli *et al.*, 2010; Correa *et al.*, 2012).

Sheeted or plastered drift

The fairly uniform thicknesses (tabular sediment architecture), the predominantly aggradational stacking pattern, and the low lateral variability of the Eifelian–Givetian facies succession (Figs 18 to 20) agree with an interpretation as a sheeted drift. Alternatively, the sheeted architecture may represent the thin upslope part of a larger plastered drift located further downslope (Preu *et al.*, 2013; Rebesco *et al.*, 2014). Such an increase in sediment thickness down the slope has been documented west and north of the Tafilalt Platform (Wendt *et al.*, 1984; Wendt, 1989; Wendt & Belka, 1991; Döring, 2002; Lubeseder *et al.*, 2010). The distribution of contourites in these basins, however, has so far remained unexplored.

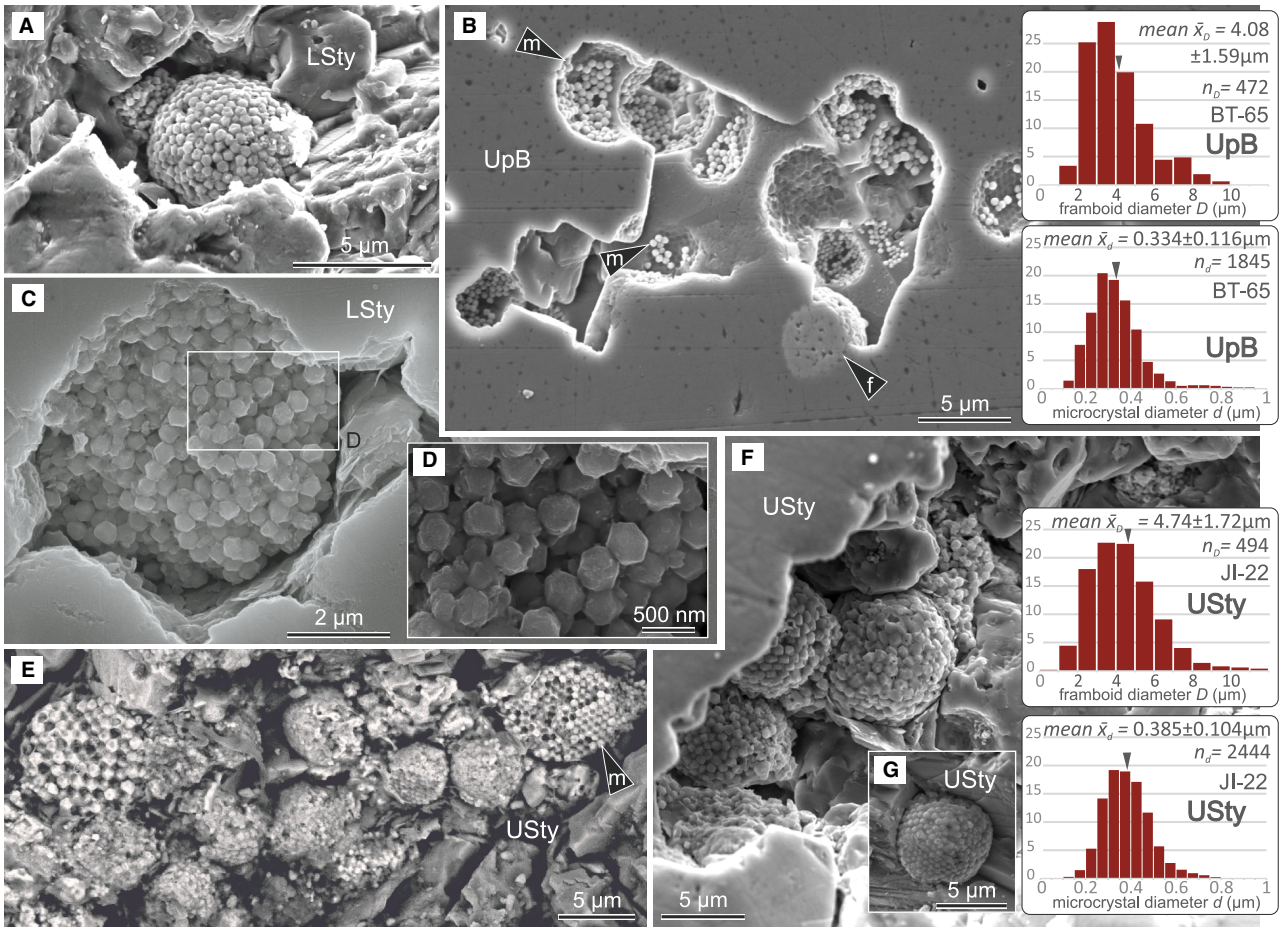

Fig. 14. Pyrite framboid micromorphology and size distribution organic-rich coquinas (FA3). (**A**) Secondary electron (SE) image of pyrite framboids of LSty at section Bou Tchrafine (BT-II-III-2-035) (Fig. 3). (**B**) SE image of a cluster of (f) small to medium-sized, (syngenetic) framboids and imprints with residual (m) microcrystals (BT65-a-48, UpB), histograms exemplify the size distribution of framboids and microcrystals of UpB at section Bou Tchrafine (BT). (**C**) InLens photomicrograph of single medium-sized framboid of LSty at section Hamar Laghdad (HL1-3 A pol 15 P4) (Fig. 5). (**D**) Detail of (C), showing well-organized equidimensional and equimorphic/equigranular pyrite microcrystals. (**E**) BSD image of framboid cluster of small to medium-sized framboids of USty at section Jebel Ihrs (JI-22-f-w3c-056) (Fig. 4); (m) fracture surface showing well-organized microcrystalline pyrite. (**F**) SE image of JI-22-f-w3b-009, histograms exemplify the size distribution of framboids and microcrystals of USty at section Jebel Ihrs (JI). (**G**) Single, partly overgrown pyrite framboid of USty at section Jebel Ihrs (JI-22-f-w3b-035).

Obstacle scours and tails

The regional thickness variations present at the eastern ridge of Hamar Laghdad (Fig. 20) suggest that the Eifelian–Givetian mud mounds formed obstacles for active bottom currents on the morphologically rather plain contourite terrace (Fig. 22B). With increasing size (up to 35 m), the Hollard Mound influenced the flow dynamics and sedimentation in the surrounding area, causing a scour in the early–mid Givetian (Fig. 20, off-mound units J and K) and a lee-side tail or a luv-side bulge in the early Frasnian (Fig. 20, unit O). Such morpho-sedimentary features typically form close to mounds associated with contourite drifts due to local turbulence and enhanced current speeds (e.g. De Mol *et al.*, 2002; Grasmueck *et al.*, 2006; Fink *et al.*, 2013; Lüdmann *et al.*, 2016).

Abraded surfaces and local erosion areas

The biostratigraphic gaps identified in the late Givetian to middle Frasnian succession (Fig. 2) result from non-deposition and submarine

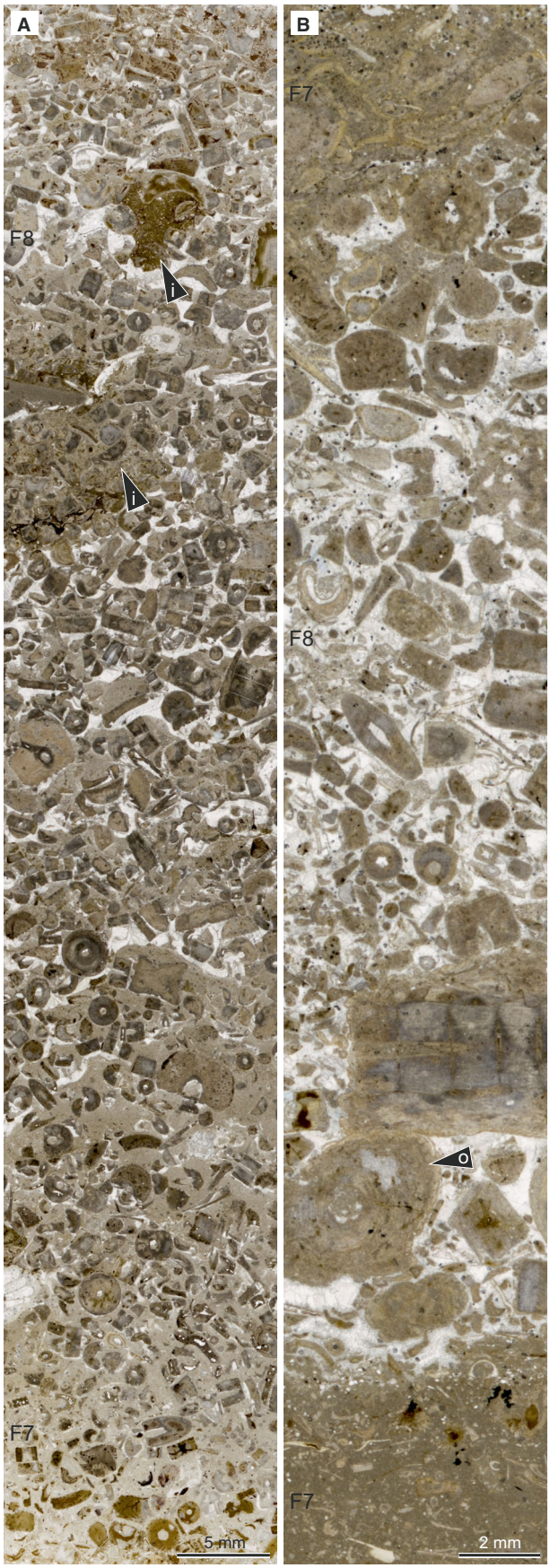

Fig. 15. Microfacies Facies Association 4 (FA4), Eifelian–Frasnian, Tafilalt Platform. (**A**) Bi-gradational sequence of crinoid floatstone (F7) and laminated crinoid rudstone (F8) formed by disarticulated crinoid ossicles together with a few intraclasts (i). Note gradual variation of grain size and mud content displaying inverse-to-normal grading. Thin section bed JI-28b, middle Frasnian (Fig. 4A). (**B**) Bi-gradational sequence of crinoid floatstone (F7) and laminated crinoid rudstone (F8) showing gradual variation of depositional texture. Note that some crinoid ossicles are the nucleus of oncoids (o). Thin section JI-31u, middle Frasnian (Fig. 4A).

erosion, which gave way to local disconform bed contacts, associated with lag deposits (Fig. 7A) and strata of different ages below the hiatus surface (Fig. 19). These features reveal that the contourite terrace was temporarily truncated by near-flat abraded surfaces produced by energetic bottom currents (Fig. 22B). Most distinctive are the two abraded surfaces that extended over the entire Tafilalt Platform during the early Frasnian (MN zones 1 and 3) (compare Fig. 2 with Figs 17 to 20). Similar surfaces of slightly lesser extent were produced during the mid–late Givetian and middle Frasnian. Abraded surfaces are regions eroded by strong tabular currents (Hernández-Molina *et al.*, 2008, 2011; Ercilla *et al.*, 2011; Rebesco *et al.*, 2014), and are often found in association with sandy contourite deposits within high-velocity zones of modern contourite depositional systems (Habgood *et al.*, 2003; Masson *et al.*, 2004; Hernández-Molina *et al.*, 2014, 2016a).

The basal Frasnian erosional disconformity (BFH, Figs 17 to 20) documents widespread sediment bypassing and more intense erosion on the south-western terrace over a period of several hundred thousand years, starting in the topmost Givetian (*norrisi* Zone), and continuing during the earliest Frasnian (lower part of MN1 zone) (Bultynck & Walliser, 2000; Aboussalam & Becker, 2007; Hartenfels *et al.*, 2018). As a result, a smooth indurated submarine surface was produced on a former muddy substrate (Figs 3 to 5, BFH). Such hardened seafloor surfaces are typical for carbonate contourite systems under conditions of energetic bottom-currents and low sediment supply (see Eberli & Betzler, 2019). Carbonates have a high diagenetic potential and cementation in deep-marine carbonates may start close to the seafloor (Milliman & Müller, 1973, 1977), a mere

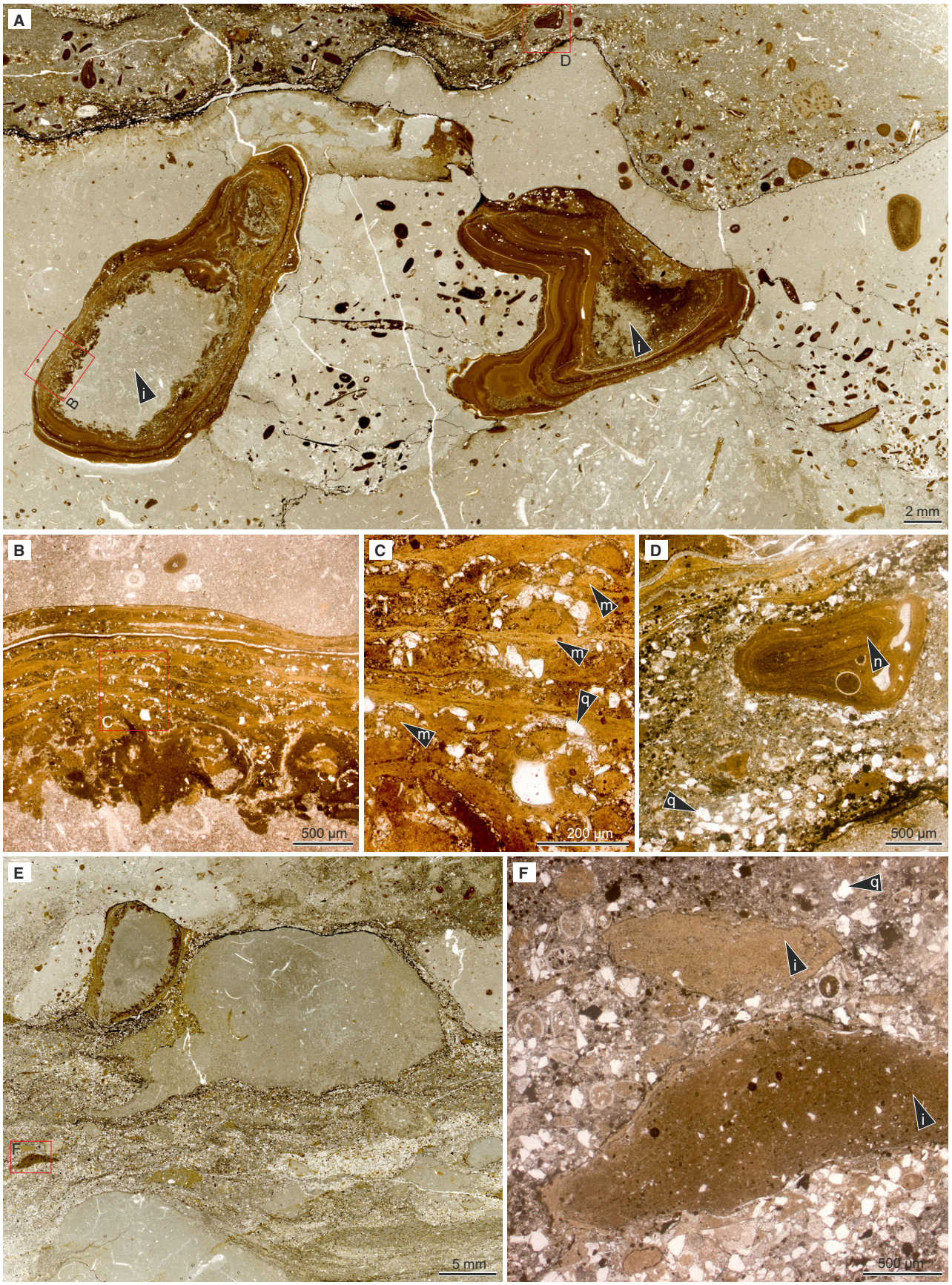

Fig. 16. Microfacies Facies Association 5 (FA5), Eifelian–Frasnian, Tafilalt Platform. (**A**) Hardground-bounded bioclast floatstone rich in ferromanganese-coated intraclasts (i) and ferromanganese nodules, which is truncated by an erosional surface and draped by a concentration of sand-sized intraclasts, quartz grains, ferromanganese nodules and bioclasts (F9.2). Thin section AM5-18, middle Frasnian (Fig. 4). (**B**) Detail of (A). Stromatolitic ferromanganese crust on lithoclast. (**C**) Detail of (B). Note spherical and hemispherical microbial structures (m) with agglutinated quartz grains (q). (**D**) Detail of (A) showing the mixture of ferromanganese nodules (n), bioclasts, abundant extraclasts (quartz grains, q), and a few intraclasts. (**E**) Carbonate–intraclast rudstone–floatstone with a packstone matrix of quartz and bioclasts in lower part (F9.1). Some of the intraclasts are impregnated by ferromanganese oxides. Thin section AM5-18u, middle Frasnian (Fig. 4). (**F**) Detail of (E) showing abundant quartz grains (q) and two different types of carbonate intraclasts (i).

reduction in sedimentation rate in current-swept areas already may result in rapid lithification of the seafloor (Mullins *et al.*, 1980; Kenter *et al.*, 2001; Malone *et al.*, 2001). Subsequent reworking of indurated mud clasts (from the hardened seafloor) by intensified currents has been reported from modern and ancient drifts (e.g. Lüdmann *et al.*, 2018; Eberli *et al.*, 2019). The Upper Marker Bed and the *Petteroceras* Bed, which occur immediately below the basal Frasnian erosional disconformity (Figs 3 to 5, BFH), are enriched in these reworked carbonate-mud clasts that occur together with concentrations of corraded goniatite shells. Both marker beds indicate widespread intraclast reworking pre-dating a period of prolonged bypassing and local erosion during earliest Frasnian. The laterally discontinuous beds and bedsets of organic-rich coquinas (FA3) found on many of these erosional disconformities indicate that (centimetre to decimetre-thick) bioclastic sand sheets and ribbons migrated as bedload across these abraded surfaces (Fig. 22B) and were preserved as the energetic currents decreased in intensity.

Numerous minor hiatuses, limited to smaller areas and not characterized by a biostratigraphic gap, occur within the depositional record of (incomplete) contourite sequences of FA2. They are likely caused by fluctuations of the interface between the two water masses in which shearing of the water masses and internal waves transported and removed the sediment, as also shown for the present-day Saya de Malha Bank (Indian Ocean; Betzler *et al.*, 2023). Alternatively, the projecting outer shelf-slope morphology of the Tafilalt Ridge (Figs 1B and 22B) may have influenced the local geostrophic currents forming non-permanent eddies (e.g. Viana & Faugéres, 1998). Wilckens *et al.* (2021) documented the link between eddy formation and localized erosional features even under conditions of low mean flow speeds on the Ewing contourite terrace of the Argentine continental margin. Such eddies are transient features and cause energetic periods during which the sediment is eroded, alternating with calm periods during which sediment deposition is favoured. The local erosion results from increased shear stress in turbulent flow compared to otherwise laminar flow (Schlichting & Gersten, 2017; Yin *et al.*, 2019).

Sandy condensation layers

The coquinas consisting of whole styliolinid shells (F5) are identified as the Devonian analogues of the globigerinid calcareous sands (Table 2) that form in modern contourite settings with limited siliciclastic sediment supply. These accumulations enriched in globigerinid foraminifera result from bottom-current induced winnowing of fine-grained pelagic mud and local bedload traction (Miller & Komar, 1977; McCave *et al.*, 1980; McCave, 2008). Miramontes *et al.* (2021) classified such sandy condensation layers as contourite features indicating environments where depositional and erosional processes balance one another. On the Tafilalt Platform, such sandy condensation units are widespread, forming both: (i) large-scale depositional features, identified as bioclastic sand sheets, decimetres to metres thick (FA3) (Figs 6B, 7B, 8A, 8B, 12, 13 and 17); and (ii) bed-scale features, comprising thin laminae of shell concentrations (F4 and F5 within FA2) (Figs 8C, 8D and 11A to F).

Channel and small mounded drift

On the south-western Tafilalt Platform, the converging disconformities, the stratigraphic sediment architecture (Figs 17B and 19), together with the lateral and vertical facies variation of the early–mid Frasnian succession display the formation of a north-west-trending channel bounded by a small mounded drift (or levée) at its north-eastern margin (Fig. 22B). A hiatus

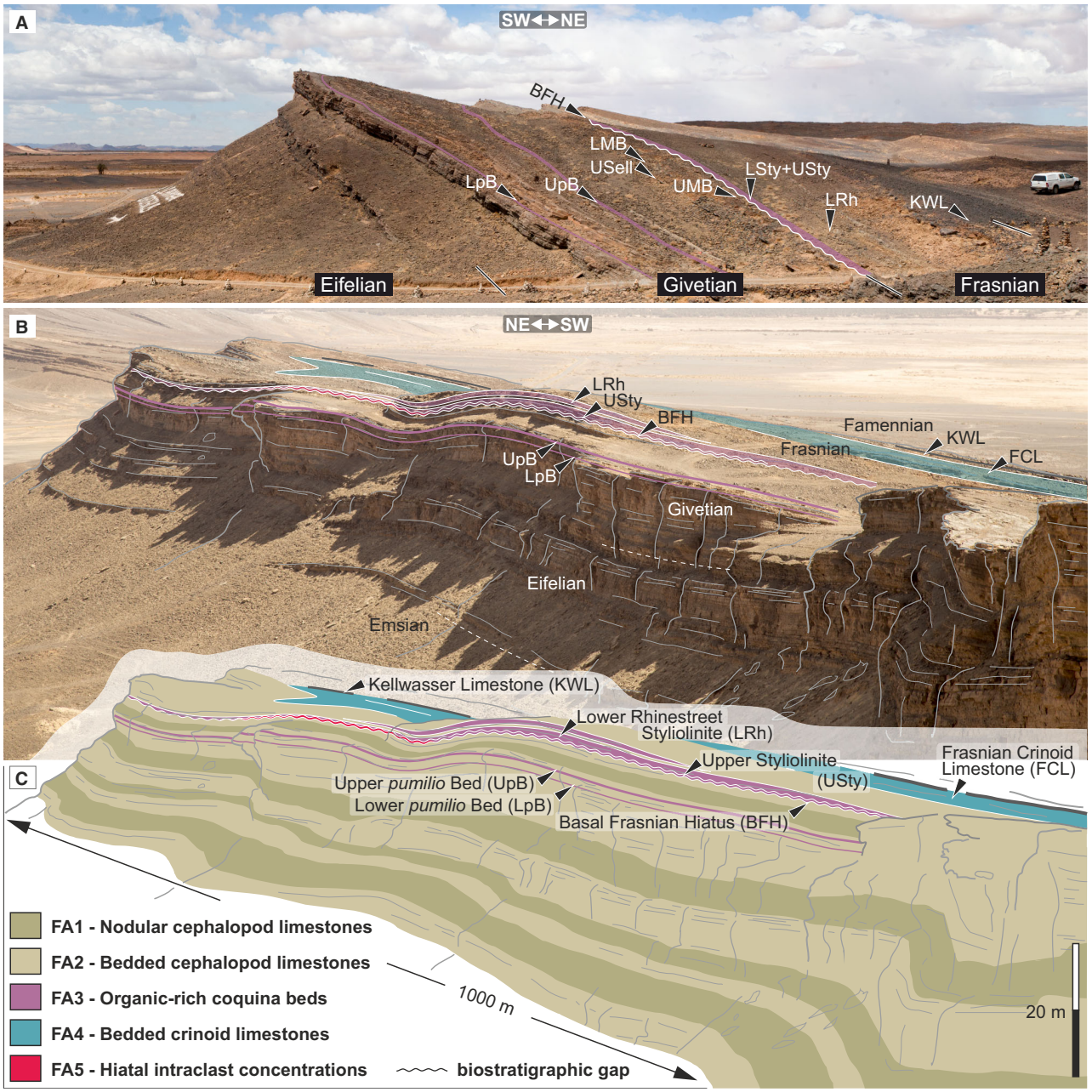

Fig. 17. Panoramic views Bou Tchrafine and Jebel Ihrs illustrating general exposed geometries and outcrop scale. (**A**) South-western scarp of Bou Tchrafine at section BT1. Overall tabular architecture, basal Frasnian hiatus (BFH), main organic-rich coquinas (FA3) and location of marker beds are highlighted (compare Fig. 18). (**B**) Oblique overview northern scarp of Jebel Ihrs (eastern part), illustrating distribution of main coarse-grained lithologies (FA3 and FA4) and hiatuses. (**C**) Sketch highlighting thickness mapping results at Jebel Ihrs (see Fig. 19). Note occurrence of hiatal intraclast concentration (FA5) above basal Frasnian hiatus. Boundaries marker beds, FA3, FA4 and FA2 were physically tracked to measure lateral thickness variation of depositional units, as gradual boundaries of FA1 and FA2 are shown schematically.

covering 7 Myr is present within the channel (Fig. 1C), that crops out at the western and south-eastern scarp of Jebel Ihrs, Mech Irdane, Rich Gaouz and El Kachla (Fig. 1C) (Wendt & Belka, 1991; Walliser, 2000; Aboussalam, 2003; Dopieralska, 2003; Hartenfels *et al.*, 2018). In central parts of the channel, such as at El Kachla (Fig. 1C), the biostratigraphic gap

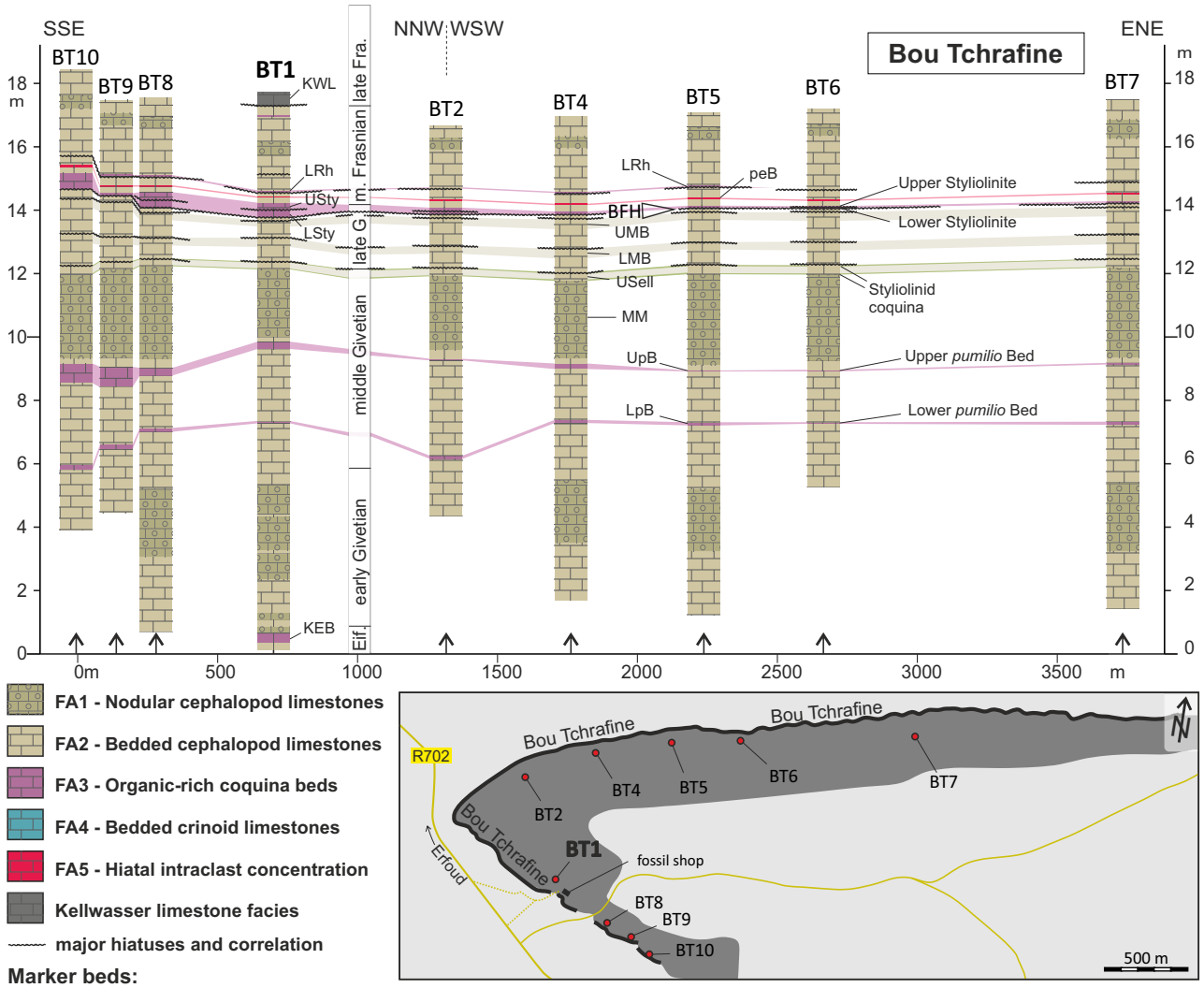

Marker beds:
FCL – Frasnian crinoidal limestones, KEB – Kačák Event Bed, KWL – Kellwasser Limestone facies, LMB – Lower Marker Bed, LpB – Lower *pumilio* Bed, LRh – Lower Rhinestreet equivalents, LSell – Lower *Sellagoniatites* Bed, LSty – Lower Styliolinite Frasnes event, Mid – Middlesex Event, MM – *Maenioceras* marl, MSell – Middle *Sellagoniatites* Bed, peB – pebble Bed, Pett – *Petteroceras* Beds, SC – *Sobolewia* coquina, TB – Twin Beds, UMB – Upper Marker Bed, UpB – Upper *pumilio* Bed, URh – Upper Rhinestreet equivalents, USell – Upper *Sellagoniatites* Bed, USty – Upper Styliolinite Timan event

Fig. 18. Event and lithostratigraphic correlation scheme Eifelian–Frasnian record in Bou Tchrafine area. Marker beds known to be isochronous were physically traced to measure lateral thickness variation of stratigraphic units. The gradual boundaries of FA1 and FA2 are shown schematically and are diachronous. Isochronous styliolinid coquinas (F5.1) associated with FA2 are marked in green. BFH, Basal Frasnian Hiatus.

comprises the *semialternans* to MN zone 10 (7 Myr), as in the northern channel margin at Jebel Ihrs the hiatus includes the *semialternans* to MN zone 4 (4 Myr) (Fig. 19A, section IH1). Initially, the channel resulted from an erosive incision (1–3 m) of the main bottom-current core into the late and middle Givetian succession during the earliest Frasnian. This can be inferred from: (i) disconform stratal patterns; and (ii) the uniform character of the late Givetian succession outside the channel, which contrasts with the early Frasnian showing facies and thickness variations together with widespread biostratigraphic gaps across the entire Tafilalt platform (compare Figs 2, 18, 19 and 20). Subsequently, during early–mid Frasnian, the channel remained largely free of sediment and became confined by low-mounded bedsets of coarse-grained contourites (FA3 and FA4), together with finer-grained contourites (FA2) at its downslope margin (Figs 17B and 19A). Compared to the central Tafilalt Platform

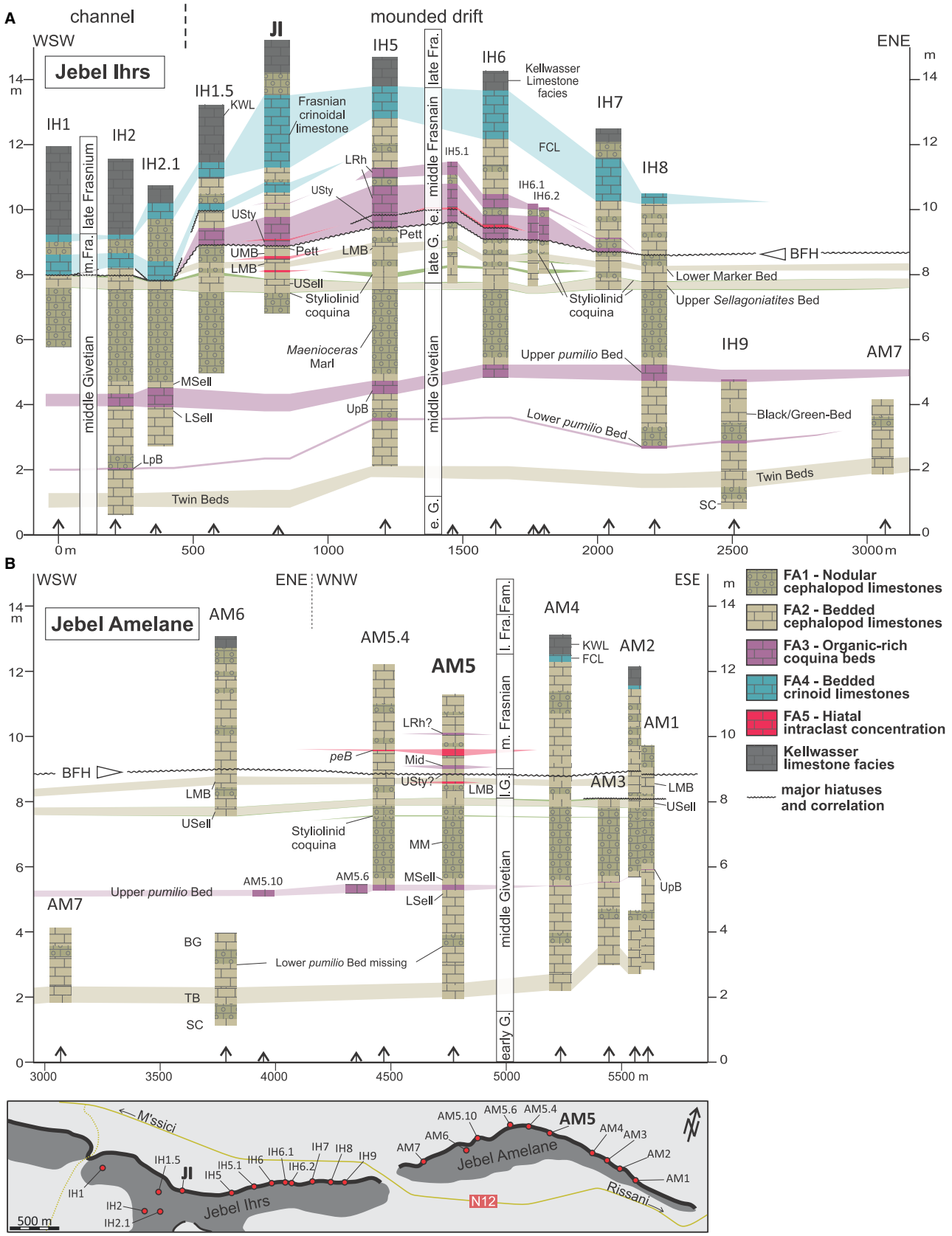

Fig. 19. Event and lithostratigraphic correlation scheme Eifelian–Frasnian record at Jebel Ihrs (**A**) and Jebel Amelane (**B**). Marker beds were traced to access lateral thickness variations of individual stratigraphic units. Gradual boundaries of FA1 and FA2 are shown schematically and are diachronous. BFH, Basal Frasnian Hiatus. For abbreviations of marker beds see Fig. 18.

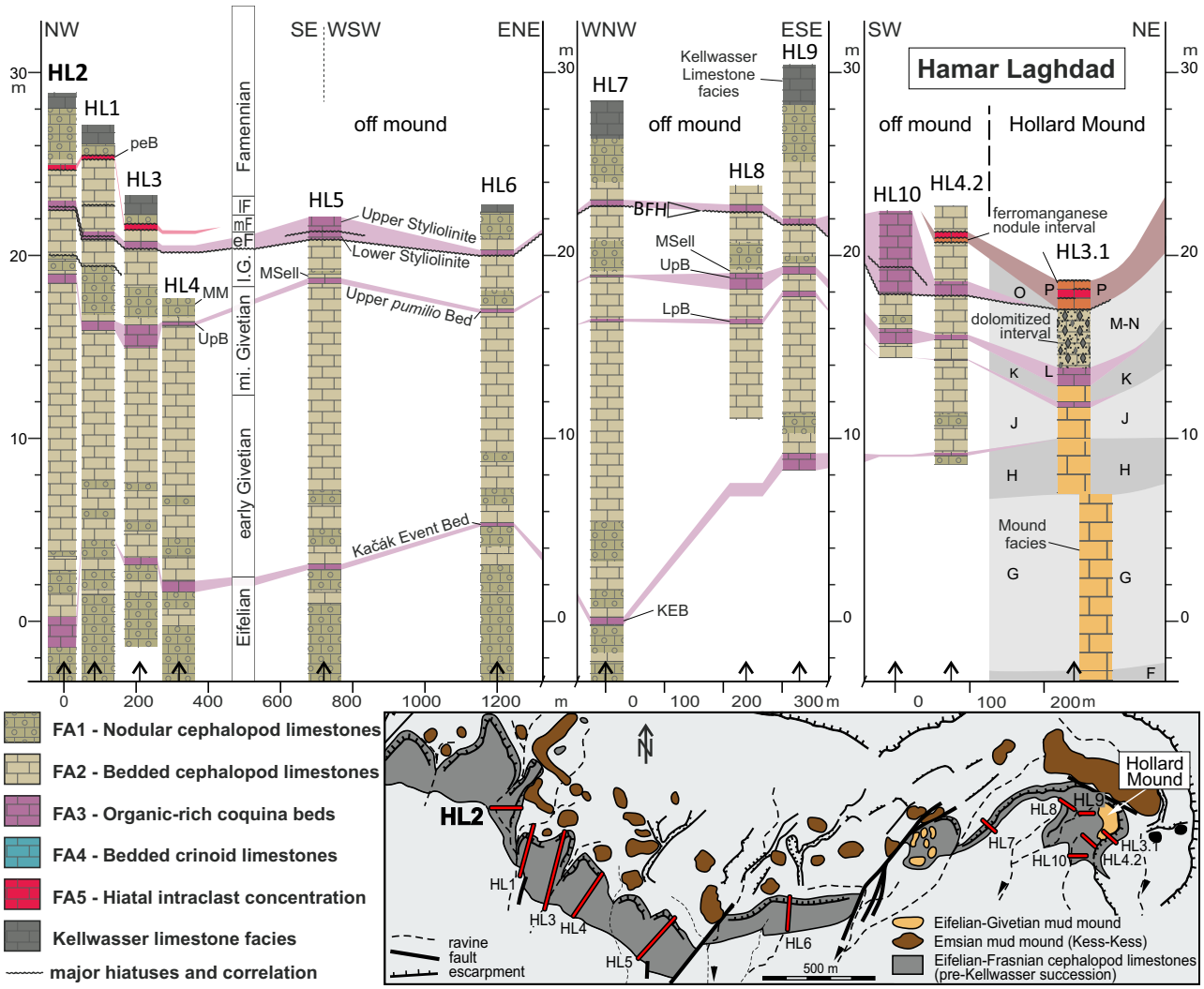

Fig. 20. Event and lithostratigraphic correlation scheme Eifelian–Frasnian record at Hamar Laghdad. Isochronous marker beds were tracked to document lateral thickness variation of stratigraphic units. Gradual boundaries of FA1 and FA2 are shown tentatively and are diachronous. BFH, Basal Frasnian Hiatus. F–P in HL3.1 refer to the lithostratigraphic subdivision of the Hollard Mound (Töneböhn, 1991). For abbreviations of marker beds see Fig. 18.

(Fig. 18), the channel-bounding drift formed by: (i) a preferred deposition of coarse-grained contourites (FA3 and FA4 >50%); (ii) a slightly increased cumulative sediment thickness; and in spite of (iii) a more fragmentary sediment accretion due to longer breaks in accumulation (Fig. 19A). Within the channel, merely coarse-grained contourites of FA4 were deposited intermittently and locally, such as during the middle Frasnian at Mech Irdane (Fig. 1C) (Aboussalam, 2003). Thus, the channel remained open until the late Frasnian due to persistent strong bottom currents, which caused sediment bypassing and erosion.

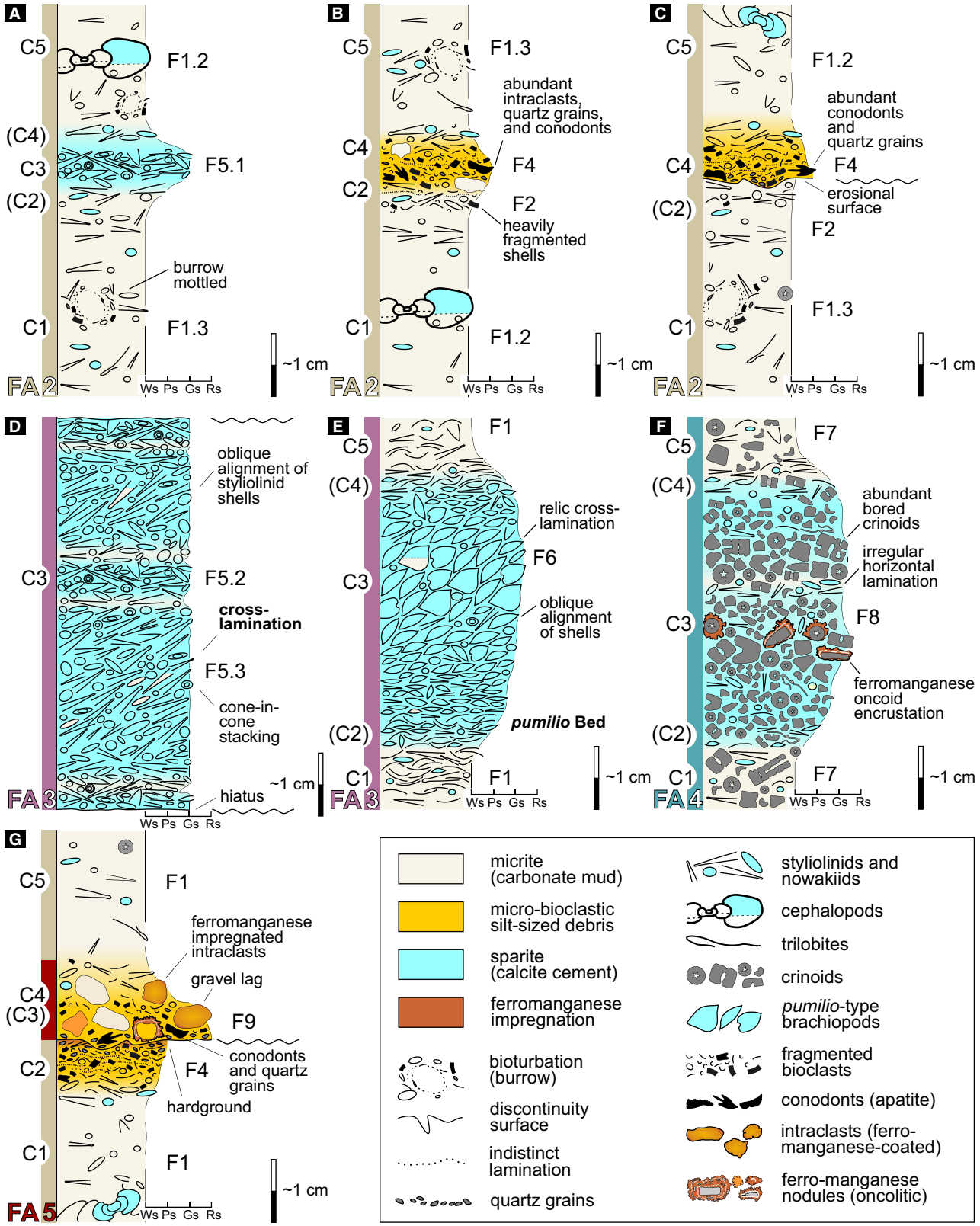

Fig. 21. Characteristic contourite facies sequences exemplifying bottom-current controlled carbonate accumulation on the Tafilalt Platform. (**A**) Bi-gradationally graded C1–(C2)–C3–(C4)–C5 sequence with styliolinid packstone (FA2). (**B**) Bi-gradationally graded C1–C2–C4–C5 sequence with micro-bioclast packstone (FA2). (**C**) Discontinuous C1–(C2)/(C4)–C5 sequence with erosional surface and normally graded upper part (FA2). (**D**) Hiatus-bounded, mid-only C3 contourite division of styliolinid grainstone, cross-laminated (FA3). (**E**) Bi-gradationally graded C1–(C2)–C3–(C4)–C5 sequence with cross-laminated brachiopod rudstone (FA3). (**F**) Bi-gradationally graded C1–(C2)–C3–(C4)–C5 sequence with laminated crinoid rudstone (FA4). (**G**) Discontinuous bi-gradational C1–C2/(C3)–C4–C5 sequence with erosional surface, hardground and central gravel lag (FA5). Depositional texture: Ws, wackestone; Ps, packstone; Gs, grainstone; Rs, rudstone. C2 and C4 intervals characterized by depositional textures of wackestone–packstone with a mean grain size of silt, but mainly consisting of micrite and sand-sized bioclasts, are designated in brackets.

An erosional truncation, such as the one associated with the basal-Frasnian hiatus at Jebel Ihrs and the locations further south (BFH in Figs 17B and 19A), is used as a main criterion to identify contourite channels (Hernández-Molina *et al.*, 2008; García *et al.*, 2009; Rebesco *et al.*, 2014; Miramontes *et al.*, 2021). Such channels can be oriented along-slope, or sinuous and oblique relative to the slope. They have been described as second-order drift features from contourite depositional systems of the eastern Gulf of Cadiz (García *et al.*, 2009; Hernández-Molina *et al.*, 2014; de Castro *et al.*, 2020b) and the Mozambique margin (Thiéblemont *et al.*, 2019; Miramontes *et al.*, 2020). In both cases, the contourite channels are bounded downslope by a small and low-mounded drift or a levée.

Basin-scale features

The interpretation of the Eifelian–Frasnian succession as deposits on a contourite terrace at the upper continental slope of Gondwana is supported by the coeval occurrence of contourite depositional and erosional features in other deep-sea domains between Gondwana and Laurussia (Oczlon, 1990; Hüneke, 2006), like the Harz, the Carnic Alps and the Moroccan Meseta (Fig. 22A), which represent parts of the Rhenish Sea shelf, the intra-Alpine terrane and the Meguma terrane (Stampfli *et al.*, 2013). This basin-wide co-occurrence indicates an overarching palaeoceanographic process as the driving mechanism behind the sediment redistribution. In all areas, the current velocities reached a maximum during the late Givetian and early Frasnian causing widespread submarine erosion and, more locally, the accumulation of coarse-grained contourites (Hüneke, 2007, 2013). Aboussalam & Becker (2011) demonstrated for the global Taghanic Biocrisis that hiatuses may reflect simultaneous erosional or non-depositional episodes in deep-marine environments of different continental margins, indicating hydrodynamic events driven by global circulation rather than regional processes.

Global palaeogeographic and plate-tectonic models show that the intensified circulation during the Givetian–Frasnian influenced different ocean basins, including the distal passive margin of Laurussia, isolated terranes (Galatian and Hanseatic terrane assemblage) and the disintegrated northern continental margin of Gondwana (see Golonka, 2002; Stampfli *et al.*, 2011, 2013; von Raumer *et al.*, 2016). The main driver of this intensified palaeocirculation is the constriction of deep-marine gateways due to the continuous convergence between Gondwana and Laurussia (Hüneke, 2006).

DISCUSSION

Hydraulic behaviour of bioclastic grains

The hydrodynamic interpretation of the Devonian bioclastic contourite sequences is mainly based on the variation in the ratio between carbonate mud and skeletal grains (Fig. 21, Table 2). Grain-size variations should be interpreted with caution because a series of studies in carbonate-dominated settings have demonstrated that grain properties, such as shape and density, also control the threshold of initiation of motion and affect the terminal settling velocity (e.g. Maiklem, 1968; Braithwaite, 1973; Flemming, 2017; de Kruijf *et al.*, 2021). The conical styliolinid shells possess different buoyancy and settling trajectories than platy brachiopods and spherical crinoids, or the contemporaneous siliciclastics. Consequently, sediment transport not only results in progressive size-sorting but also shape-sorting (Flemming, 2017). This feature is

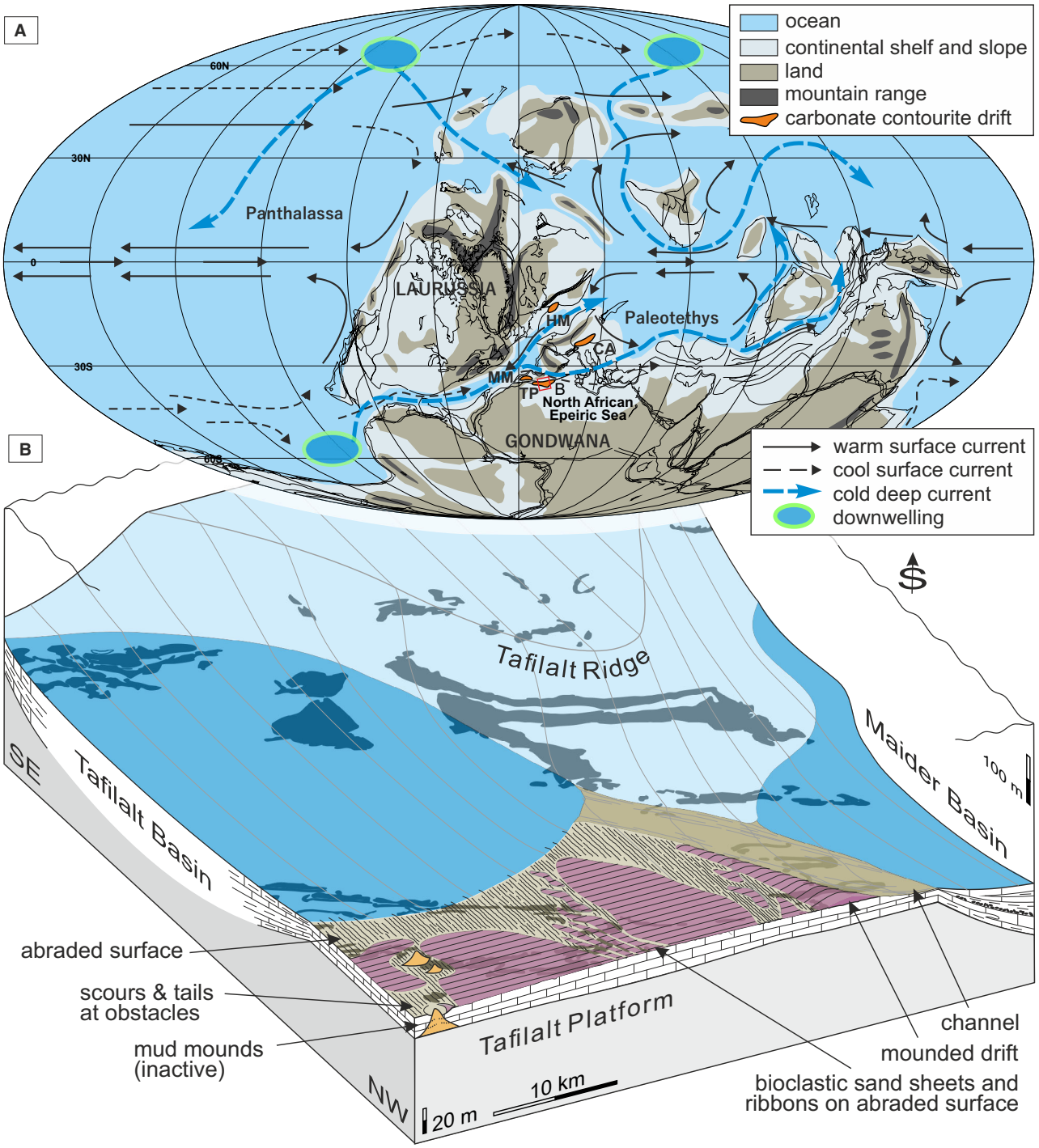

Fig. 22. Givetian–Frasnian palaeogeography. (**A**) Reconstruction of Golonka (2002) showing expected pattern of ocean circulation (modified from Hüneke, 2006; Crasquin & Horne, 2018), downwelling sites (de Vleeschouwer *et al.*, 2014), and deep-marine gateways between Gondwana and Laurussia (map provided by Kiessling, 2002). Bioclastic contourite drifts: HM, Harz Mountains; CA, Carnic Alps; MM, Moroccan Meseta; TP, Tafilalt. The western part of the North African Epeiric Sea comprises the Reggane, Ahnet, Mouydir, Illizi and Ghadames basins. (**B**) Contourite erosional and depositional features on the Tafilalt Platform during the early Frasnian. The palaeogeographic context of platforms and basins (see Fig. 1B) is adapted from Wendt *et al.* (1984), Wendt & Aigner (1985) and Belka & Wendt (1992). Eifelian–Frasnian sediment thickness, contourite morphological features and water depth are shown at different scales. The depth of the contourite terrace is estimated at 200 to 300 m water depth. Dark-grey areas are the locations of Devonian outcrops.

ascribed to the higher drag effect, i.e. higher resistance to motion, of irregularly shaped particles. Differences in particle shape can thus lead to progressive separation and selective concentration of individual shape groups in different lateral and vertical positions within a deposit (Flemming, 2017; de Kruijf *et al.*, 2021).

The effective density of the ubiquitous styliolinid shells, plugged with water by capillary force, varies between 1.4 g cm^{-3} and 1.6 g cm^{-3} (Hladil *et al.*, 1991). Lottmann (1990) estimated that the settling velocity of whole styliolinid shells is equivalent to that of quartz spheres of a diameter approximately four times less than the maximum length of the conical test, whereby large variations from this mode occur resulting from the percentage of mud-filled shells. Complete beds of styliolinid packstone to grainstone (F5), accordingly, typically show a grain size of medium to very coarse sand, and therefore are comparable to sediments dominated by very fine to fine-grained quartz sand. Current speeds between 19 cm s^{-1} and 23 cm s^{-1} were calculated for the mobilization of such styliolinid-rich coquinas (Hüneke, 2013).

Depositional setting

Contourite terraces, which are considered to result from sedimentary processes varying between deposition and erosion (Ercilla *et al.*, 2016; Miramontes *et al.*, 2021), are a sedimentary environment known primarily from modern continental slopes (Viana & Faugéres, 1998; Mutti *et al.*, 2014; Llave *et al.*, 2015; Hernández-Molina *et al.*, 2017; Eberli & Betzler, 2019; Thiéblemont *et al.*, 2019; de Castro *et al.*, 2021; Wilckens *et al.*, 2021). The Moroccan Tafilalt Platform is identified as part of such a mixed (depositional/erosional) system positioned at the uppermost slope off the North African Epicontinental Sea (Fig. 22A) (for example, Reggane, Ahnet, Ghadames basins; Lüning *et al.*, 2004; Soua, 2014). Bed-scale and drift-scale features show that the flow conditions varied between tranquil (for example, C1–C2–C4–C5 contourite sequences of FA2) and vigorous (for example, C3–C4–C5 sequences with a sharp erosive base and stand-alone C3 intervals of FA3, FA4 and FA5). From the Eifelian to the middle Givetian, long periods with continuous sediment accumulation at overall low accumulation rates alternated with times of winnowing and reworking (prevailing FA1 and FA2 in Fig. 3, Table 2). As of the late Givetian to middle Frasnian, sediment accumulation became increasingly interrupted by bottom-current induced winnowing and reworking over longer periods of time (see FA3, FA4 and FA5, and abundant erosional surfaces in Figs 3 to 5). During early–mid Frasnian, long-lasting periods of non-deposition and even erosion occurred (compare biostratigraphic gaps in Fig. 2 and Figs 17 to 20).

The bathymetric position of major water-mass interfaces and their vertical variations in time are known to exert primary control on the configuration of contourite terraces, including morphological changes along the slope gradient (Hernández-Molina *et al.*, 2009, 2016a,b; Preu *et al.*, 2013; Llave *et al.*, 2015; Ercilla *et al.*, 2016; Steinmann *et al.*, 2020; Miramontes *et al.*, 2021; Wilckens *et al.*, 2021). In addition, density contrasts are important components of these water-mass interfaces. So far, however, very few facies criteria have been developed to characterize the effects of the various palaeoceanographic processes on sedimentation and terrace formation.

In the succession studied, contourites with widespread shell concentrations, mainly planktonic and nektonic organisms (F4, F5), evidence periods of increased hydrodynamic agitation due to a position of the water-mass interface close to the water depth of the Tafilalt Platform (Fig. 23). The formation of such contourite terraces is attributed to strong along-slope currents (Miramontes *et al.*, 2019, 2020) and turbulent hydrodynamic processes at the density gradient (Hernández-Molina *et al.*, 2009; Steinmann *et al.*, 2020), which may cause widespread sediment reworking even when both geostrophic currents flow in the same direction. The contourite channel identified at the southern margin of the Tafilalt terrace, agrees with the observation that vigorous currents are observed only in the inner (landward) part of the contourite terraces, while the central and external (basinward) parts are affected by weaker bottom currents (Wilckens *et al.*, 2021). Extensive hiatuses and lag deposits (F9) were caused in periods of a downward shifting water-mass interface or accelerating geostrophic currents, while mud-rich contourites and pelagites (F1 and F2) were deposited in periods of an upward shifting interface or decelerating currents.

Internal waves and tidal waves are secondary processes that may influence sedimentation on contourite terraces (Hernández-Molina *et al.*, 2009, 2016b; Preu *et al.*, 2013; Ercilla *et al.*, 2016; Yin *et al.*, 2019; Llave *et al.*, 2020). Comparable processes were identified in deep-marine dunes along the Jurassic South–Iberian margin (Pomar *et al.*, 2012, 2019) and in a contourite channel of

the Miocene Rifian corridor (de Weger *et al.*, 2021). In the Devonian succession, however, sedimentary features indicative of oscillatory flows were not observed.

In carbonate systems, where terraces are often the result of drowned and back-stepped platform margins (e.g. Mullins & Neumann, 1979; Schlager, 1981; Rankey & Doolittle, 2012; Betzler *et al.*, 2016; Courgeon *et al.*, 2016), current-induced seafloor cementation together with the precipitation of ferromanganese crusts and phosphates have been described as important processes influencing the impact of hydrodynamic processes that form contourites (Kenter *et al.*, 2001; Heck *et al.*, 2004; Eberli *et al.*, 2010; Chabaud *et al.*, 2016; Föllmi, 2016; Wunsch *et al.*, 2017; Eberli & Betzler, 2019). As of the abundant mud intraclasts and ferromanganese nodules in many of the Devonian facies types (F2, F3, F4 and F9), similar conditions can be assumed for the Tafilalt terrace.

The contourite interpretation outlined above contradicts previous assumptions of frequent and widespread sediment redistribution by storm waves (Wendt *et al.*, 1984; Wendt, 1989, 1995; Wendt & Belka, 1991; Lubeseder *et al.*, 2010). The main arguments in favour of a periodic deposition from bottom currents opposing event deposition from storm-generated oscillatory flows and combined flows are: (i) the frequent integration of coquinas into bi-gradational sequences instead of exclusively normally-graded event beds; (ii) features of syndepositional bioturbation instead of post-depositional burrowing; (iii) the bioclastic composition corresponding to the interbedded pelagic sediments; (iv) the absence of particles with a shallow-water origin; (v) the close association of shell and intraclast concentrations with hardgrounds; and (vi) the absence of hummocky cross-stratification and oscillation ripples. These characteristics also allow to differentiate basecut-out (normally graded) contourite sequences from fine-grained turbidites, which usually show post-depositional burrowing, grain compositions contrasting with the host sediment, an erosional base without features of a long-lasting break in sedimentation, and turbidite-specific facies sequences (see Stow & Shanmugam, 1980; Stow & Smillie, 2020).

The palaeoenvironment of contourites is generally interpreted as deep marine (Fig. 22B), since contourite terraces are commonly found on the upper and middle slopes (Hernández-Molina *et al.*, 2008; Preu *et al.*, 2013; Miramontes *et al.*, 2021) and on the outer shelves (Eberli & Betzler, 2019). This interpretation agrees with the absence of light-dependent benthic organisms such as photosymbiotic colonial corals, stromatoporoids and calcareous algae within both the carbonate contourites and the interbedded pelagic limestones. Their absence suggests that the sediments were deposited in the aphotic zone, which comprises parts of the deep shelf and the deep-sea bottom further downslope (Flügel, 2010). The frequent preservation of complete goniatite shells, which have a calculated implosion depth of <300 m (Hewitt, 1996), provides a lower water-depth limit and implies terrace formation on the deep shelf or on the uppermost slope (200–300 m).

The basin-ridge topography in the eastern Anti-Atlas is basically the result of tectonic processes and differential subsidence that increased as of the early Eifelian (Wendt, 1985, 2021a; Baidder *et al.*, 2008; Lubeseder *et al.*, 2010). The documented morphosedimentary features indicate a distinct influence of bottom currents and associated palaeoceanographic processes. On the Tafilalt Platform, bioclastic contourites and pelagites formed a contourite terrace and gave way to a thin series of partially condensed carbonates (10–30 m). A much thicker Eifelian–Frasnian succession is known from the Maider, Tafilalt and Rheris basins, which preserve the sediments deposited further downslope in the west, east and north, respectively (Fig. 22B). As an example, the stratal record on the slope towards the Maider Basin is up to 350 m thick (Ottara section) and correlates with more than 600 m thick deposits in the central part of the basin (Bou Dib section) (Hollard, 1974; Wendt *et al.*, 1984; Döring & Kazmierczak, 2001; Döring, 2002; Lubeseder *et al.*, 2010).

A thicker Eifelian–Frasnian succession is also preserved on the Tafilalt Ridge in the south of the Tafilalt Platform (Wendt *et al.*, 1984; Lubeseder *et al.*, 2010; Klug & Pohle, 2018). The succession with nodular limestones, peloid-rich laminated limestones, marls and claystones, as well as normally-graded limestone beds, coral-rich conglomerates and quartziferous deposits thickens upslope from 80 m (Bou Maiz Syncline) to locally 400 m (Amessoui Syncline) (Fig. 23). The spur-like upslope area, rich in gravity-flow deposits, connects the Tafilalt Platform with a shallow-water carbonate factory with hermatypic corals and stromatoporoids, possibly connected with the Maider Platform further to the south-west (Döring & Kazmierczak,

2001; Döring, 2002) (Fig. 22B). Palaeocurrent measurements from turbidites (cross-lamination) and the orientation of slump folds (fold planes) indicate a predominant north-west-directed sediment transport, i.e. parallel to the spur of the Tafilalt Ridge (Lubeseder *et al.*, 2010). Latter authors also identified iron-rich hardgrounds on the Tafilalt Ridge that could be correlated with submarine hiatuses on the Tafilalt Platform. Together these sedimentary features suggest that the Tafilalt Ridge was less affected by winnowing, reworking, non-deposition and erosion when compared with the Tafilalt Platform. The preserved sedimentary record is thicker, more complete, and the particle composition of the interbedded gravity-flow deposits signals a shallowing towards a euphotic depositional environment to the south.

Aforementioned regional features contradict the hypothesis of repeated storm-induced reworking and erosion of the carbonate muds as the main mechanism for condensed sediment deposition on the Tafilalt Platform (Wendt *et al.*, 1984; Wendt, 1989, 1995; Wendt & Belka, 1991; Lubeseder *et al.*, 2010). In general, there is no empirical basis in assuming any particular bimodal separation in the size of fair-weather and storm waves, or in the manifestation of such differences in the sedimentary record (Peters & Loss, 2012). In addition, storm waves and associated combined flows are most severe in shallow water and less intense in deeper parts of the shelf. Incomplete successions with erosional surfaces as numerous tempestites mark proximal (shallow) settings and more complete records with less-abundant, non-erosive tempestites prevail in distal (deep) settings (Duke, 1990; Myrow & Southard, 1991, 1996; Seilacher & Aigner, 1991; Einsele, 2000; Jelby *et al.*, 2020). The distribution of shell concentrations and hiatuses on the Tafilalt Platform and the Tafilalt Ridge contradicts the aforementioned depth relationship.

A contourite terrace provides a more adequate depositional model for the Tafilalt Platform. Above and below the bathymetric level of the interrelated water-mass interface, hydrodynamic effects are less intense and, thus, sediment deposition is more continuous and occurs at a higher accumulation rate, frequently giving way to plastered contourite drifts (Fig. 23). The styliolinid coquinas identified in the successions above (Tafilalt Ridge) and below (Maider and Tafilalt basins) the bathymetric level of the Tafilalt Platform (Fig. 22B) are probably part of contourite drifts formed under mainly depositional conditions.

At the south-western (upslope) edge of the Tafilalt contourite terrace, an erosional channel was formed during the early Frasnian, flanked (downslope) by a small mounded drift rich in bioclastic coarse-grained contourites (Fig. 23). Such erosional elements are often associated with the main current-cores of dense water masses, which are usually adjusted parallel to the isobaths (e.g. McCave & Tucholke, 1986; Faugères *et al.*, 1999; Rebesco & Stow, 2001; Stow *et al.*, 2002, 2009; Rebesco & Camerlenghi, 2008; Faugères & Mulder, 2011).

Energetic bottom currents and oxygen restriction

The organic-rich coquinas classified as FA3 (Table 3) formed simultaneous to Devonian biotic crises (Lottmann, 1990; Ebert, 1993; Walliser, 1996; Aboussalam & Becker, 2011; Becker *et al.*, 2016) and their depositional conditions are of key importance for palaeoceanographic reconstructions. These coarse-grained contourites are interpreted to result from energetic bottom currents of a mostly anoxic water mass, because bioturbation in these beds is absent or sparse (BI 0–1). The morphology and size distribution of framboidal pyrites (and microcrystals) reflects syngenetic and rarely early-diagenetic formation (Sagemann *et al.*, 1991; Wignall, 1994, 2005; Wilkin & Barnes, 1997; Uchman & Wetzel, 2011). These pyrites (Fig. 14) that occur in most investigated organic-rich coquinas (for example, LpB, UpB, LSty, USty and LRh in Fig. 2) are indicative of anoxic conditions (Wilkin *et al.*, 1996; Liu *et al.*, 2019). The FA3 deposits are organic-rich (Table 3) and characterize conditions of enhanced organic-carbon burial, especially because the analysed samples are from shell concentrations with very low proportions of carbonate mud (Figs 12 and 13). Organic matter is preferentially transported as suspension load and occurs concentrated in fine-grained sediments, because most organic particles are hydrodynamically equivalent to clay-grade and silt-grade particles (Tyson, 1987).

The TOC contents measured in outcrop agree with values identified in borehole samples from Frasnian petroleum source rocks in the Ghadames Basin (0.8 to 2.8%, Riboulleau *et al.*, 2018). In this basin and other parts of the spacious epicontinental sea of North Africa (Fig. 22A), organic matter accumulation was temporarily widespread during the

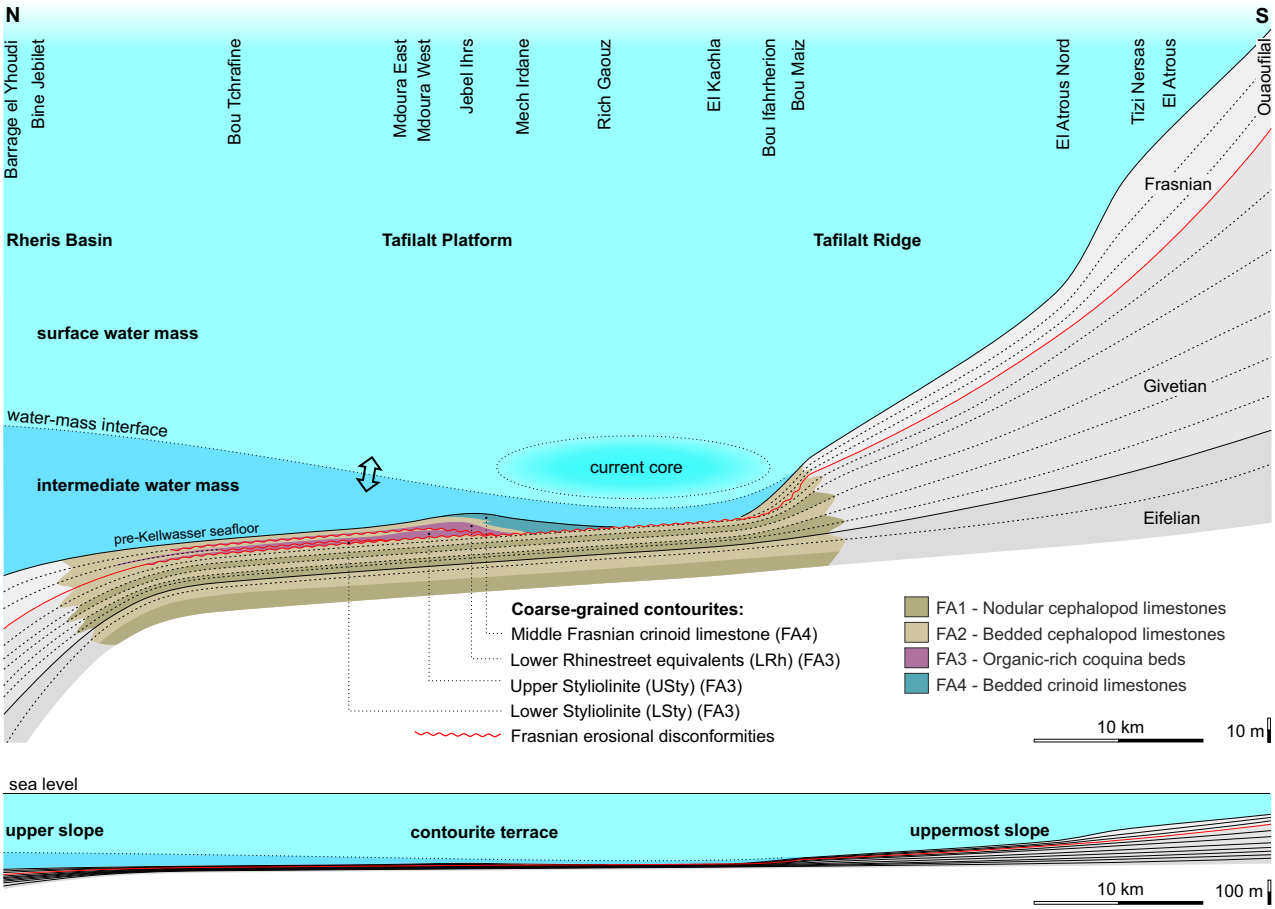

Fig. 23. Schematic north–south cross-section of the Tafilalt Platform displaying thickness variation of the Eifelian–Frasnian lithologies, palaeogeographic interpretation and inferred water-mass interface during the middle Frasnian (compare Fig. 1C). The partially condensed succession between Bou Tchrafine and El Kachla mainly shows a sheeted architecture. Frasnian carbonates display a small mounded drift at Mdoura and Jebel Ihrs, which is recognized at the downslope margin of a channel located further south. The distribution of FA1 and FA2 is shown schematically. Sediment thicknesses from Wendt & Belka (1991), Klug (2002), Aboussalam (2003), Aboussalam & Becker (2007), Lubeseder *et al.* (2010), publications in Becker *et al.* (2013), Hartenfels *et al.* (2018) and own data.

Frasnian and early Famennian, resulting in organic-rich shales and limestones, in part >200 m thick and TOC values of up to 14%, the so-called hot shales (Lüning *et al.*, 2003, 2004; Soua, 2014). Sections studied at the margin of the Ahnet Basin indicate the presence of a major anoxic phase during Frasnian conodont zones MN1–2 and shortly thereafter (Lüning *et al.*, 2004). For the same time interval, this study documents the formation of erosional disconformities and organic-rich coarse-grained contourite beds (FA3) on the Tafilalt Platform. Based on this stratigraphic correlation, Lüning *et al.* (2003) inferred the formation of an oxygen minimum zone that expanded during the early Frasnian at the upper continental slope and inundated the shelf with oxygen-poor water masses.

The organic-carbon enrichment in styliolinid coquinas on the Tafilalt Platform was interpreted to result from either episodically enhanced primary productivity (regional plankton blooms, enabling blooms of planktonic dacryoconarids and plankton-feeding brachiopods), or the presence of an oxygen-minimum zone (Wendt & Belka, 1991; Lüning *et al.*, 2003; Aboussalam & Becker, 2011). Such increased supply and burial of organic matter, however, does not necessarily signify deposition under tranquil and stagnant anoxic conditions. Intensified currents preferentially operating at water-mass boundaries may be closely associated with conditions of pronounced oxygen-minimum zones. The Namibian continental margin provides an example (Hanz *et al.*, 2019), where

the relatively sharp upper boundary of the oxygen-minimum zone (150–200 m below sea level) corresponds with the interface between the South Atlantic Subtropical Surface Water at the surface and South Atlantic Central Water below.

A similar ocean stratification and combination of environmental conditions is assumed for the organic-rich facies of styliolinid and brachiopod coquinas (FA3), which result from deposition with increased hydrodynamic energy from an anoxic water mass rich in particulate organic matter. The main evidence includes: (i) grain-supported depositional texture; (ii) layer-specific distinct orientation patterns of styliolinid cones; (iii) monomict composition of well to very-well sorted bioclastic particles and the partial or complete lack of interstitial carbonate mud; (iv) frequent cone-in-cone stacking of the shells; (v) current-ripple cross lamination; and (vi) parallel lamination; together with (vii) aggregations of organic matter within skeletal grains and carbonate mud; (viii) syngenetic framboidal pyrites; and (ix) absent to sparse bioturbation. The identified hiatuses and gravel lags, which may occur at the base and the top of those beds, are additional criteria for a vigorous bottom current, supporting this interpretation.

An unclear aspect of the contourite interpretation of the *pumilio*-type brachiopod coquinas (F6) is their composition. The predominant brachiopod shells must have been supplied from a source outside the Tafilalt Platform, since these shells are not found within the host succession, and their provenance is unknown. A possible source area were hemipelagic outer-shelf sediments rich in *pumilio*-type brachiopod colonies, preserved in the Dra Valley west of the Tafilalt (Ebbighausen *et al.*, 2004, 2011).

CONCLUSIONS

This study identified the Moroccan Tafilalt Platform as part of a contourite depositional system at the uppermost slope that connects the Gondwana mainland with the Meseta domain further north. The bioclastic carbonate drift is one of the rare fossil analogues of modern carbonate contourites that was formed under greenhouse climate conditions. The contourite interpretation is based on independent lines of evidence at the microfacies, bed, drift and basin scale.

The microfacies reflects repeated changes between suspension deposition, sediment bypassing, winnowing of fines, bedload traction and erosion, together with concomitant seafloor cementation. Shell concentrations (coquinas) of mainly planktonic and nektonic organisms are identified as integral parts of bi-gradational contourite sequences showing inverse and normal grading as a result of gradual variation in mean grain size, depositional texture and degree of shell fragmentation. Coquinas with whole shells constitute the C3 intervals of contourite sequences, as coquinas made up of heavily fragmented shells represent the C2 and C4 intervals. Hiatal lag concentrations of carbonate intraclasts, ferromanganese nodules and conodonts drape hardgrounds and erosional surfaces. These lag deposits contain mechanically robust shells and highly fragmented less robust shells, which result from current-induced mechanical erosion. Widespread shell-in-shell structures and layer-specific orientation patterns of the conical styliolinid shells display unidirectional flow behaviour of varying direction and speed.

The bedsets of calcareous muddy to sandy contourites (wackestone to grainstone) form coarsening-up and fining-up sequences, and display long-term increasing and decreasing current velocities. Traction structures preserved in organic-rich contourites evidence current-induced bedload transport mostly under subcritical flow conditions. Ferromanganese and calcareous gravel-lag contourites (rudstone to packstone) often drape hardgrounds and erosional surfaces that coincide with biostratigraphic gaps, suggesting very low net accumulation rates at moderate to strong current speeds.

At the drift scale, the overall sheeted architecture of the Eifelian–Frasnian succession results from an interplay between depositional and erosional processes on a contourite terrace that presumably constitutes the thin upslope part of a larger plastered drift. Abraded surfaces and sandy condensation layers are most widespread in the late Givetian to middle Frasnian part of the drift. Obstacle scours and tails occur in the vicinity of closely associated carbonate mud mounds. The upper contourite terrace is characterized by a Frasnian contourite channel and a small mounded drift at its downslope margin, which are oriented quasi-parallel to the continental slope.

The coeval occurrence of contourite depositional and erosional features in other areas of the oceanic domain between Gondwana and Laurussia indicates an overarching palaeoceanographic process driving sediment redistribution. Individual hiatuses and coarse-grained contourites can be linked to synchronous contourite deposits on the Laurussian continental margin.

Devonian global evolutionary events and crises, known to be linked to widespread deposition of organic-carbon-rich sediments in outer shelf settings, relate to the formation of coarse-grained contourites and hiatuses, both indicating intensified bottom-current dynamics. The coincidence of intensified thermohaline deep-marine circulation with hypoxic and anoxic conditions, affecting individual basins and perhaps even spreading into the ocean, point to common palaeoceanographic causes.

ACKNOWLEDGEMENTS

The financial and logistical support of the *Deutsche Forschungsgemeinschaft* (DFG) is gratefully acknowledged. This study received funding from and contributes to the DFG-project "Devonian contourites in oceanic passageways between Gondwana and Laurussia" (HU 804/8-1). We would also like to thank Ahmed Benlakhdim, Directeur de la Géologie (Ministère de l'Energie, des Mines et de l'Environnement, Maroc), for field work permission and advice, and Aissam El Khlifi, Chef de la Division des Infrastructures de Géologiques Maroc, for export permission of rock samples. We thank Torsten Haberzettl and Mike Steinich for the organic-carbon measurements. Special thanks go to Sylvia Weinert, for her careful and meticulous preparation of the excellent thin sections. We gratefully acknowledge Michael Böttcher, Georg Grathoff and Markus Peltz for discussions, scientific input and analytical support. We thank Marie-Elaine van Egmond for correcting our English and helping us to focus our statements. The authors are grateful to the editor Alexander Brasier, the handling editor John Reijmer and the anonymous reviewers of a first and a revised manuscript version for their valuable comments, which greatly improved the publication. Open Access funding enabled and organized by Projekt DEAL.

DATA AVAILABILITY STATEMENT

Data available on request from the authors.

REFERENCES

Aboussalam, Z.S. (2003) Das "Taghanic-Event" im höheren Mittel-Devon von West-Europa und Marokko. *Münstersche Forschungen zur Geologie und Paläontologie*, **97**, 1–332.

Aboussalam, Z.S. and **Becker, R.T.** (2007) New upper Givetian to basal Frasnian conodont faunas from the Tafilalt (Anti-Atlas, Southern Morocco). *Geol. Quarterly*, **51**, 345–374.

Aboussalam, Z.S. and **Becker, R.T.** (2011) The global Taghanic Biocrisis (Givetian) in the eastern Anti-Atlas, Morocco. *Palaeogeogr. Palaeoclimatol. Palaeoecol.*, **304**, 136–164.

Abram, M.B. and **Holz, M.** (2020) Early to Middle Devonian ironstone and phosphorite in the northwestern Gondwana Parnaíba Basin, Brazil: a record of an epeiric margin paleoceanographic changes. *Sed. Geol.*, **402**, 105646.

Accotto, C., **Poyatos, D.M.**, **Azor, A.**, **Talavera, C.**, **Evans, N.J.**, **Jabaloy-Sánchez, A.**, **Azdimousa, A.**, **Tahiri, A.** and **El Hadi, H.** (2021) Syn-collisional detrital zircon source evolution in the northern Moroccan Variscides. *Gondwana Res.*, **93**, 73–88.

Aitken, S.A., **Collom, C.J.**, **Henderson, C.M.** and **Johnston, P.A.** (2002) Stratigraphy, paleoecology, and origin of Lower Devonian (Emsian) carbonate mud buildups, Hamar Laghdad, eastern Anti-Atlas, Morocco. *Africa. Bull. Can. Petrol. Geol.*, **50**, 217–243.

Allen, J.R.L. (1984) Sedimentary structures: their character and physical basis. *Dev. Sedimentol.*, **30**, 1–663.

Ashley, G. (1990) Classification of large-scale subaqueous bedforms: a new look at an old problem. *J. Sed. Petrol.*, **60**, 160–172.

Baccelle, L. and **Bosellini, A.** (1965) Diagrammi per la stima visiva della composizione percentuale nelle rocce sedimentarie. *Ann. Univ. Ferrara, N.S., Sez. IX, Sci. Geol. Paleont.*, **1**, 59–62.

Baidder, L., **Raddi, Y.**, **Tahiri, M.** and **Michard, A.** (2008) Devonian extension of the Pan-African crust north of the West African Craton and its bearing on the Variscan foreland deformation: evidence from eastern Anti-Atlas (Morocco). In: *The Boundaries of the West African Craton* (Eds Ennih, N. and Liégeois, J.P.), *Geol. Soc. London Spec. Publ*, **297**, 453–465.

Baidder, L., **Michard, A.**, **Soulaimani, A.**, **Fekkak, A.**, **Eddebbi, A.**, **Rjimati, E.-C.** and **Raddi, Y.** (2016) Fold interference pattern in thick-skinned tectonics; a case study from the external Variscan belt of Eastern Anti-Atlas, Morocco. *J. Afr. Earth Sci.*, **119**, 204–225.

Becker, R.T. and **House, M.R.** (1994) International Devonian goniatite zonation, Emsian to Givetian, with new records from Morocco. *Courier Forschungsinstitut Senckenberg*, **169**, 79–135.

Becker, R.T. and **House, M.R.** (2000) Devonian ammonoid succession at Jbel Amelane (Western Tafilalt, Southern Morocco). *Notes et Mém. Serv. Géol. Maroc*, **399**, 49–56.

Becker, R.T. and **Kirchgasser, W.T.** (2007) Devonian events and correlations. *Geol. Soc. London Spec. Publ.*, **278**, 1–299.

Becker, R.T., **El Hassani, A.** and **Tahiri, A.** (2013) The Devonian and lower Carboniferous of northern Gondwana, international field symposium, field guidebook. *Document de l'Institut Scientifique Rabat*, **27**, 1–150.

Becker, R.T., **Königshof, P.** and **Brett, C.E.** (2016) Devonian climate, sea level and evolutionary events: an introduction. *Geol. Soc. London Spec. Publ.*, **423**, 1–10.

Becker, R.T., **Marshall, J.E.A.**, **Da-Silva, A.-C.**, **Agterberg, F.P.**, **Gradstein, F.M.** and **Ogg, J.G.** (2020) The devonian period. In: *Geological Time Scale 2020* (Eds Gradstein, F.M., Ogg, J.G., Schmitz, M.D. and Ogg, G.M.), Vol. **2**, pp. 733–810. Elsevier, Amsterdam.

Belka, Z. (1991) Conodont colour alteration patterns in Devonian rocks of the eastern Anti-Atlas, Morocco. *J. Afr. Earth Sci.*, **12**, 417–428.

Belka, Z. (1998) Early Devonian Kess-Kess carbonate mud mounds of the eastern Anti-Atlas (Morocco), and their relation to submarine hydrothermal venting. *J. Sediment. Res.*, **68**, 368–377.

Belka, Z. and **Wendt, J.** (1992) Conodont biofacies patterns in the Kellwasser facies (upper Frasnian/lower Famennian) of the eastern Anti-Atlas, Morocco. *Palaeogeogr. Palaeoclimatol. Palaeoecol.*, **91**, 143–173.

Belka, Z., **Kaufmann, B.** and **Bultynck, P.** (1997) A conodont-based quantitative biostratigraphy for the Eifelian of the eastern Anti-Atlas, Morocco. *Geol. Soc. Am. Bull.*, **109**, 643–651.

Belka, Z., **Klug, C.**, **Kaufmann, B.**, **Korn, D.**, **Döring, S.**, **Feist, R.** and **Wendt, J.** (1999) Devonian conodont and ammonoid succession of the eastern Tafilalt (Ouidane Chebbi section), Anti-Atlas, Morocco. *Acta Geol. Pol.*, **49**, 1–23.

Benninger, L.M. and **Hein, J.R.** (2000) Diagenetic evolution of seamount phosphorite. In: *Marine Authigenesis: From Global to Microbial* (Eds Glenn, C.R., Prévôt-Lucas, L. and Lucas, J.), *SEPM Spec. Publ*, **66**, 245–256.

Berner, R.A. (1984) Sedimentary pyrite formation: an update. *Geochim. Cosmochim. Acta*, **48**, 605–615.

Best, J. and **Bridge, J.** (1992) The morphology and dynamics of low amplitude bedwaves upon upper stage plane beds and the preservation of planar laminae. *Sedimentology*, **39**, 737–752.

Betzler, C., **Lüdmann, T.**, **Hübscher, C.** and **Fürstenau, J.** (2013) Current and sea-level signals in periplatform ooze (Neogene, Maldives, Indian Ocean). *Sed. Geol.*, **290**, 126–137.

Betzler, C., **Lindhorst, S.**, **Eberli, G.P.**, **Lüdmann, T.**, **Möbius, J.**, **Ludwig, J.**, **Schutter, I.**, **Wunsch, M.**, **Reijmer, J.J.G.** and **Hübscher, C.** (2014) Periplatform drift: the combined result of contour current and off-bank transport along carbonate platforms. *Geology*, **42**, 871–874.

Betzler, C., **Hübscher, C.**, **Lindhorst, S.**, **Lüdmann, T.**, **Reijmer, J.J.G.** and **Braga, J.-C.** (2016) Lowstand wedges in carbonate platform slopes (Quaternary, Maldives, Indian Ocean). *Deposit Rec.*, **2**, 196–207.

Betzler, C., **Eberli, G.P.**, **Alvarez Zarikian, C.A.**, **Alonso-García, M.**, **Bialik, O.M.**, **Blättler, C.L.**, **Guo, J.A.**, **Haffen, S.**, **Horozal, S.**, **Inoue, M.**, **Jovane, L.**, **Kroon, D.**, **Lanci, L.**, **Laya, J.C.**, **Ling Hui Mee, A.**, **Lüdmann, T.**, **Nakakuni, M.**, **Nath, B.N.**, **Niino, K.**, **Petruny, L.M.**, **Pratiwi, S.D.**, **Reijmer, J.J.G.**, **Reolid, J.**, **Slagle, A.L.**, **Sloss, C.R.**, **Su, X.**, **Swart, P.K.**, **Wright, J.D.**, **Yao, Z.** and **Young, J.R.** (2017) Expedition 359 summary. In: *Maldives Monsoon and Sea Level* (Eds Betzler, C., Eberli, G.P. and Zarikian, C.A.A.), *Proc. IODP*, **359**, 1–31.

Betzler, C., **Lindhorst, S.**, **Reijmer, J.J.G.**, **Braga, J.C.**, **Lüdmann, T.**, **Bialik, O.M.**, **Reolid, J.**, **Geßner, A.-L.**, **Hainbucher, D.** and **Bissessur, D.** (2023) Carbonate platform drowning caught in the act: the sedimentology of Saya de Malha Bank (Indian Ocean). *Sedimentology*, **70**, 78–99. https://doi.org/10.1111/sed.13032.

Blakey, R. (2016) Devonian - 370 Ma, global paleogeography and tectonics in deep time series. In: *Deep Time Maps™ Paleogeography*. Available at: https://deeptimemaps.com.

Bond, D., **Wignall, P.B.** and **Racki, G.** (2004) Extent and duration of marine anoxia during the Frasnian–Famennian (Late Devonian) mass extinction in Poland, Germany, Austria and France. *Geol. Mag.*, **141**, 173–193.

Brachert, T.C., **Buggisch, W.**, **Flügel, E.**, **Hüssner, H.M.**, **Joachimski, M.M.**, **Tourneur, F.** and **Walliser, O.H.** (1992) Controls of mud mound formation: the Early Devonian Kess-Kess carbonates of the Hamar Laghdad, Antiatlas, Morocco. *Geol. Rundsch.*, **81**, 15–44.

Brackenridge, R.E., **Stow, D.A.V.** and **Hernández-Molina, F.J.** (2011) Contourites within a deep-water sequence stratigraphic framework. *Geo-Mar. Lett.*, **31**, 343–360.

Brackenridge, R.E., **Stow, D.A.V.**, **Hernández-Molina, F.J.**, **Jones, C.**, **Mena, A.**, **Alejo, I.**, **Ducassou, E.**, **Llave, E.**, **Ercilla, G.**, **Nombela, M.A.**, **Perez-Arlucea, M.** and **Frances, G.** (2018) Textural characteristics and facies of sand-rich contourite depositional systems. *Sedimentology*, **65**, 2223–2252.

Braithwaite, C.J.R. (1973) Settling behaviour related to sieve analysis of skeletal sands. *Sedimentology*, **20**, 251–262.

Brett, C.E., **McLaughlin, P.I.**, **Histon, K.**, **Schindler, E.** and **Ferretti, A.** (2012) Time-specific aspects of facies: state of the art, examples, and possible causes. *Palaeogeogr. Palaeoclimatol. Palaeoecol.*, **367**, 6–18.

Bultynck, P. (1986) Accuracy and reliability of conodont zones: the Polygnathus asymmetricus "zone" and the Givetian-Frasnian boundary. *Bull. Inst. Roy. Sci. Nat. Belg.*, **56**, 269–280.

Bultynck, P. and **Walliser, O.H.** (2000) Emsian to Middle Frasnian sections in the northern Tafilalt. *Notes et Mém. Serv. Géol. Maroc*, **399**, 11–20.

Burkhard, M., **Caritg, S.**, **Helg, U.**, **Robert-Charrue, C.** and **Soulaimani, A.** (2006) Tectonics of the anti-atlas of Morocco. In: *Recent Developments on the Maghreb Geodynamics* (Eds de Lamotte, D.F., Saddiqi, O. and Michard, A.), *CR Geoscience*, **338**, 11–24.

Carmichael, S.K., **Waters, J.A.**, **Königshof, P.**, **Suttner, T.J.** and **Kido, E.** (2019) Paleogeography and paleoenvironments of the Late Devonian Kellwasser event: a review of its sedimentological and geochemical expression. *Global Planet. Change*, **183**, 102984.

de Castro, S., **Hernández-Molina, F.J.**, **Rodríguez-Tovar, F.J.**, **Llave, E.**, **Ng, Z.L.**, **Nishida, N.** and **Mena, A.** (2020a) Contourites and bottom current reworked sands: bed facies model and implications. *Mar. Geol.*, **428**, 106267.

de Castro, S., **Hernández-Molina, F.J.**, **de Weger, W.**, **Jiménez-Espejo, F.J.**, **Rodriguez-Tovar, F.J.**, **Mena, A.**, **Llave, E.** and **Sierro, F.J.** (2020b) Contourite characterisation and its discrimination from other deepwater deposits in the Gulf of Cadiz contourite depositional system. *Sedimentology*, **68**, 987–1027.

de Castro, S., **Miramontes, E.**, **Dorador, J.**, **Jouet, G.**, **Cattaneo, A.**, **Rodríguez-Tovar, F.J.** and **Hernández-Molina, F.J.** (2021) Siliciclastic and bioclastic contouritic sands: textural and geochemical characterisation. *Marine Petrol. Geol.*, **128**, 105002.

Chabaud, L., **Ducassou, E.**, **Tournadour, E.**, **Mulder, T.**, **Reijmer, J.J.G.**, **Conesa, G.**, **Giraudeau, J.**, **Hanquiez, V.**, **Borgomano, J.** and **Ross, L.** (2016) Sedimentary processes determining the modern carbonate periplatform drift of Little Bahama Bank. *Mar. Geol.*, **378**, 216–229.

Clerc, S., **Buoncristiani, J.-F.**, **Guiraud, M.**, **Vennin, E.**, **Desaubliaux, G.** and **Portier, E.** (2013) Subglacial to proglacial depositional environments in an Ordovician glacial tunnel valley, Alnif, Morocco. *Palaeogeogr. Palaeoclimatol. Palaeoecol.*, **370**, 127–144.

Copper, P. (1986) Frasnian/Famennian mass extinction and cold-water oceans. *Geology*, **14**, 835–839.

Copper, P. (2002) Silurian and Devonian reefs: 80 million years of global greenhouse between two ice ages. In:

Phanerozoic Reef Patterns (Eds Kiessling, W., Flügel, E. and Golonka, J.), *Soc. Sedim. Geol. Spec. Publ*, **72**, 181–239.

Correa, T.B.S., **Eberli, G.P.**, **Grasmueck, M.**, **Reed, J.K.** and **Correa, A.M.S.** (2012) Genesis and morphology of cold-water coral ridges in a unidirectional current regime. *Mar. Geol.*, **326–328**, 14–27.

Courgeon, S., **Jorry, S.J.**, **Camoin, G.F.**, **BouDagher-Fadel, M.K.**, **Jouet, G.**, **Révillon, S.**, **Bachèlery, P.**, **Pelleter, E.**, **Borgomano, J.**, **Poli, E.** and **Droxler, A.W.** (2016) Growth and demise of Cenozoic isolated carbonate platforms: new insights from the Mozambique Channel seamounts (SW Indian Ocean). *Mar. Geol.*, **380**, 90–105.

Craig, J., **Rizzi, C.**, **Said, F.**, **Thusu, B.**, **Luning, S.**, **Asbali, A.I.** and **Hamblett, C.** (2008) Structural styles and prospectivity in the Precambrian and Palaeozoic hydrocarbon systems of North Africa. *Geol. East Libya*, **4**, 51–122.

Crasquin, S. and **Horne, D.J.** (2018) The palaeopsychrosphere in the Devonian. *Lethaia*, **51**, 547–563.

Dalziel, I.W.D., **Dalla Salda, L.H.** and **Gahagan, L.M.** (1994) Paleozoic Laurentia-Gondwana interaction and the origin of the Appalachian-Andean mountain system. *Geol. Soc. Am. Bull.*, **106**, 243–252.

Davies, A.J., **Duineveld, G.C.A.**, **Lavaleye, M.S.S.**, **Bergman, M.J.N.**, **van Haren, H.** and **Roberts, J.M.** (2009) Downwelling and deep-water bottom currents as food supply mechanisms to the cold-water coral Lophelia pertusa (Scleractinia) at the Mingulay Reef Complex. *Limnol. Oceanogr.*, **54**, 620–629.

De Mol, B., **Van Rensbergen, P.**, **Pillen, S.**, **Van Herreweghe, K.**, **Van Rooij, D.**, **McDonnell, A.**, **Huvenne, V.**, **Ivanov, M.**, **Swennen, R.** and **Henriet, J.-P.** (2002) Large deep-water coral banks in the Porcupine Basin, southwest of Ireland. *Mar. Geol.*, **188**, 193–231.

Destombes, J., **Hollard, H.** and **Willefert, S.** (1985) Lower Palaeozoic rocks of Morocco. In: *Lower Palaeozoic Rocks of North-Western and West-Central Africa* (Ed. Holland, C.H.), pp. 91–336. John Wiley, Chichester.

Domeier, M. and **Torsvik, T.H.** (2014) Plate tectonics in the late Paleozoic. *Geosci. Frontiers*, **5**, 303–350.

Dopieralska, J. (2003) *Neodymiumisotopic Composition of Conodonts as a Palaeoceanographic Proxy in the Variscan Oceanic System*. PhD Thesis. Univ. Giessen, Giessen.

Dopieralska, J. (2009) Reconstructing seawater circulation on the Moroccan shelf of Gondwana during the Late Devonian: evidence from Nd isotope composition of conodonts. *Geochem. Geophys. Geosyst.*, **10**, Q03015.

Dopieralska, J., **Belka, Z.** and **Haack, U.** (2006) Geochemical decoupling of water masses in the Variscan oceanic system during Late Devonian times. *Palaeogeogr. Palaeoclimatol. Palaeoecol.*, **240**, 108–119.

Döring, S. (2002) *Sedimentological Evolution of the Late Emsian to Early Givetian Carbonate Ramp in the Maider (Eastern Anti-Atlas, SE-Morocco)*. PhD Thesis. Univ. Tübingen, Tübingen.

Döring, S. and **Kazmierczak, M.** (2001) Stratigraphy, geometry, and facies of a Middle Devonian ramp-to-basin transect (Eastern Anti-Atlas, SE Morocco). *Facies*, **44**, 137–150.

Dorschel, B., **Hebbeln, D.**, **Foubert, A.**, **White, M.** and **Wheeler, A.J.** (2007) Hydrodynamics and cold-water coral facies distribution related to recent sedimentary processes at Galway Mound west of Ireland. *Mar. Geol.*, **244**, 184–195.

Duan, T., **Gao, Z.**, **Zeng, Y.** and **Stow, D.** (1993) A fossil carbonate contourite drift on the Lower Ordovician palaeocontinental margin of the middle Yangtze Terrane, Jiuxi, northern Hunan, southern China. *Sed. Geol.*, **82**, 271–284.

Duineveld, G.C.A., **Lavaleye, M.S.S.**, **Bergman, M.J.N.**, **De Stigter, H.** and **Mienis, F.** (2007) Trophic structure of a cold-water coral mound community (Rockall Bank, NE Atlantic) in relation to the near-bottom particle supply and current regime. *Bull. Mar. Sci.*, **81**, 449–467.

Duke, W.L. (1990) Geostrophic circulation or shallow marine turbidity currents? The dilemma of paleoflow patterns in storm-influenced prograding shoreline systems. *J. Sed. Petrol.*, **60**, 870–883.

Dunham, R.J. (1962) Classification of carbonate rocks according to depositional texture. In: *Classification of Carbonate Rocks* (Ed. Ham, W.E.), *AAPG Mem*, **1**, 108–121.

Ebbighausen, V., **Bockwinkel, J.**, **Becker, R.T.**, **Aboussalam, Z.S.**, **Bultynck, P.**, **El Hassani, A.** and **Nübel, H.** (2004) Late Emsian and Eifelian stratigraphy at Oufrane (Tata region, eastern Dra Valley, Morocco). *Document de l' Institut Scientifique Rabat*, **19**, 44–52.

Ebbighausen, V., **Becker, R.T.** and **Bockwinkel, J.** (2011) Emsian and Eifelian ammonoids from Oufrane, eastern Dra Valley (Anti-Atlas, Morocco) – taxonomy, stratigraphy and correlation. *Neues Jb. Geol. Paläontol. Abh.*, **259**, 313–379.

Eberli, G.P. and **Betzler, C.** (2019) Characteristics of modern carbonate contourite drifts. *Sedimentology*, **66**, 1163–1191.

Eberli, G.P., **Anselmetti, F.S.**, **Isern, A.R.** and **Delius, H.** (2010) Timing of changes in sea level and currents along Miocene platforms on the Marion Plateau. In: *Cenozoic Carbonate Systems of Australasia* (Eds Morgan, W.A., George, A.D., Harris, P.M., Kupecz, J.A. and Sarg, J.F.), *SEPM Spec. Publ*, **95**, 219–242.

Eberli, G.P., **Bernoulli, D.**, **Vecsei, A.**, **Sekti, R.**, **Grasmueck, M.**, **Lüdmann, T.**, **Anselmetti, F.S.**, **Mutti, M.** and **Della Porta, G.** (2019) A Cretaceous carbonate delta drift in the Montagna della Maiella, Italy. *Sedimentology*, **66**, 1266–1301.

Ebert, J. (1993) Globale Events im Grenz-Bereich Mittel-/Oberdevon. *Göttinger Arb. Geol. Paläont.*, **59**, 1–106.

Eichholt, S. and **Becker, R.T.** (2016) Middle Devonian reef facies and development in the Oued Cherrat Zone and adjacent regions (Moroccan Meseta). *Facies*, **62**, 7.

Einsele, G. (2000) *Sedimentary Basins. Evolution, Facies, and Sediment Budget*. Springer, Berlin, 700 pp.

Ekdale, A.A. and **Mason, T.R.** (1988) Characteristic trace fossil associations in oxygen-poor sedimentary environments. *Geology*, **16**, 720–723.

El Hassani, A., **Tahiri, A.** and **Walliser, O.H.** (2003) The Variscan crust between Gondwana and Baltica. *Courier Forschungsinstitut Senckenberg*, **242**, 81–87.

Embry, A.F. and **Klovan, J.E.** (1972) Absolute water depth limits of Late Devonian palecological zones. *Geol. Rundsch.*, **61**, 672–686.

Ercilla, G., **Casas, D.**, **Vázquez, J.T.**, **Iglesias, J.**, **Somoza, L.**, **Juan, C.**, **Medialdea, T.**, **León, R.**, **Estrada, F.**, **García-Gil, S.**, **Farran, M.**, **Bohoyo, F.**, **García, M.** and **Maestro, A.** (2011) Imaging the recent sediment dynamics of the Galicia Bank region (Atlantic, NW Iberian Peninsula). *Mar. Geophys. Res.*, **32**, 99–126.

Ercilla, G., **Juan, C.**, **Hernández-Molina, F.J.**, **Bruno, M.**, **Estrada, F.**, **Alonso, B.**, **Casas, D.**, **Farran, M.**, **Llave, E.**, **García, M.**, **Vázquez, J.T.**, **D'Acremont, E.**, **Gorini, C.**, **Palomino, D.**, **Valencia, J.**, **El Moumni, B.** and **Ammar, A.** (2016) Significance of bottom currents in deep-sea morphodynamics: an example from the Alboran Sea. *Mar. Geol.*, **378**, 157–170.

Faugères, J.C. and **Mulder, T.** (2011) Contour currents and contourite drifts. In: *Deep-Sea Sediments* (Eds Hüneke, H. and Mulder, T.), *Dev. Sedimentol.*, **63**, 149–214.

Faugéres, J.C., **Gonthier, E.** and **Stow, D.A.V.** (1984) Contourite drift moulded by deep Mediterranean outflow. *Geology*, **12**, 296–300.

Faugères, J.-C., **Stow, D.A.V.**, **Imbert, P.** and **Viana, A.R.** (1999) Seismic features diagnostic of contourite drifts. *Mar. Geol.*, **162**, 1–38.

Fink, H.G., **Wienberg, C.**, **Pol-Holtz, R.**, **Wintersteller, P.** and **Hebbeln, D.** (2013) Cold-water coral growth in the Alboran Sea related to high productivity during the Late Pleistocene and Holocene. *Mar. Geol.*, **339**, 71–82.

Flemming, B.W. (2017) Particle shape-controlled sorting and transport behaviour of mixed siliciclastic/bioclastic sediments in a mesotidal lagoon, South Africa. *Geo-Mar. Lett.*, **37**, 397–410.

Flügel, E. (2010) *Microfacies of Carbonate Rocks. Analysis, Interpretation and Application*. Springer, Berlin, 976 pp.

Folk, R.A. (1962) Spectral subdivision of limestone types. In: *Classification of Carbonate Rocks* (Ed. Ham, W.E.), *AAPG Mem*, **1**, 62–84.

Föllmi, K.B. (2016) Sedimentary condensation. *Earth-Sci. Rev.*, **152**, 143–180.

Föllmi, K.B., **Delamette, M.** and **Ouwehand, P.J.** (2011) Aptian to Cenomanian deeper-water hiatal stromatolites from the northern Tethyan margin. In: *Stromatolites: Interaction of Microbes with Sediments* (Eds Tewari, V.C. and Seckbach, J.), pp. 159–186. Springer, Berlin.

Franchi, F., **Cavalazzi, B.**, **Pierre, C.** and **Barbieri, R.** (2015) New evidence of hydrothermal fluids circulation at the Devonian Kess Kess mounds, Hamar Laghdad (eastern Anti-Atlas, Morocco). *Geol. J.*, **50**, 634–650.

García, M., **Hernández-Molina, F.J.**, **Llave, E.**, **Stow, D.A.V.**, **León, R.**, **Fernández-Puga, M.C.**, **Diaz del Río, V.** and **Somoza, L.** (2009) Contourite erosive features caused by the Mediterranean Outflow Water in the Gulf of Cadiz: quaternary tectonic and oceanographic implications. *Mar. Geol.*, **257**, 24–40.

Gereke, M. and **Schindler, E.** (2012) "Time-Specific Facies" and biological crises — The Kellwasser Event interval near the Frasnian/Famennian boundary (Late Devonian). *Palaeogeogr. Palaeoclimatol. Palaeoecol.*, **367–368**, 19–29.

Ghienne, J.-F., **Desrochers, A.**, **Vandenbroucke, T.R.A.**, **Achab, A.**, **Asselin, E.**, **Dabard, M.P.**, **Farley, C.**, **Loi, A.**, **Paris, F.**, **Wickson, S.** and **Veizer, J.** (2014) A Cenozoic style scenario for the end-Ordovician glaciation. *Nat. Commun.*, **5**, 4485.

Giresse, P. (2008) Some aspects of diagenesis in contourites. In: *Contourites* (Eds Rebesco, M. and Camerlenghi, A.), *Dev. Sedimentol.*, **60**, 203–221.

Glasby, G.P. and **Read, A.J.** (1976) Deep-sea manganese nodules. In: *Handbook of Strata-Bound and Stratiform Ore Deposits* (Ed. Wolf, R.H.), pp. 295–340. Elsevier, Amsterdam.

Golonka, J. (2002) Plate-tectonic maps of the Phanerozoic. In: *Phanerozoic Reef Patterns* (Eds Kiessling, W., Flügel, E. and Golonka, J.), *Soc. Sedim. Geol. Spec. Publ*, **72**, 21–75.

Golonka, J. (2020) Late Devonian paleogeography in the framework of global plate tectonics. *Global Planet. Change*, **186**, 103129.

Gonthier, E., **Faugères, J.-C.** and **Stow, D.A.V.** (1984) Contourite facies of the Faro Drift, Gulf of Cadiz. In: *Fine-Grained Sediments, Deep-Water Processes and Facies* (Eds Stow, D.A.V. and Piper, D.J.W.), *Geol. Soc. London Spec. Publ.*, **15**, 275–292.

Gouwy, S., **Haydukiewicz, J.** and **Bultynck, P.** (2007) Conodont-based graphic correlation of upper Givetian-Frasnian sections of the East ern Anti-Atlas (Morocco). *Geol. Quarterly*, **51**, 375–392.

Grasmueck, M., **Eberli, G.**, **Viggiano, D.A.**, **Correa, T.**, **Rathwell, G.** and **Luo, J.** (2006) Autonomous Underwater Vehicle (AUV) mapping reveals coral mound distribution, morphology and oceanography in deep water of the Straits of Florida. *Geophys. Res. Lett.*, **33**, L23616.

Habgood, E.L., **Kenyon, N.H.**, **Akhmetzhanov, A.**, **Weaver, P.P.E.**, **Masson, D.G.**, **Gardner, J.** and **Mulder, T.** (2003) Deep-water sediment wave fields, bottom current sand channels and gravity flow channel-lobe systems: Gulf of Cadiz, NE Atlantic. *Sedimentology*, **50**, 483–510.

Halbach, P., **Scherhag, C.**, **Hebisch, U.** and **Marchig, V.** (1981) Geochemical and mineralogical control of different genetic types of deep-sea nodules from the Pacific Ocean. *Mineral. Deposita*, **16**, 59–84.

Hanz, U., **Wienberg, C.**, **Hebbeln, D.**, **Duineveld, G.**, **Lavaleye, M.**, **Juva, K.**, **Dullo, W.C.**, **Freiwald, A.**, **Tamborrino, L.**, **Reichart, G.J.**, **Flögel, S.** and **Mienis, F.** (2019) Environmental factors influencing cold water coral ecosystems in the oxygen minimum zones on the Angolan and Namibian margins. *Biogeosciences*, **16**, 4337–4356.

Hartenfels, S., Becker, R.T., El Hassani, A. and **Lüddecke, F.** (Eds) (2018) 10th International Symposium "Cephalopods – Present and Past", Field Guidebook. *Münstersche Forschungen zur Geologie und Paläontologie*, **110**, 145–306.

Hartmann, M., **Segl, M.**, **Mangini, A.**, **Beer, J.**, **Bonani, G.**, **Suter, M.** and **Wölfli, W.** (1989) The 1460 manganese nodules of the Kane Gap (East Atlantic). Indicators of sedimentation–erosion changes. *Geol. Rundsch.*, **78**, 943–958.

Heck, P.R., **Frank, M.**, **Anselmetti, F.S.** and **Kubik, P.W.** (2004) Origin and age of submarine ferromanganese hardgrounds from the Marion Plateau, offshore northeast Australia. In: *Proceedings of the Ocean Drilling Program* (Eds Anselmetti, F.S., Isern, A.R., Blum, P. and Betzler, C.), *Sci. Res*, **194**, 1–22.

Heckel, P.H. and **Witzke, B.J.** (1979) Devonian world palaeogeography determined from distribution of carbonates and related lithic palaeoclimatic indicators. In: *The Devonian System* (Eds House, M.R., Scrutton, C.T. and Basset, M.G.), *Spec. Pap. Palaeont*, **23**, 99–123.

Hein, J.R. and **Koschinsky, A.** (2014) Deep-ocean ferromanganese crusts and nodules. In: *Treatise on Geochemistry* (Eds Holland, H.D. and Turekian, K.K.), pp. 273–291. Elsevier, Amsterdam.

Hein, J.R. and **Peterson, S.** (2013) The geology of manganese nodules. In: *Deep Sea Minerals: Manganese Nodules, a Physical, Biological, Environmental, and Technical Review* (Eds Baker, E. and Beaudoin, Y.), *Secretariat of the Pacific Community*, **1B**, 7–18.

Hein, J.R., **Spinardi, F.**, **Okamoto, N.**, **Mizell, K.**, **Thorburn, D.** and **Tawake, A.** (2015) Critical metals in manganese nodules from the Cook Islands EEZ, abundances and distributions. *Ore Geol. Rev.*, **68**, 97–116.

Hernández-Molina, F.J., **Llave, E.**, **Stow, D.A.V.**, **García, M.**, **Somoza, L.**, **Vázquez, J.T.**, **Lobo, F.**, **Maestro, A.**, **Díaz del Río, V.**, **León, R.**, **Medialdea, T.** and **Gardner, J.** (2006) The Contourite Depositional System of the Gulf of Cadiz: a sedimentary model related to the bottom current activity

of the Mediterranean Outflow Water and the continental margin characteristics. *Deep-Sea Res. I*, **53**, 1420–1463.

Hernández-Molina, F.J., **Stow, D.A.V.** and **Llave, E.** (2008) Continental slope contourites. In: *Contourites* (Eds Rebesco, M. and Camerlenghi, A.), *Dev. Sedimentol*, **60**, 379–408.

Hernández-Molina, F.J., **Paterlini, M.**, **Violante, R.**, **Marshall, P.**, **de Isasi, M.**, **Somoza, L.** and **Rebesco, M.** (2009) Contourite depositional system on the Argentine Slope: an exceptional record of the influence of Antarctic water masses. *Geology*, **37**, 507–510.

Hernández-Molina, F.J., **Serra, N.**, **Stow, D.A.V.**, **Llave, E.**, **Ercilla, G.** and **Van Rooij, D.** (2011) Along-slope oceanographic processes and sedimentary products around the Iberian margin. *Geo-Mar. Lett.*, **31**, 315–341.

Hernández-Molina, F.J., **Llave, E.**, **Preu, B.**, **Ercilla, G.**, **Fontan, A.**, **Bruno, M.**, **Serra, N.**, **Gomiz, J.J.**, **Brackenridge, R.E.**, **Sierro, F.J.**, **Stow, D.A.V.**, **García, M.**, **Juan, C.**, **Sandoval, N.** and **Arnaiz, A.** (2014) Contourite processes associated to the Mediterranean outflow water after its exit from the Gibraltar strait: global and conceptual implications. *Geology*, **42**, 227–230.

Hernández-Molina, F.J., **Sierro, F.J.**, **Llave, E.**, **Roque, C.**, **Stow, D.A.V.**, **Williams, T.**, **Lofi, J.**, **Van der Schee, M.**, **Arnaiz, A.**, **Ledesma, S.**, **Rosales, C.**, **Rodriguez-Tovar, F.J.**, **Pardo-Iguzquiza, E.** and **Brackenridge, R.E.** (2016a) Evolution of the Gulf of Cadiz margin and southwest Portugal contourite depositional system: tectonic, sedimentary and paleoceanographic implications from IODP expedition 339. *Mar. Geol.*, **337**, 7–39.

Hernández-Molina, F.J., **Wåhlin, A.**, **Bruno, M.**, **Ercilla, G.**, **Llave, E.**, **Serra, N.**, **Roson, G.**, **Puig, P.**, **Rebesco, M.**, **Van Rooij, D.**, **Roque, C.**, **González-Pola, C.**, **Sánchez, F.**, **Gómez, M.**, **Preu, B.**, **Schwenk, T.**, **Hanebuth, T.J.J.**, **Sánchez-Leal, R.F.**, **García-Lafuente, J.**, **Brackenridge, R.E.**, **Juan, C.**, **Stow, D.A.V.** and **Sánchez-González, J.M.** (2016b) Oceanographic processes and products around the Iberian margin: a new multidisciplinary approach. *Mar. Geol.*, **378**, 127–156.

Hernández-Molina, F.J., **Soto, M.**, **Piola, A.R.**, **Tomasini, J.**, **Preu, B.**, **Thompson, P.**, **Badalini, G.**, **Creaser, A.**, **Violante, R.A.**, **Morales, E.**, **Paterlini, M.** and **De Santa Ana, H.** (2016c) A contourite depositional system along the Uruguayan continental margin: sedimentary, oceanographic and paleoceanographic implications. *Mar. Geol.*, **378**, 333–349.

Hernández-Molina, F.J., **Campbell, S.**, **Badalini, G.**, **Thompson, P.**, **Walker, R.**, **Soto, M.**, **Conti, B.**, **Preu, B.**, **Thieblemont, A.**, **Hyslop, L.**, **Miramontes, E.** and **Morales, E.** (2017) Large bedforms on contourite terraces: sedimentary and conceptual implications. *Geology*, **46**, 27–30.

Hewitt, R. (1996) Architecture and strength of the ammonoid shell. In: *Ammonoid Paleobiology* (Eds Landman, N., Tanabe, K. and Davies, R.A.), *Top. Geobiol*, **13**, 297–339.

Hladil, J., **Čejchan, P.** and **Beroušek, P.** (1991) Orientation of the conical tests of tentaculites: internal waves an aqueous environments. *Časopsis mineral. geol.*, **36**, 115–130.

Hoepffner, C., **Houari, M.R.** and **Bouabdelli, M.** (2006) Tectonics of the North African Variscides (Morocco, Western Algeria), an outline. In: *Recent Developments on the Maghreb Geodynamics* (Eds de Lamotte, D.F., Saddiqi, O. and Michard, A.), *C. R. Geoscience*, **338**, 25–40.

Hollard, H. (1963) Un tableau stratigraphique du Dévonien du Sud de l′Anti-Atlas. *Notes Serv. Géol. Maroc*, **23**, 105–109.

Hollard, H. (1974) Recherches sur la stratigraphie des formations du Dévonien moyen, de L′Emsien supérieur au Frasnien, dans le Sud du Tafilalt et dans le Ma′der (Anti-Atlas oriental, Maroc). *Notes Serv. Géol. Maroc*, **264**, 7–68.

Hollard, H. (1981) Principaux caractères des formations dévoniennes de l′Anti-Atlas. *Notes Serv. Géol. Maroc*, **308**, 15–22.

House, M.R. (1985) Correlation of mid-Palaeozoic ammonoid evolutionary events with global sedimentary perturbations. *Nature*, **313**, 17–22.

House, M.R. (2002) Strength, timing, setting and cause of Mid-Palaeozoic extinctions. *Palaeogeogr. Palaeoclimatol. Palaeoecol.*, **181**, 5–25.

Hovikoski, J., **Uchman, A.**, **Weibel, R.**, **Nøhr-Hansen, H.**, **Sheldon, E.**, **Ineson, J.**, **Bjerager, M.**, **Therkelsen, J.**, **Olivarius, M.**, **Larsen, M.**, **Alsen, P.** and **Bojesen-Koefoed, J.** (2020) Upper Cretaceous bottom current deposits, north-east Greenland. *Sedimentology*, **67**, 3619–3654.

Hubbard, S.M., **Maceachern, J.A.** and **Bann, K.** (2012) Slopes. In: *Trace Fossils as Indicators of Sedimentary Environments* (Eds Knaust, D. and Bromley, R.J.), *Dev. Sedimentol*, **64**, 607–642.

Hübscher, C., **Dullo, W.C.**, **Flögel, S.**, **Titschack, J.** and **Schönfeld, J.** (2010) Contourite drift evolution and related coral growth in the eastern Gulf of Mexico and its gateways. *Int. J. Earth Sci.*, **99**, S191–S206.

Hübscher, C., **Hseinat, M.A.**, **Schneider, M.** and **Betzler, C.** (2019) Evolution of contourite systems in the late Cretaceous Chalk Sea along the Tornquist Zone. *Sedimentology*, **66**, 1341–1360.

Hüneke, H. (2006) Erosion and deposition from bottom currents during the Givetian and Frasnian: response to intensified oceanic circulation between Gondwana and Laurussia. *Palaeogeogr. Palaeoclimatol. Palaeoecol.*, **234**, 146–167.

Hüneke, H. (2007) Pelagic carbonate ooze reworked by bottom currents during Devonian approach of the continents Gondwana and Laurussia. In: *Economic and Palaeoceanographic Significance of Contourite Deposits* (Eds Viana, A.R. and Rebesco, M.), *Geol. Soc. London Spec. Publ*, **276**, 299–328.

Hüneke, H. (2013) Bioclastic contourites: depositional model for bottom-current redeposited pelagic carbonate ooze (Devonian, Moroccan Central Massif). *Z. Dt. Ges. Geowiss.*, **164**, 253–277.

Hüneke, H. and **Stow, D.A.V.** (2008) Identification of ancient contourites: problems and palaeoceanographic significance. In: *Contourites* (Eds Rebesco, M. and Camerlenghi, A.), *Dev. Sedimentol*, **60**, 323–344.

Hüneke, H., **Hernández-Molina, F.J.**, **Rodríguez-Tovar, F.J.**, **Llave, E.**, **Chiarella, D.**, **Mena, A.** and **Stow, D.A.** (2021) Diagnostic criteria using microfacies for calcareous contourites, turbidites and pelagites in the Eocene-Miocene slope succession, southern Cyprus. *Sedimentology*, **68**, 557–592.

Isern, A.R., **Anselmetti, F.S.** and **Blum, P.** (2002) Constraining Miocene sea-level change from carbonate platform evolution, Marion Plateau, Northeast Australia, Sites 1192–1199. *Proc. ODP Init. Rep.*, **194**, 1–88.

Isern, A.R., **Anselmetti, F.S.** and **Blum, P.** (2005) A Neogene carbonate platform, slope, and shelf edifice shaped by sea level and ocean currents, Marion Plateau (northeast Australia). In: *Seismic Imaging of Carbonate Reservoirs and Systems* (Eds Eberli, G.P., Massaferro, J.L. and Sarg, J.F.), *AAPG Memoir*, **81**, 291–307.

Jelby, M.E., **Grundvåg, S.A.**, **Helland-Hansen, W.**, **Olaussen, S.** and **Stemmerik, L.** (2020) Tempestite facies variability and storm-depositional processes across a wide ramp: towards a polygenetic model for hummocky cross-stratification. *Sedimentology*, **67**, 742–781.

Kenter, J.A.M., **Ginsburg, R.N.** and **Troelstra, S.R.** (2001) Sea-level-driven sedimentation patterns on the slope and margin. In: *Subsurface Geology of a Prograding Carbonate Platform Margin, Great Bahama Bank: Results of the Bahamas Drilling Project* (Ed. Ginsburg, R.N.), *SEPM Spec. Publ*, **70**, 61–100.

Kidwell, S.M. (1991a) The stratigraphy of shell concentrations. In: *Taphonomy: Releasing the Data Locked in the Fossil Record* (Eds Briggs, D.E.G. and Allison, P.A.), pp. 221–290. Plenum Press, New York, NY.

Kidwell, S.M. (1991b) Condensed deposits in siliciclastic sequences. In: *Cycles and Events in Stratigraphy* (Eds Einsele, G., Ricken, W. and Seilacher, A.), pp. 682–695. Springer, Berlin.

Kiessling, W. (2002) Secular variations in the Phanerozoic reef ecosystem. *Spec. Publ. Soc. Econ. Paleontol. Mineral.*, **72**, 625–690.

Klug, C. (2002) Quantitative stratigraphy and taxonomy of late Emsian and Eifelian ammonoids of the eastern Anti-Atlas (Morocco). *Cour. Forschungsinstitut Senckenberg*, **238**, 1–109.

Klug, C. and **Pohle, A.** (2018) The eastern Amessoui Syncline – a hotspot for Silurian to Carboniferous cephalopod research. *Münstersche Forschungen zur Geologie und Paläontologie*, **110**, 244–260.

Klug, C., **Samankassou, E.**, **Pohle, A.**, **De Baets, K.**, **Franchi, F.** and **Korn, D.** (2018) Oases of biodiversity: early Devonian palaeoecology at Hamar Laghdad, Morocco. *N. Jb. Geol. Paläont. Abh.*, **290**, 9–48.

Knutz, P.C. (2008) Paleoceanographic significance of contourite drifts. In: *Contourites* (Eds Rebesco, M. and Camerlenghi, A.), *Dev. Sedimentol*, **60**, 511–535.

de Kruijf, M., **Slootman, A.**, **de Boer, R.A.** and **Reijmer, J.J.G.** (2021) On the settling of marine carbonate grains: review and challenges. *Earth-Sci. Rev.*, **217**, 103532.

Lewandowski, M. (2003) Assembly of Pangea: combined paleomagnetic and paleoclimatic approach. *Adv Geophys.*, **46**, 199–236.

Lindhorst, S., **Betzler, C.** and **Kroon, D.** (2019) Wind variability over the northern Indian Ocean during the past 4 million years – insights from coarse aeolian dust (IODP exp. 359, site U1467, Maldives). *Palaeogeogr. Palaeoclimatol. Palaeoecol.*, **536**, 109371.

Liu, Z., **Chen, D.**, **Zhang, J.**, **Lü, X.**, **Wang, Z.**, **Liao, W.**, **Shi, X.**, **Tang, J.** and **Xie, G.** (2019) Pyrite morphology as an indicator of Paleoredox conditions and shale gas content of the Longmaxi and Wufeng Shales in the middle Yangtze Area, South China. *Minerals*, **9**, 428.

Llave, E., **Hernández-Molina, F.J.**, **Ercilla, G.**, **Roque, C.**, **Van Rooij, D.**, **García, M.**, **Juan, C.**, **Mena, A.**, **Brackenridge, R.**, **Jané, G.** and **Stow, D.A.V.** (2015) Bottom current processes along the Iberian continental margin. *Boletín Geológico y Minero*, **126**, 219–256.

Llave, E., **Hernández-Molina, F.J.**, **García, M.**, **Ercilla, G.**, **Roque, C.**, **Juan, C.** and **Stow, D.** (2020) Contourites along the Iberian continental margins: conceptual and economic implications. *Geol. Soc. Lond. Spec. Publ.*, **476**, 403–436.

Lokier, S.W. and **Al Junaibi, M.** (2016) The petrographic description of carbonate facies: are we all speaking the same language? *Sedimentology*, **63**, 1843–1885.

Lottmann, J. (1990) Die *pumilio*-Events (Mittel-Devon). *Göttinger Arb. Geol. Paläont.*, **44**, 1–98.

Lubeseder, S., **Rath, J.**, **Rücklin, M.** and **Messbacher, R.** (2010) Controls on Devonian hemi-pelagic limestone deposition analysed on cephalopod ridge to slope sections, Eastern Anti-Atlas, Morocco. *Facies*, **56**, 295–315.

Lüdmann, T., **Kalvelage, C.**, **Betzler, C.**, **Fürstenau, J.** and **Hübscher, C.** (2013) The Maldives, a giant isolated carbonate platform dominated by bottom currents. *Mar. Petrol. Geol.*, **43**, 326–340.

Lüdmann, T., **Paulat, M.**, **Betzler, C.**, **Möbius, J.**, **Lindhorst, S.**, **Wunsch, M.** and **Eberli, G.P.** (2016) Carbonate mounds in the Santaren Channel, Bahamas: a current-dominated periplatform depositional regime. *Mar. Geol.*, **376**, 69–85.

Lüdmann, T., **Betzler, C.**, **Eberli, G.P.**, **Reolid, J.** and **the IODP Expedition 359 Scientists** (2018) Carbonate drift delta: a new sediment drift type. *Mar. Geol.*, **401**, 98–111.

Lüning, S., **Adamson, K.** and **Craig, J.** (2003) Frasnian organic-rich shales in North Africa: regional distribution and depositional model. In: *Petroleum Systems and Emerging Technologies in African Exploration and Production* (Eds Arthur, T.J., Macgregor, D.S. and Cameron, N.), *Geol. Soc. London Spec. Publ*, **207**, 165–184.

Lüning, S., **Wendt, J.**, **Belka, Z.** and **Kaufmann, B.** (2004) Temporal-spatial reconstruction of the early Frasnian (Late Devonian) anoxia in NW Africa: new field data from the Ahnet Basin (Algeria). *Sed. Geol.*, **163**, 237–264.

Maiklem, W.R. (1968) Some hydraulic properties of bioclastic carbonate grains. *Sedimentology*, **10**, 101–109.

Malone, M.J., **Slowey, N.C.** and **Henderson, G.M.** (2001) Early diagenesis of shallow-water periplatform carbonate sediments, leeward margin, Great Bahama Bank (Ocean Drilling Program Leg 166). *Geol. Soc. Am. Bull.*, **113**, 881–894.

Martín-Chivelet, J., **Fregenal-Martínez, M.A.** and **Chacón, B.** (2008) Traction structures in contourites. In: *Contourites* (Eds Rebesco, M. and Camerlenghi, A.), *Dev. Sedimentol*, **60**, 159–181.

Massa, D., **Combaz, A.** and **Manderscheid, G.** (1965) Observations sur les séries siluro-dévoniennes des confins algéro-marocains du sud (1954–1955). *Notes Mém Comp Franç Petrol*, **8**, 1–187.

Masson, D.G., **Wynn, R.B.** and **Bett, B.J.** (2004) Sedimentary environment of the Faeroe-Shetland Channel and Faeroe Bank channels, NE Atlantic, and the use of bedforms as indicators of bottom current velocity in the deep ocean. *Sedimentology*, **51**, 1–35.

Matthew, A.J., **Woods, A.J.** and **Oliver, C.** (1991) Spots before eyes: new comparison charts for visual percentage estimation in archaeological material. In: *Recent Developments in Ceramic Petrology* (Eds Middleton, A. and Freestone, I.), *Brit. Mus. Occasional Paper*, **81**, 211–263.

McCave, I.N. (2008) Size sorting during transport and deposition of fine sediments: sortable silt and flow speed. In: *Contourites* (Eds Rebesco, M. and Camerlenghi, A.), *Dev. Sedimentol*, **60**, 121–142.

McCave, I.N. and **Tucholke, B.E.** (1986) Deep current-controlled sedimentation in the western North Atlantic. In: *The Geology of North America The Western North Atlantic Region, Decade of North American Geology* (Eds Vogt, P.R. and Tucholke, B.E.), pp. 451–468. Geological Society of America, Boulder, CO.

McCave, I.N., **Lonsdale, P.F.**, **Hollister, C.D.** and **Gardner, W.D.** (1980) Sediment transport over the Hatton and Gardar contourite drifts. *J. Sediment. Petrol.*, **50**, 1049–1062.

McGhee, G.R., **Clapham, M.E.**, **Sheehan, P.M.**, **Bottjer, D.J.** and **Droser, M.L.** (2013) A new ecological-severity ranking of major Phanerozoic biodiversity crises. *Palaeogeogr. Palaeoclimatol. Palaeoecol.*, **370**, 260–270.

McKerrow, W.S., **Mac Niocaill, C.**, **Ahlberg, P.E.**, **Clayton, G.**, **Cleal, C.J.** and **Eagar, R.M.C.** (2000) The late Palaeozoic relations between Gondwana and Laurussia. In: *Orogenic Processes: Quantification and Modelling in the Variscan Belt* (Eds Franke, W., Haak, V., Oncken, O. and Tanner, D.), *Geol. Soc. London Spec. Pub*, **179**, 9–20.

Michard, A., **Hoepffner, C.**, **Soulaimani, A.** and **Baidder, L.** (2008) The variscan belt. In: *Continental Evolution: The Geology of Morocco* (Eds Michard, A., Saddiqi, O., Chalouan, A. and de Lamotte, D.F.), *Lec. Notes Earth Sci*, **116**, 65–131.

Michard, A., **Soulaimani, A.**, **Hoepffner, C.**, **Ouanaimi, H.**, **Baidder, L.**, **Rjimati, E.C.** and **Saddiqi, O.** (2010) The south-western branch of the variscan belt: evidence from Morocco. *Tectonophysics*, **492**, 1–24.

Mienis, F., **de Stigter, H.C.**, **de Haas, H.**, **van der Land, C.** and **van Weering, T.C.E.** (2012a) Hydrodynamic conditions in a cold-water coral mound area on the Renard Ridge, southern Gulf of Cadiz. *J. Mar. Syst.*, **96–97**, 61–71.

Mienis, F., **Duineveld, G.C.A.**, **Davies, A.J.**, **Ross, S.W.**, **Seim, H.**, **Bane, J.** and **van Weering, T.C.E.** (2012b) The influence of near-bed hydrodynamic conditions on cold-water corals in the Viosca Knoll area, Gulf of Mexico. *Deep-Sea Res. I*, **60**, 32–45.

Miller, M.C. and **Komar, P.D.** (1977) Development of sediment threshold curves for unusual environments (Mars) and for inadequately studied materials (foram sands). *Sedimentology*, **24**, 709–721.

Milliman, J.D. and **Müller, J.** (1973) Precipitation and lithification of magnesian calcite in the deep-sea sediments of the eastern Mediterranean Sea. *Sedimentology*, **20**, 29–45.

Milliman, J.D. and **Müller, J.** (1977) Characteristics and genesis of shallow-water and deep-sea limestones. In: *The Fate of Fossil Fuel CO_2 in the Oceans* (Eds Andersen, N.R. and Malahoff, A.), pp. 655–672. Plenum Publ. Co, New York, NY.

Miramontes, E., **Jorry, S.J.**, **Jouet, G.**, **Counts, J.W.**, **Courgeon, S.**, **Roy, P.L.**, **Guerin, C.** and **Hernández-Molina, F.J.** (2019) Deep-water dunes on drowned isolated carbonate terraces (Mozambique Channel, south-west Indian Ocean). *Sedimentology*, **66**, 1222–1242.

Miramontes, E., **Jouet, G.**, **Thereau, E.**, **Bruno, M.**, **Penven, P.**, **Guerin, C.**, **Le Roy, P.**, **Droz, L.**, **Jorry, S.J.**, **Hernández-Molina, F.J.**, **Thíeblemont, A.**, **Silva Jacinto, R.** and **Cattaneo, A.** (2020) The impact of internal waves on upper continental slopes: insights from the Mozambican margin (Southwest Indian Ocean). *Earth Surf. Process. Landf.*, **45**, 1469–1482.

Miramontes, E., **Thíeblemont, A.**, **Babonneau, N.**, **Penven, P.**, **Raisson, F.**, **Droz, L.**, **Jorry, S.J.**, **Fierens, R.**, **Counts, J.W.**, **Wilckens, H.**, **Cattaneo, A.** and **Jouet, G.** (2021) Contourite and mixed turbidite-contourite systems in the Mozambique Channel (SW Indian Ocean): link between geometry, sediment characteristics and modelled bottom currents. *Mar. Geol.*, **437**, 106502.

Montenat, C., **Baidder, L.**, **Barrier, P.**, **Hilali, A.**, **Lachkem, H.** and **Mennig, J.** (1996) Contrôle tectonique de l´edition des monticules biosédimentaires dévoniens du hmar Lakhdad d´Erfoud (Anti-Atlas oriental, Maroc). *Compte Rendu de l´Academie Sciences*, **323**, 297–304.

Mulder, T., **Ducassou, E.**, **Eberli, G.P.**, **Hanquiez, V.**, **Gonthier, E.**, **Kindler, P.**, **Principaud, M.**, **Fournier, F.**, **Léonide, P.**, **Billeaud, I.**, **Marsset, B.**, **Reijmer, J.J.G.**, **Bondu, C.**, **Joussiaume, R.** and **Pakiades, M.** (2012) New insights into the morphology and sedimentary processes along the western slope of Great Bahama Bank. *Geology*, **40**, 603–606.

Mulder, T., **Hassan, R.**, **Ducassou, E.**, **Zaragosi, S.**, **Gonthier, E.**, **Hanquiez, V.**, **Marchès, E.** and **Toucanne, S.** (2013) Contourites in the Gulf of Cadiz: a cautionary note on potentially ambiguous indicators of bottom current velocity. *Geo-Mar. Lett.*, **33**, 357–367.

Mulder, T., **Ducassou, E.**, **Hanquiez, V.**, **Principaud, M.**, **Fauquembergue, K.**, **Tournadour, E.**, **Chabaud, L.**, **Reijmer, J.**, **Recouvreur, A.**, **Gillet, H.**, **Borgomano, J.**, **Schmitt, A.** and **Moal, P.** (2019) Contour current imprints and contourite drifts in the Bahamian archipelago. *Sedimentology*, **66**, 1192–1221.

Mullins, H.T. and **Neumann, A.C.** (1979) Geology of the Miami terrace and its paleoceanographic implications. *Mar. Geol.*, **30**, 205–232.

Mullins, H.T., **Neumann, A.C.**, **Wilber, R.J.**, **Hine, A.C.** and **Chinburg, S.J.** (1980) Carbonate sediment drifts in northern Straits of Florida. *AAPG Bull.*, **64**, 1701–1717.

Munnecke, A. and **Servais, T.** (2008) Palaeozoic calcareous plankton: evidence from the Silurian of Gotland. *Lethaia*, **41**, 185–194.

Mutti, E., **Cunha, R.S.**, **Bulhoes, E.M.**, **Arienti, L.M.** and **Viana, A.R.** (2014) Contourites and turbidites of the Brazilian marginal basins. *AAPG Search Discov.*, **51069**, 1–46.

Myrow, P.M. and **Southard, J.B.** (1991) Combined-flow model for vertical stratification sequences in shallow marine storm-deposited beds. *J. Sed. Petrol.*, **61**, 202–210.

Myrow, P.M. and **Southard, J.B.** (1996) Tempestite deposition. *J. Sed. Res.*, **66**, 875–887.

Narkiewicz, K. and **Bultynck, P.** (2010) The upper Givetian (Middle Devonian) *subterminus* conodont zone in North America, Europe and North Africa. *J. Paleont.*, **84**, 588–625.

Oczlon, M. (1990) Ocean currents and unconformities: the north Gondwana Middle Devonian. *Geology*, **18**, 509–512.

Ono, K., **Plink-Björklund, P.**, **Eggenhuisen, J.T.** and **Cartigny, M.J.B.** (2021) Froude supercritical flow processes and sedimentary structures: new insights from experiments with a wide range of grain sizes. *Sedimentology*, **68**, 1328–1357.

Ouanaimi, H. and **Lazreq, N.** (2008) The rich group of the Draa plain (lower Devonian, Anti-Atlas, Morocco): a sedimentary and tectonic integrated approach. In: *The Boundaries of the West African Craton* (Eds Ennih, N. and Liégeois, J.P.), *Geol. Soc. London Spec. Publ*, **297**, 467–489.

Paola, C., **Wiele, S.M.** and **Reinhart, M.A.** (1989) Upper-regime parallel lamination as the result of turbulent sediment transport and low-amplitude bed forms. *Sedimentology*, **36**, 47–59.

Paulat, M., **Lüdmann, T.**, **Betzler, C.** and **Eberli, G.P.** (2019) Neogene palaeoceanographic changes recorded in a carbonate contourite drift (Santaren Channel, Bahamas). *Sedimentology*, **66**, 1361–1385.

Percival, L.M.E., **Bond, D.P.G.**, **Rakociński, M.**, **Marynowski, L.**, **Hood, A.V.S.**, **Adatte, T.**, **Spangenberg, J.E.** and **Föllmi, K.B.** (2020) Phosphorus-cycle disturbances during the Late Devonian anoxic events. *Global Planet. Change*, **184**, 103070.

Peters, S.E. and **Loss, D.P.** (2012) Storm and fair-weather wave base: a relevant distinction? *Geology*, **40**, 511–514.

Pomar, L., **Morsilli, M.**, **Hallock, P.** and **Bádenas, B.** (2012) Internal waves, an under-explored source of turbulence events in the sedimentary record. *Earth Sci. Rev.*, **111**, 56–81.

Pomar, L., **Molina, J.M.**, **Ruiz-Ortiz, P.A.** and **Vera, J.A.** (2019) Storms in the deep: tempestite- and beach-like deposits in pelagic sequences (Jurassic, Subbetic, South of Spain). *Mar. Petrol. Geol.*, **107**, 365–381.

Preat, A., **El Hassani, A.** and **Mamet, B.** (2008) Iron bacteria in Devonian carbonates (Tafilalt, Anti-Atlas, Morocco). *Facies*, **54**, 107–120.

Preu, B., **Hernández-Molina, F.J.**, **Violante, R.**, **Piola, A.R.**, **Paterlini, C.M.**, **Schwenk, T.**, **Voigt, I.**, **Krastel, S.** and **Spiess, V.** (2013) Morphosedimentary and hydrographic features of the northern Argentine margin: the interplay between erosive, depositional and gravitational processes and its conceptual implications. *Deep-Sea Res. I*, **75**, 157–174.

Racki, G. (2005) Toward understanding Late Devonian global events: few answers, many questions. In: *Understanding Late Devonian and Permian-Triassic Biotic and Climatic Events: Towards an Integrated Approach* (Eds Over, D.J., Morrow, J.R. and Wignall, P.B.), *Dev. Palaeont. Strat*, **20**, 5–36.

Racki, G. (2020) A volcanic scenario for the Frasnian–Famennian major biotic crisis and other Late Devonian global changes: more answers than questions? *Global Planet. Change*, **189**, 103174.

Raddi, Y., **Baidder, L.**, **Michard, A.** and **Tahiri, M.** (2007) Variscan deformation at the northern border of the West African Craton, eastern Anti-Atlas, Morocco: compression of a mosaic of tilted blocks. *Bull. Soc. Geol. Fr.*, **178**, 343–352.

Rankey, E.C. and **Doolittle, D.F.** (2012) Geomorphology of carbonate platform-marginal uppermost slopes: insights from a Holocene analogue, Little Bahama Bank, Bahamas. *Sedimentology*, **59**, 2146–2171.

von Raumer, J.F. and **Stampfli, G.M.** (2008) The birth of the Rheic Ocean — Early Palaeozoic subsidence patterns and subsequent tectonic plate scenarios. *Tectonophysics*, **461**, 9–20.

von Raumer, J.F., **Nesbor, H.D.** and **Stampfli, G.M.** (2016) The north-subducting Rheic Ocean during the Devonian: consequences for the Rhenohercynian ore sites. *Int. J. Earth Sci.*, **106**, 2279–2296.

Rebesco, M. and **Camerlenghi, A.** (2008) Contourites. *Dev. Sedimentol.*, **60**, 1–663.

Rebesco, M. and **Stow, D.A.V.** (2001) Seismic expression of contourites and related deposits: a preface. *Mar. Geophys. Res.*, **22**, 303–308.

Rebesco, M., **Hernández-Molina, F.J.**, **Van Rooij, D.** and **Wahlin, A.** (2014) Contourites and associated sediments controlled by deep-water circulation processes: state-of-the-art and future considerations. *Mar. Geol.*, **352**, 111–154.

Reid, J.L., **Nowlin, W.D.** and **Patzert, W.C.** (1977) On the characteristics and circulation of the Southwestern Atlantic Ocean. *J. Phys. Oceanogr.*, **7**, 62–91.

Reolid, J. and **Betzler, C.** (2019) The ichnology of carbonate drifts. *Sedimentology*, **66**, 1427–1448.

Reolid, M. and **Nieto, L.M.** (2010) Jurassic Fe-Mn macro-oncoids from pelagic swells of the External Subbetic (Spain): evidences of microbial origin. *Geol. Acta*, **8**, 151–168.

Reolid, J., **Betzler, C.** and **Lüdmann, T.** (2019) Facies and sedimentology of a carbonate delta drift (Miocene, Maldives). *Sedimentology*, **66**, 1243–1265.

Reolid, J., **Betzler, C.**, **Bialik, O.M.** and **Waldman, N.** (2020) Lenticular-bedding-like bioturbation and the onshore recognition of carbonate drifts (Oligocene, Cyprus). *J. Sed. Res.*, **90**, 1667–1677.

Riboulleau, A., **Spina, A.**, **Vecoli, M.**, **Riquier, L.**, **Quijada, M.**, **Tribovillard, N.** and **Averbuch, O.** (2018) Organic matter deposition in the Ghadames Basin (Libya) during the Late Devonian – a multidisciplinary approach. *Palaeogeogr., Palaeoclimatol., Palaeoecol.*, **497**, 37–51.

Rodrigues, S., **Hernández-Molina, F.J.** and **Kirby, A.** (2021) A Late Cretaceous hybrid (turbidite-contourite) system along the Argentine Margin: paleoceanographic and conceptual implications. *Mar. and Petrol. Geol.*, **123**, 104768.

Rodríguez-Tovar, F.J., **Hernández-Molina, F.J.**, **Hüneke, H.**, **Llave, E.** and **Stow, D.** (2019) Contourite facies model: improving contourite characterization based on the ichnological analysis. *Sed. Geol.*, **384**, 60–69.

Ruiz, G.M.H., **Helg, U.**, **Negro, F.**, **Adatte, T.** and **Burkhard, M.** (2008) Illite crystallinity patterns in the Anti-Atlas of Morocco. *Swiss J. Geosci.*, **101**, 387–395.

Sagemann, B.B., **Wignall, P.B.** and **Kaufmann, E.G.** (1991) Biofacies models for oxygen-deficient facies in epicontinental seas: tool for palaeoenvironmental analysis. In: *Cycles and Events in Stratigraphy* (Eds Einsele, G., Riecken, W. and Seilacher, A.), pp. 543–564. Springer, Berlin.

Schlager, W. (1981) The paradox of drowned reefs and carbonate platforms. *Geol. Soc. Am. Bull.*, **92**, 197–211.

Schlichting, H. and **Gersten, K.** (2017) *Boundary Layer Theory*. Springer, Berlin, 805 pp.

Seilacher, A. and **Aigner, T.** (1991) Storm deposits at hte bed, facies, and basin scale: the geologic perspective. In: *Cycles and Events in Stratigraphy* (Eds Einsele, G., Riecken, W. and Seilacher, A.), pp. 227–248. Springer, Berlin.

Servais, T., **Perrier, V.**, **Danelian, T.**, **Klug, C.**, **Martin, R.**, **Munnecke, A.**, **Nowak, H.**, **Nützel, A.**, **Vandenbroucke, T.R.A.**, **Williams, M.** and **Rasmussen, C.M.Ø.** (2016) The onset of the 'Ordovician Plankton Revolution' in the late Cambrian. *Palaeogeogr. Palaeoclimatol. Palaeoecol.*, **458**, 12–28.

Shanmugam, G. (2017) Contourites: physical oceanography, process sedimentology, and petroleum geology. *Petrol. Explor. Develop.*, **44**, 183–216.

Soua, M. (2014) Paleozoic oil/gas shale reservoirs in southern Tunisia: an overview. *J. Afr. Earth Sci.*, **100**, 450–492.

Soulaimani, A. and **Burkhard, M.** (2008) The Anti-Atlas chain (Morocco): the southern margin of the Variscan belt along the edge of the West African craton. In: *The Boundaries of the West African Craton* (Eds Ennih, N. and Liégeois, J.P.), *Geol. Soc. London Spec. Publ*, **279**, 433–452.

Soulaimani, A., **Pique, A.** and **Bouabdelli, M.** (2003) L'extension continentale au Protérozoique terminal – Cambrien basal dans l'Anti-Atlas (Maroc). *Bull. Soc. Geol. Fr.*, **174**, 83–92.

Southard, J.B. and **Bouguchwal, L.A.** (1990) Bed configurations in steady unidirectional water flows. Part 1. Synthesis of flume data. *J. Sed. Petrol.*, **60**, 658–679.

Stampfli, G.M. and **Borel, G.** (2002) A plate tectonic model for the Palaeozoic and Mesozoic constrained by dynamic plate boundaries and restored synthetic oceanic isochrones. *Earth Planet. Sci. Lett.*, **169**, 17–33.

Stampfli, G.M., **von Raumer, J.** and **Wilhem, C.** (2011) The distribution of Gondwana derived terranes in the early Paleozoic. In: *The Ordovician of the World* (Eds Gutiérrez-Marco, J.C., Rábano, I. and García-Bellido, D.), *Cuadernos del Museo Geominero*, **14**, 567–574.

Stampfli, G.M., **Hochard, C.**, **Vérard, C.**, **Wilhem, C.** and **von Raumer, J.** (2013) The formation of Pangea. *Tectonophysics*, **593**, 1–19.

Steinmann, L., **Baques, M.**, **Wenau, S.**, **Schwenk, T.**, **Spiess, V.**, **Piola, A.R.**, **Bozzano, G.**, **Violante, R.** and **Kasten, S.** (2020) Discovery of a giant cold-water coral mound province along the northern Argentine margin and its link to the regional Contourite Depositional System and oceanographic setting. *Mar. Geol.*, **427**, 106223.

Stigall, A.L. (2012) Speciation collapse and invasive species dynamics during the Late Devonian "Mass Extinction". *GSA Today*, **22**, 4–9.

Stow, D.A.V. and **Faugères, J.C.** (2008) Contourite facies and the facies model. In: *Contourites* (Eds Rebesco, M. and Camerlenghi, A.), *Dev. Sedimentol*, **60**, 223–256.

Stow, D.A. and **Shanmugam, G.** (1980) Sequence of structures in fine-grained turbidites: comparison of recent deep-sea and ancient flysch sediments. *Sed. Geol.*, **25**, 23–42.

Stow, D.A.V. and **Smillie, Z.** (2020) Distinguishing between deep-water sediment facies: turbidites, contourites and hemipelagites. *Geosciences*, **10**, 68.

Stow, D.A.V., **Faugères, J.-C.** and **Gonthier, E.** (1986) Facies distribution and textural variation in Faro Drift contourites: velocity fluctuation and drift growth. *Mar. Geol.*, **72**, 71–100.

Stow, D.A.V., **Pudsey, C.J.**, **Howe, J.A.**, **Faugères, J.-C.** and **Viana, A.R.** (Eds) (2002) Deep-water contourite systems: modern drifts and ancient series, seismic and sedimentary characteristics. *Geol. Soc. London Memoirs*, **22**, 1–464.

Stow, D.A.V., **Hernández-Molina, F.J.**, **Llave, E.**, **Sayago-Gil, M.**, **Díaz-del Río, V.** and **Branson, A.** (2009) Bedform-velocity matrix: the estimation of bottom current velocity from bedform observations. *Geology*, **37**, 327–330.

Surlyk, F. and **Lykke-Andersen, H.** (2007) Contourite drifts, moats and channels in the Upper Cretaceous chalk of the Danish Basin. *Sedimentology*, **42**, 405–422.

Svarda, C.E. (2012) Chalk and related deep-marine carbonates. In: *Trace Fossils as Indicators of Sedimentary Environments* (Eds Knaust, D. and Bromley, R.J.), *Dev. Sedimentol*, **64**, 777–806.

Svarda, C.E., **Bottjer, D.J.** and **Seilacher, A.** (1991) Redox-related benthic events. In: *Cycles and Events in Stratigraphy* (Eds Einsele, G., Riecken, W. and Seilacher, A.), pp. 524–541. Springer, Berlin.

Tait, J., **Schätz, M.**, **Bachtadse, V.** and **Soffel, H.** (2000) Palaeomagnetism and Palaeozoic palaeogeography of Gondwana and European terranes. In: *Orogenic Processes: Quantification and Modelling in the Variscan Belt* (Eds Franke, W., Haak, V., Oncken, O. and Tanner, D.), *Geol. Soc. London Spec. Pub*, **179**, 21–34.

Taviani, M., **Angeletti, L.**, **Beuck, L.**, **Campiani, E.**, **Canese, S.**, **Foglini, F.**, **Freiwald, A.**, **Montagna, P.** and **Trincardi, F.** (2016) On and off the beaten track: megafaunal sessile life and Adriatic cascading processes. *Mar. Geol.*, **375**, 146–160.

Taylor, A.M. and **Goldring, R.** (1993) Description and analysis of bioturbation and ichnofabric. *J. Geol. Soc. London*, **150**, 141–148.

Thiéblemont, A., **Hernández-Molina, F.J.**, **Miramontes, E.**, **Raisson, F.** and **Penven, P.** (2019) Contourite depositional systems along the Mozambique channel: the interplay between bottom currents and sedimentary processes. *Deep-Sea Res. I*, **147**, 79–99.

Töneböhn, R. (1991) Bildungsbedingungen epikontinentaler Cephalopodenkalke (Devon, SE-Marokko). *Göttinger Arb. Geol. Paläont.*, **47**, 1–114.

Torsvik, T.H. and **Cocks, L.R.M.** (2004) Earth geography from 400 to 250 Ma: a palaeomagnetic, faunal and facies review. *J. Geol. Soc. London*, **161**, 555–572.

Torsvik, T.H. and **Cocks, L.R.M.** (2013) Gondwana from top to base in space and time. *Gondwana Res.*, **24**, 999–1030.

Toucanne, S., **Soulet, G.**, **Riveiros, N.V.**, **Boswell, S.M.**, **Dennielou, B.**, **Waelbroeck, C.**, **Bayon, G.**, **Mojtahid, M.**, **Bosq, M.**, **Sabine, M.**, **Zaragosi, S.**, **Bourillet, J.F.** and **Mercier, H.** (2021) The North Atlantic Glacial Eastern Boundary Current as a key driver for ice-sheet—AMOC interactions and climate instability. *Paleoceanogr. Paleoclimatol.*, **36**, e2020PA004068.

Tournadour, E., **Mulder, T.**, **Borgomano, J.**, **Hanquiez, V.**, **Ducassou, E.** and **Gillet, H.** (2015) Origin and architecture of a Mass Transport Complex on the northwest slope of Little Bahama Bank (Bahamas): relations between off-bank transport, bottom current sedimentation and submarine landslides. *Sed. Geol.*, **317**, 9–26.

Tucker, M.E. (1974) Sedimentology of Palaeozoic pelagic limestones: the Griotte (Southern France) and Cephalopodenkalk (Germany). In: *Pelagic Sediments: On Land and Under the Sea* (Eds Hsü, K.J. and Jenkyns, H.C.), *Spec. Publ. Int. Ass. Sediment*, **1**, 71–92.

Tucker, M.E. (1990) Carbonate depositional systems II: deeper-water facies of pelagic and resedimented limestones. In: *Carbonate Sedimentology* (Eds Tucker, M.E. and Wright, V.P.), pp. 228–283. Blackwell, Oxford.

Tyson, R.V. (1987) The genesis and palynofacies characteristics of marine petroleum source rocks. In: *Marine Petroleum Source Rocks* (Eds Brooks, J. and Fleet, A.J.), *Geol. Soc. London Spec. Publ*, **26**, 47–67.

Uchman, A. and **Wetzel, A.** (2011) Deep-sea ichnology: the relationships between depositional environment and endobenthic organisms. In: *Deep-Sea Sediments* (Eds Hüneke, H. and Mulder, T.), *Dev. Sedimentol*, **63**, 517–556.

Usui, A., **Nishimura, A.** and **Mita, N.** (1993) Composition and growth history of surficial and buried manganese nodules in the Penrhyn Basin, Southwestern Pacific. *Mar. Geol.*, **114**, 133–153.

Van der Voo, R. (1993) *Paleomagnetism of the Atlantic, Tethys and Iapetus Oceans*. Cambridge Univ. Press, Cambridge, 411 pp.

Viana, A.R. (2001) Seismic expression of shallow- to deep-water contourites along the south-eastern Brazilian margin. *Mar. Geophys. Res.*, **22**, 509–521.

Viana, A.R. and **Faugéres, J.-C.** (1998) Upper slope sand deposits: the example of Campos Basin, a latest Pleistocene/Holocene record of the interaction between along and across slope currents. In: *Geological Processes on Continental Margins – Sedimentation, Mass-Wasting and Stability* (Eds Stoker, M.S., Evans, D. and Cramp, A.), *Geol. Soc. London Spec. Publ*, **129**, 287–316.

Viana, A.R., **Almeida, W., Jr.** and **Almeida, C.F.W.** (2002a) Upper slope sands–the late quaternary shallow-water sandy contourites of campos basin SW atlantic margin. In: *Deep-Water Contourite Systems: Modern Drifts and Ancient Series, Seismic and Sedimentary Characteristics*

(Eds Stow, D.A.V., Pudsey, C.J., Howe, J.A., Faugères, J.C. and Viana, A.R.), *Geol. Soc. London Mem*, **22**, 261–270.

Viana, A.R., **Hercos, C.M.**, **Almeida, W., Jr.**, **Magalhães, J.L.C.** and **Andrade, S.B.** (2002b) Evidence of bottom current influence on the Neogene to quaternary sedimentation along the Northern Campos Slope, SW Atlantic Margin. In: *Deep-Water Contourite Systems: Modern Drifts and Ancient Series, Seismic and Sedimentary Characteristics* (Eds Stow, D.A.V., Pudsey, C.J., Howe, J.A., Faugères, J.C. and Viana, A.R.), *Geol. Soc. London Mem*, **22**, 249–259.

de Vleeschouwer, D., **Crucifix, M.**, **Bounceur, N.** and **Claeys, P.** (2014) The impact of astronomical forcing on the Late Devonian greenhouse climate. *Global Planet. Change*, **120**, 65–80.

Walliser, O.H. (1996) Global events in the Devonian and Carboniferous. In: *Global Events and Event Stratigraphy* (Ed. Walliser, O.H.), pp. 225–250. Springer, Berlin.

Walliser, O.H. (2000) The Jebel Mech Irdane section. *Notes Mém. Serv. Géol. Maroc*, **399**, 57–62.

Walliser, O.H. and **Reitner, J.** (1999) Coquinas of pelagic fossils in pelagic facies: allodapic or autochthonous? *Neues Jb Geol. Paläontol. Abh.*, **214**, 111–128.

Walliser, O.H., **Bultynck, P.**, **Weddige, K.**, **Becker, R.T.** and **House, M.R.** (1995) Definition of the Eifelian-Givetian stage boundary. *Episodes*, **18**, 107–115.

de Weger, W., **Hernández-Molina, F.J.**, **Flecker, R.**, **Sierro, F.J.**, **Chiarella, D.**, **Krijgsman, W.** and **Manar, M.A.** (2020) Late Miocene contourite channel system reveals intermittent overflow behavior. *Geology*, **48**, 1194–1199.

de Weger, W., **Hernández-Molina, F.J.**, **Miguez-Salas, O.**, **de Castro, S.**, **Bruno, M.**, **Chiarella, D.**, **Sierro, F.J.**, **Blackbourn, G.** and **Manar, M.A.** (2021) Contourite depositional system after the exit of a strait: case study from the late Miocene South Rifian Corridor, Morocco. *Sedimentology*, **68**, 2996–3032.

Wendt, J. (1985) Disintegration of the continental margin of northwestern Gondwana, Late Devonian of the eastern Anti-Atlas (Morocco). *Geology*, **13**, 815–818.

Wendt, J. (1988) Condensed carbonate sedimentation in the late Devonian of the eastern Anti-Atlas (Morocco). *Eclogae Geol. Helv.*, **81**, 155–173.

Wendt, J. (1989) Facies pattern and paleogeography of the Middle and Late Devonian in the eastern Anti-Atlas (Morocco). In: *Devonian of the World, II* (Eds McMillan, N.J., Embry, A.F. and Glass, D.E.), *Can. Soc. Petrol. Geol. Mem*, **14**, 531–539.

Wendt, J. (1995) Shell direction as a tool in palaeocurrent analysis. *Sed. Geol.*, **95**, 161–186.

Wendt, J. (2021a) Middle and Late Devonian paleogeography of the eastern Anti-Atlas (Morocco). *Int. J. Earth Sci.*, **110**, 1531–1544.

Wendt, J. (2021b) Middle and Late Devonian sea-level changes and synsedimentary tectonics in the eastern Anti-Atlas (Morocco). *J. Afr. Earth Sci.*, **182**, 104247.

Wendt, J. and **Aigner, T.** (1985) Facies patterns and depositional environments of Palaeozoic cephalopod limestones. *Sed. Geol.*, **44**, 263–300.

Wendt, J. and **Belka, Z.** (1991) Age and depositional environment of Upper Devonian (Early Frasnian to Early Famennian) black shales and limestones (Kellwasser facies) in the eastern Anti-Atlas, Morocco. *Facies*, **25**, 51–90.

Wendt, J., **Aigner, T.** and **Neugebauer, J.** (1984) Cephalopod limestone deposition on a shallow pelagic ridge: the Tafilalt Platform (Upper Devonian, eastern Anti-Atlas, Morocco). *Sedimentology*, **31**, 601–625.

Wetzel, A., **Werner, F.** and **Stow, D.A.V.** (2008) Bioturbation and biogenic sedimentary structures in contourites. In: *Contourites* (Eds Rebesco, M. and Camerlenghi, A.), *Dev. Sedimentol*, **60**, 183–202.

Whalen, C.D. and **Briggs, D.E.G.** (2018) The Palaeozoic colonization of the water column and the rise of global nekton. *Proc. R. Soc. B*, **285**, 20180883.

Wignall, P.B. (1994) *Black Shales*. Oxford University Press, Oxford, 144 pp.

Wignall, P.B. (2005) Anoxic environments. In: *Encyclopedia of Geology* (Eds Selley, R.C., Cocks, L.R.M. and Plimer, I.R.), pp. 495–501. Elsevier, Amsterdam.

Wilckens, H., **Miramontes, E.**, **Schwenk, T.**, **Artan, C.**, **Zhang, W.**, **Piola, A.**, **Baques, M.**, **Provost, C.**, **Hernández-Molina, J.**, **Felgendreher, M.**, **Spieß, V.** and **Kasten, S.** (2021) The erosive power of the Malvinas Current: influence of bottom currents on morpho-sedimentary features along the northern Argentine margin (SW Atlantic Ocean). *Mar. Geol.*, **439**, 106539.

Wilkin, R.T. and **Barnes, H.L.** (1997) Formation processes of framboidal pyrite. *Geochim. Cosmochim. Acta*, **61**, 323–339.

Wilkin, R.T., **Barnes, H.L.** and **Brantley, S.L.** (1996) The size distribution of framboidal pyrite in modern sediments: an indicator of redox conditions. *Geochim. Cosmochim. Acta*, **60**, 3897–3912.

Wunsch, M., **Betzler, C.**, **Lindhorst, S.**, **Lüdmann, T.** and **Eberli, G.P.** (2017) Sedimentary dynamics along carbonate slopes (Bahamas archipelago). *Sedimentology*, **64**, 631–657.

Wunsch, M., **Betzler, C.**, **Eberli, G.P.**, **Lindhorst, S.**, **Lüdmann, T.** and **Reijmer, J.J.G.** (2018) Sedimentary dynamics and high-frequency sequence stratigraphy of the southwestern slope of Great Bahama Bank. *Sed. Geol.*, **363**, 96–117.

Yin, S., **Hernández-Molina, F.J.**, **Zhang, W.**, **Li, J.**, **Wang, L.**, **Ding, W.** and **Ding, W.** (2019) The influence of oceanographic processes on contourite features: a multidisciplinary study of the northern South China Sea. *Mar. Geol.*, **415**, 105967.

Ziegler, P.A. (1989) *Evolution of Laurussia: A Study in Late Palaeozoic Plate Tectonics*. Kluver Academic Publishers, Dordrecht, 129 pp.

Manuscript received 17 March 2022; revision accepted 24 January 2023

